University of Alberta
Department of Civil Engineering

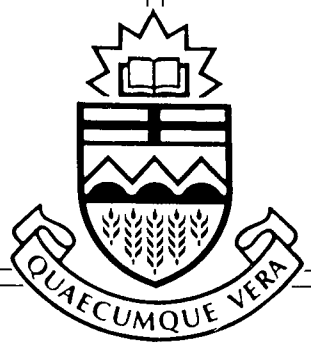

Structural Engineering Report No. 195

SOME BEHAVIOURAL ASPECTS OF COMPOSITE TRUSSES

by

Berhanu F. Woldegiorgis

and

D.J. Laurie Kennedy

January 1994

Structural Engineering Report 195

SOME BEHAVIOURAL ASPECTS OF COMPOSITE TRUSSES

by

Berhanu F. Woldegiorgis

and

D.J. Laurie Kennedy

Department of Civil Engineering

University of Alberta

Edmonton, Alberta, Canada

T6G 2G7

January, 1994

Acknowledgment

The author expresses his deepest appreciation to Dr. D.J.L. Kennedy for his invaluable counselling and supervision throughout this work. Special thanks are extended to Dr. D.W. Murray, Dr. T.M. Hrudey and Dr. S.H. Simmonds for their helpful comments and interest.

This work is based on tests conducted by Anita Brattland in the I.F. Morrison Structural Laboratory at the University of Alberta. The author would like to express his appreciation to Anita Brattland for her sincere cooperation in providing the test data. The financial support of the Natural Sciences and Energy Research Council in the form of an operating grant to Dr. Kennedy is also gratefully acknowledged.

The assistance of C.M. Matthews, Manager of Downhole Technology at C-FER, Roy Gitzel and Dale Lathe, Electronic technicians in Department of Civil Engineering and Albert Huizinga, Electronic technician in Department of Electrical Engineering is very much appreciated.

TABLE OF CONTENTS

Chapter Page

LIST OF FIGURES

Figure

Figure

Page

LIST OF SYMBOLS

A	cross-sectional area, mm^2
A_m	area of model stud, mm^2
A_p	area of prototype stud, mm^2
a_0	peak acceleration, m/sec^2
a_1	peak acceleration, first cycle, m/sec^2
a_n	peak acceleration, n^{th} cycle, m/sec^2
a,b,c	distance of strain gauges on a cross-section, mm
E	modulus of Elasticity, MP_a
EI	flexural stiffness, Nmm^2
e	eccentricity, mm
e_b	bottom end eccentricity, mm
e_t	top end eccentricity, mm
f	frequency, Hz
I	impulse, N.sec
I_e	effective moment of inertia, mm^4
I_m	moment of inertia of model stud, mm^4
I_p	moment of inertia of prototype stud, mm^4
I_s	moment of inertia of steel truss, mm^4
j	$\sqrt{\frac{EI}{P}}$, mm
L	length of member, mm
L_m	length of model stud, mm
L_p	length of prototype stud, mm
M_{cb}	moment in connection at bottom end of web member, kN.m
M_{ct}	moment in connection at top end of web member, kN.m
M_b	moment at bottom end of web member, kN.m
M_t	moment at top end of web member, kN.m

$\bar{m}$ mass per unit length, Kg/m

n number of cycles

P concentrated load, kN

p the decimal fraction of shear connection

R^2 multiple coefficient of determination

u L/j; subscript relating to major principal axis; deflection parallel to the u axis

v subscript relating to minor principal axis; deflection parallel to the v axis

x deflection parallel to the x axis; subscript relating to a rectangular axis of a member; centroidal distance

y deflection parallel to the y axis; subscript relating to a rectangular axis of a member; centroidal distance

z distance along web member, mm

β damping ratio

ε_{st} steel strain at the beginning of strain hardening, $\mu\varepsilon$

ε_u steel strain at ultimate strength, $\mu\varepsilon$

ε_y steel strain at yield strength, $\mu\varepsilon$

ω natural circular frequency, rad/sec

CHAPTER 1
INTRODUCTION

1.1 General

Composite steel-concrete trusses may be used for the floor systems of high-rise buildings where large clear spans are seen to be advantageous. A composite truss consists of a triangulated steel framework connected to a concrete slab by means of shear connectors. The concrete slab, generally reinforced with welded wire mesh, is frequently cast on wide-rib profile steel deck spanning between the steel trusses. Different components and configurations may be used for the steel trusses. Designers need to understand the behaviour of composite trusses and their components so that safe, serviceable and economical trusses can be made. Two aspects of composite trusses worthy of consideration are: the behaviour of double angle web members that are not interconnected and the vibration characteristics of the steel trusses before they are made composite and of the composite trusses.

Double angle web members, frequently used in composite trusses, may also be used in non-composite construction. Although the double angle web members may be interconnected at a point or points between their ends the question arises whether or not such interconnections are needed. Interconnection reduces the effective slenderness ratio of the members and, as well, may reduce the effect of moments introduced in the web members because they are connected to the chord of the truss by one leg only. These moments tend to cause the web members to deflect out of the plane of the

truss. The increased cost of the larger web members required when interconnection is not provided may be more than offset by the cost of the interconnection. This is particularly true when hollow structural sections are used for the chords of the truss and the two angles constituting a web member are separated by the width of the hollow structural section.

Long span composite truss floor systems may exhibit undesirable vibration characteristics when subjected to transient or steady-state vibrations. This problem is exacerbated by the flexibility of the systems and, for transient vibration, by the lack of damping.

1.2 Objectives

The overall objectives of this study were to examine:

1. the behaviour of non-interconnected double angle web members and

2. the vibration characteristics of steel and composite steel-concrete trusses.

1.3 Scope

In testing two composite trusses to failure, Brattland and Kennedy (1986, 1992) also instrumented the angle web members to examine their behaviour. Their analyses of the web members were very limited. A more general and complete analysis is presented here for all those web members instrumented by Brattland and

Kennedy which provided meaningful results. Data developed on the geometric and material properties of the angles by them were used in these analyses. Effective or actual end eccentricities when the web members are attached by welding to one leg are determined. An effective end eccentricity is defined as the moment about any axis divided by the axial force in the member. Based on the analyses of the behaviour, recommendations for the design of non-interconnected angle web members are developed.

The results of 20 heel-drop tests on each of the steel and composite steel-concrete trusses tested by Brattland and Kennedy are analyzed to determine the relevant vibration characteristics of frequency, peak acceleration and percent critical damping and conclusions are drawn.

1.4 Outline

Review of the literature presented in this chapter, revealed that only a limited amount of research has been done on the behaviour of angle web members. In the literature on the vibration of steel and composite flexural members a more or less standard heel-drop test and annoyance criteria for vibration have been developed. The test specimen design and instrumentation is discussed in chapter 2. In chapter 3 the behaviour of the web members is analyzed. Chapter 4 discusses the results of the heel-drop tests. The work is summarized and conclusions are presented in chapter 5.

1.5 Literature review

1.5.1 Angle web members

Brattland and Kennedy (1986, 1992) conducted tests and compiled the necessary data for the investigation of web members as part of their shrinkage and flexural full-scale composite truss tests. Ten web members were gauged to determine their behaviour. The data of two web members were analyzed by them. Brattland and Kennedy recommended that double angle web members be designed for their axial loads together with their portion of the in-plane joint eccentricity moment plus 1/3 of the out-of-plane connection eccentricity moment. They also recommended that the welds connecting double angle web members to chords be designed for the axial force and in-plane moments.

Elgaaly et al. (1991) designed a program to test 50 single-angle web members as part of a truss. The ends of the web members were connected to the chords by one or two bolts. They integrated strain gauge readings at a single cross-section at mid length to determine the axial load at failure and also determined the in-plane and out-of-plane displacements at this location. The failure load was compared with those predicted given by the American Institute of Steel Construction (AISC 1986) and the American Society of Civil Engineers Manual 52 (ASCE 1988) without any consideration of the effective end eccentricities of the applied loads. In other words, the angles were assumed to be concentrically loaded when in fact they were not. Adluri and Madugula (1992, 1993) suggested that single angles connected by one leg be designed as beam columns with biaxial

bending.

Bathon et al. (1993) tested 75 single equal and unequal leg angles connected by one leg with two, three or five bolts. They compared the test failure loads with those predicted by ASCE Manual 52 (ASCE 1988) for angles with normal framing eccentricity. The mean test-to-predicted ratio was 0.70 with a coefficient of variation of 0.13 indicating that this approach is not a good one or that the tests were poor or both.

As discussed subsequently, this work shows that double angle web members should be designed for the effective out-of-plane end eccentricities that are only a fraction of the centroidal distance from the connection interface to the centroidal axes. In-plane end eccentricities to be considered include joint eccentricities and connection eccentricity moments.

1.5.2 Floor vibration

Reiher and Meister (1931) developed a scale for the perception of vibrations by standing and reclining people when subjected to steady state vibrations. Lenzen and Keller (1960) modified the Reiher-Meister scale to include transient vibration induced by humans.

Wiss and Parmelee (1974) developed a human response formula based on subjective ratings of transient vibrations. Allen and Rainer (1976) developed annoyance threshold curves as functions of frequency, initial peak acceleration and damping. This material is given in Appendix G of CAN/CSA standard S16.1-M89 (CSA 1989).

Lenzen (1966) showed that a strong dependence existed between acceptable floor accelerations and damping. Lenzen and Keller (1960) developed the " T-Beam Analogy" to predict frequencies of vibration of steel joist-concrete slab floor systems. Lenzen and Murray (1969) developed the heel drop test to assess the vibration characteristics of floor systems.

In this work vibration characteristics of the steel and steel-concrete composite trusses determined from the analysis of the heel-drop tests conducted by Brattland and Kennedy in accordance with the procedures of Lenzen and Murray (1969) are compared to the annoyance threshold curves developed by Allen and Rainer (1976).

CHAPTER 2

TEST SPECIMEN DESIGN AND INSTRUMENTATION

2.1. General

The composite trusses consisted of Grade 350W hollow structural section (HSS) top and bottom chords with Grade 300W double angle web members in a Warren configuration supporting a 76 mm deep wide-rib profile steel deck and a 65 mm thick cover slab of normal density 20 MPa concrete as shown in Figure 2.1. The fabricator substituted the next higher imperial size angles for the metric angles that had been specified. The slab reinforcement consisted of one or two layers of 152x152xMW9.1xMW9.1 welded wire mesh.

Because in previous composite truss tests, Cran (1972) and Bjorhovde (1981), failure was precipitated by buckling of the first compression diagonals, the diagonals were designed to resist forces consistent with the ultimate tensile strength of the bottom chord. The information that follows deals chiefly with the design and instrumentation of the web members as they are the focus of this investigation.

2.2 Web member properties

All web members were rolled to CSA Standard CAN3-G40.21-M81 Grade 300W steel (CSA 1981b) by Manitoba Rolling Mills. Web members of the same cross-section were supplied from the same heat of steel. The chemical composition for the angles given in Table

2.1 is within the limits specified in the standard. The cross-sectional dimensions (Brattland and Kennedy 1986) given in Table 2.2 are within the rolling tolerances of CSA standard CAN3-G40.20-M81 (CSA 1981a). In no case is the measured dimension as much as 1% less than the specified value. The measured cross-sectional properties (Brattland and Kennedy 1992) are given in Table 2.3. The areas were determined by geometric and volumetric methods. The geometric method was based on the measured dimensions assuming that all rounded corners were circular arcs of radius equal to one-half the leg thickness. In the volumetric method the area is calculated from the measured mass and length of specimens and the density of rolled steel. The average mechanical properties for the five angle sections based on two tension coupon tests per angle are given in Table 2.4. These properties exceed the requirements of the standards with the exception of the yield strength of the angle L 2-1/2x2-1/2x3/8 which is 2% under the specified minimum..

2.3 Web member configuration

To accommodate the welds, joint eccentricities at the bottom chord of 20 to 30 mm measured along the axis of the bottom chord were needed. This joint eccentricity is defined as the distance, measured along the axis of the chord, between the points where the longitudinal axes of the two web members at a joint intersect the axis of the chord. The web members were positioned on the top chord in such a manner that their centroidal axes meet at the mid-depth of the cover slab. Besides providing enough space to

accommodate the welds on the top chord, this positioning reduced the top chord panel length and effected reduced axial force-bending moment interaction values of the top chord for the construction stage. This configuration also minimizes the joint eccentricities of the composite truss.

2.4 Web member connections

The web members were connected to the vertical webs of the HSS chord by welding along one leg. This, of course, introduces out-of-plane connection eccentricities. The welds were designed to transfer the axial loads of the member and its in-plane yield moment, neglecting the out-of-plane moments due to connection eccentricity (Brattland and Kennedy 1992).

2.5 Web member eccentricity moments

Moments may develop at the ends of the web members due to out-of-plane and in-plane connection eccentricities and due to joint eccentricities. Connection eccentricities arise when the resisting force in the welds is not concentric with the axis of the member. Out-of-plane connection eccentricities exist when the angles are connected by one leg as discussed in section 2.4. In-plane connection eccentricities occur when the cenroid of the connecting welds does not lie on the longitudinal axis of the member. Joint eccentricities arise when all members do not intersect at a common point as discussed in section 2.3. Brattland and Kennedy (1992) argued that

the web members need not be designed for the connection eccentricity moments, but should be designed for the proportion of the in-plane joint eccentricity moment they attract based on their relative flexural stiffness. These in-plane moments would then be resolved into moments about the principal axes of the angles for use in an axial force-moment interaction equation.

2.6 Test procedure

The behaviour of the double angle web members was investigated as constituent parts of the two composite steel-concrete trusses. The trusses were loaded to failure with four point loading as shown in Figure 2.2. From this diagram it can be inferred that the axial force in the diagonals on either end would be twice that in the next four and zero in the central four diagonals if the loads and the structure were symmetrical. The bending moment diagram shows that this four point loading arrangement results in a moment diagram closely approximated with that from a uniformly distributed load.

By loading the web members as part of the overall structure the end connection effects are automatically accounted for. Most tests on angle members have been conducted on isolated members with end conditions simulating those of the actual structure. Elgaaly et al. (1991) tested angles with bolted end connections as part of a truss but did not assess the end eccentricities or moments. They analyzed the angles as axially loaded members.

2.7 Instrumentation

Calibrated load cells were used to measure the four loads and two reactions. Statics therefore provided a check on the load cell readings.

Figures 2.3 and 2.4 show the web members that were strain gauged on composite trusses 1 and 2 respectively. Only one angle of the double web members was strain gauged at each location. From the experience gained in the testing of the first truss, more of the heavily loaded compression diagonals were strain gauged in the second truss.

Using the alpha-numeric designation for the web members and adding the designation T1 for truss 1 and T2 for truss 2 the web members that were gauged were: W9T1, W10T1, W11T1, W14T1, and W15T1 on composite truss 1 and W2T2, W4T2, W13T2, W14T2, and W15T2 on composite truss 2. For the web members in the Warren configuration that were strain gauged, assuming symmetry exists, all members are in compression with the exception of W14T1, W14T2 which are in tension and W9T1, W10T1 which are nominally zero force members.

Figure 2.5 shows the location of each of the six strain gauges mounted on an angle at a given cross-section. The nominal values of the distances a, b, and c shown in the figure are given in Table 2.6 for the different sizes of the angles used. The measured values of these distances, which could vary by approximately $\pm$ 2 mm from the nominal values were, of course, used in the calculations.

Three cross-sections, approximately at the mid-length and quarter points of the angles were strain gauged as shown in Figure 2.6. The distances are again nominal values, with measured value used in the calculation. The separation of the double angle compression members, 2T1, 15T1, 2T2, 4T2, 6T2, 11T2, 13T2, and 15T2 were monitored with linear variable displacement transformers (LVDT's).

For the proper functioning of all electrical instrumentation, the power supply voltage was regularly monitored and adjusted as necessary to ensure accurate output. The overall voltage did not vary by more than 0.8% on test 1 and 1.8% on test 2. All the output from the electric resistance strain gauges, LVDT's and load cells were automatically recorded using the Data General Eclipse S/120 data acquisition system. The data were transferred subsequently to the University of Alberta's Amdahl 5860 mainframe computer and processed.

Table 2.1 Chemical composition of angle sections

Size of angle	Chemical composition, %				
	C	Mn	P	S	Si
L 2-1/2x2-1/2x3/8	0.18	1.13	0.025	0.033	0.24
L 2x2x3/8	0.18	1.06	0.027	0.040	0.25
L 2x2x1/4	0.12	0.70	0.021	0.035	-
L 1-1/2x1-1/2x1/4	0.13	0.78	0.028	0.044	-
L 1-1/2x1-1/2x3/16	0.12	0.69	0.011	0.032	-

Table 2.2 Cross-sectional dimensions of angle sections

Size of angle	Dimension	Number of measurments	Mean value mm	C.O.V	Measured / Specified	Tolerance
L 2-1/2x2-1/2x3/8	Width	110	63.11	0.0031	0.994	61.50 - 65.50
	Thickness	112	9.49	0.0075	0.996	9.12 - 9.92
L 2x2x3/8	Width	110	51.11	0.0031	1.006	49.80 - 51.80
	Thickness	112	9.45	0.0051	0.993	9.32 - 9.72
L 2x2x1/4	Width	158	50.97	0.0100	1.003	49.80 - 51.80
	Thickness	160	6.32	0.0104	0.995	6.15 - 6.55
L1-1/2x1-1/2x1/4	Width	158	38.54	0.0088	1.012	37.10 - 39.10
	Thickness	160	6.34	0.0100	0.999	6.15 - 6.55
L1-1/2x1-1/2x3/16	Width	160	37.99	0.0016	0.997	36.10 - 39.10
	Thickness	160	4.78	0.0117	1.004	4.56 - 4.96

Table 2.3 Cross-sectional properties of angle sections

Size of angle	Measured cross-sectional properties			
	Area, mm^2		Location of centroid mm	Moment of inertia mm^4
	Volumetric method	Geometric method		
L 2-1/2x2-1/2x3/8	1099	1104	19.0	390×10^3
L 2x2x3/8	858	868	15.9	193×10^3
L 2x2x1/4	604	606	14.9	143×10^3
L 1-1/2x1-1/2x1/4	447	447	11.9	59×10^3
L 1-1/2x1-1/2x3/16	340	341	11.1	45×10^3

Table 2.4 Average of the tension coupon results

Size of angle	Modulus of elasticity MPa	Static yield strength MPa	ε_y με	ε_{st} με	Ultimate strength MPa	ε_u με
L 2-1/2x2-1/2x3/8	206 800	294	1610	15 500	488	200 000
L 2x2x3/8	206 000	304	2070	13 800	509	190 000
L 2x2x1/4	203 600	309	1620	17 000	496	200 000
L 1-1/2x1-1/2x1/4	205 400	302	1610	17 800	488	209 000
L 1-1/2x1-1/2x3/16	206 800	318	2220	18 000	488	205 000

Table 2.5 Nominal values of strain gauge locations on the cross-section

Size of angle	Nominal value of distances, mm		
	a	b	c
L 2-1/2x2-1/2x3/8	5	31	56
L 2x2x1/4	5	25	45
L 1-1/2x1-1/2x1/4	5	19	33
L 1-1/2x1-1/2x3/16	5	18	32

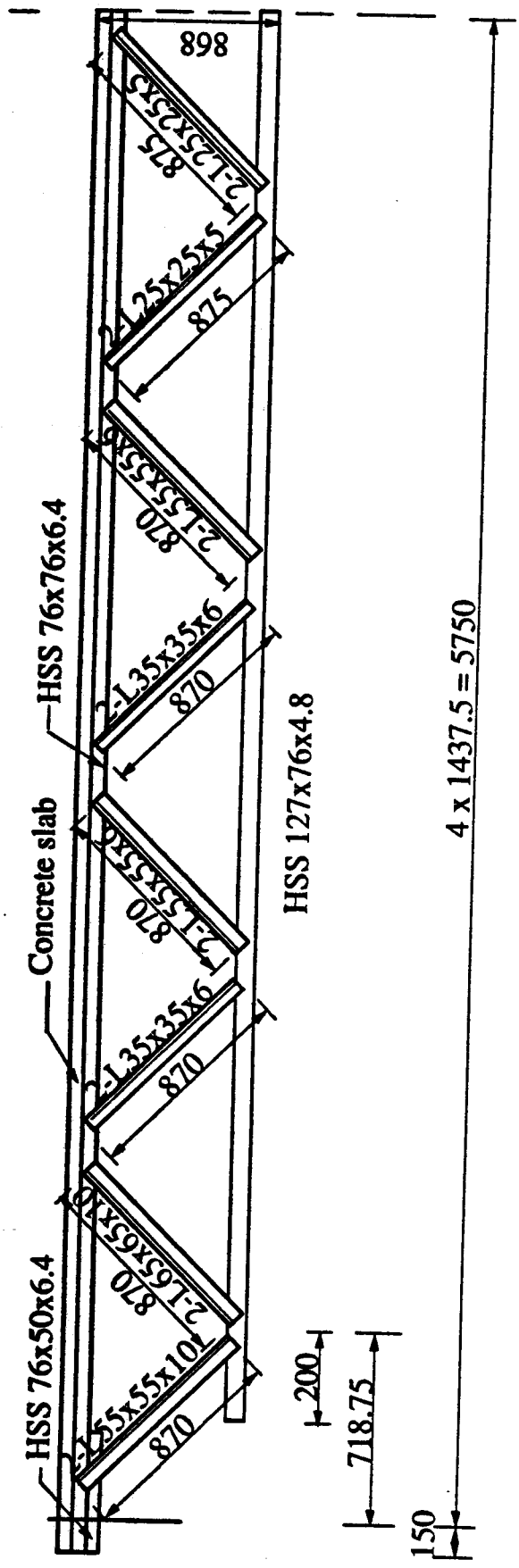

Figure 2.1. Half-elevation of a composite truss

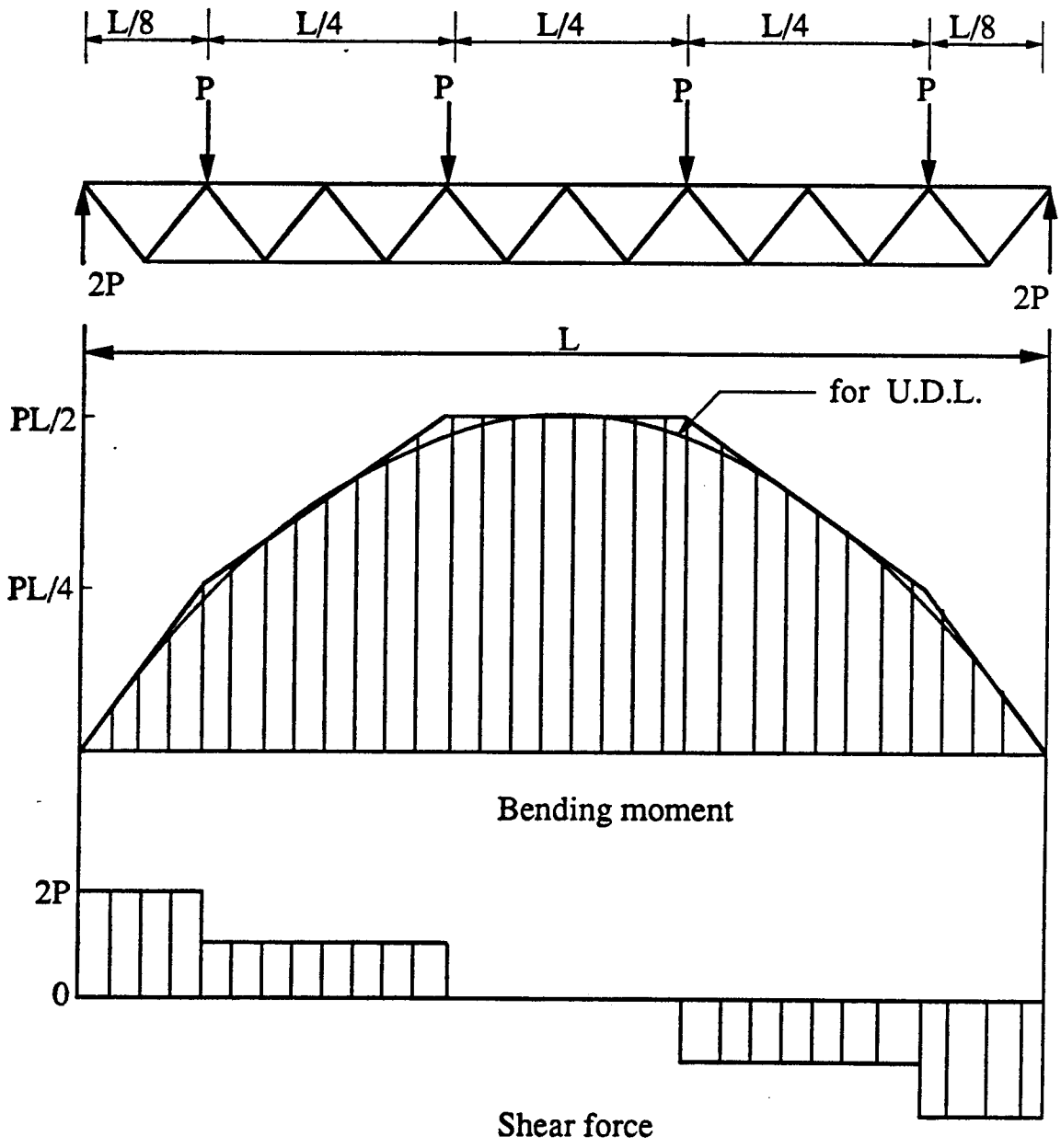

Figure 2.2 Load, bending moment, and shear force diagrams

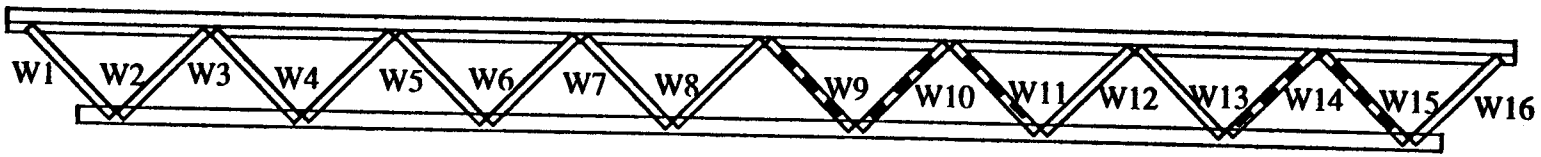

Figure 2.3 Web members with strain gauges on composite truss 1

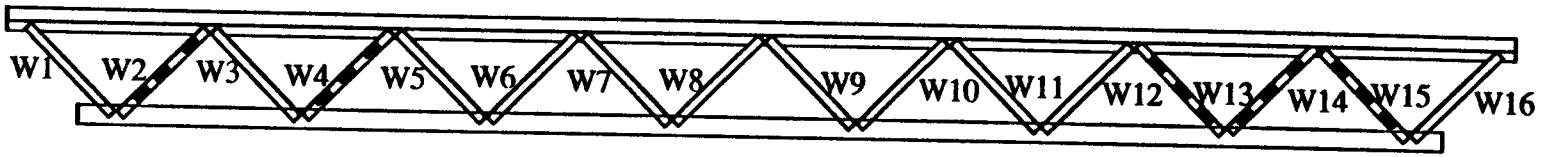

Figure 2.4 Web members with strain gauges on composite truss 2

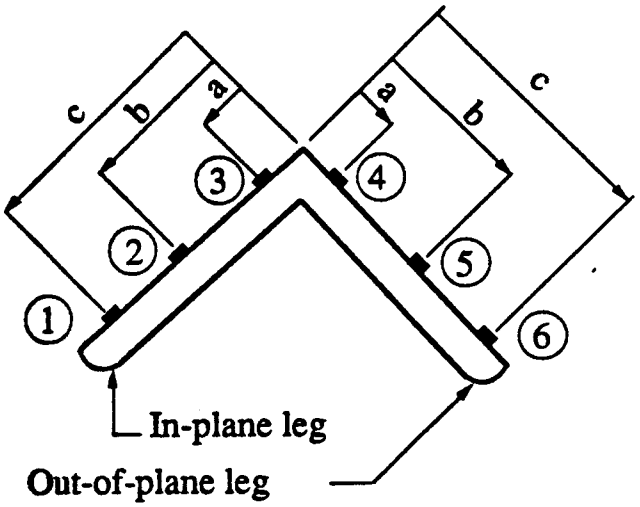

Figure 2.5 Typical strain gauge locations on a cross-section

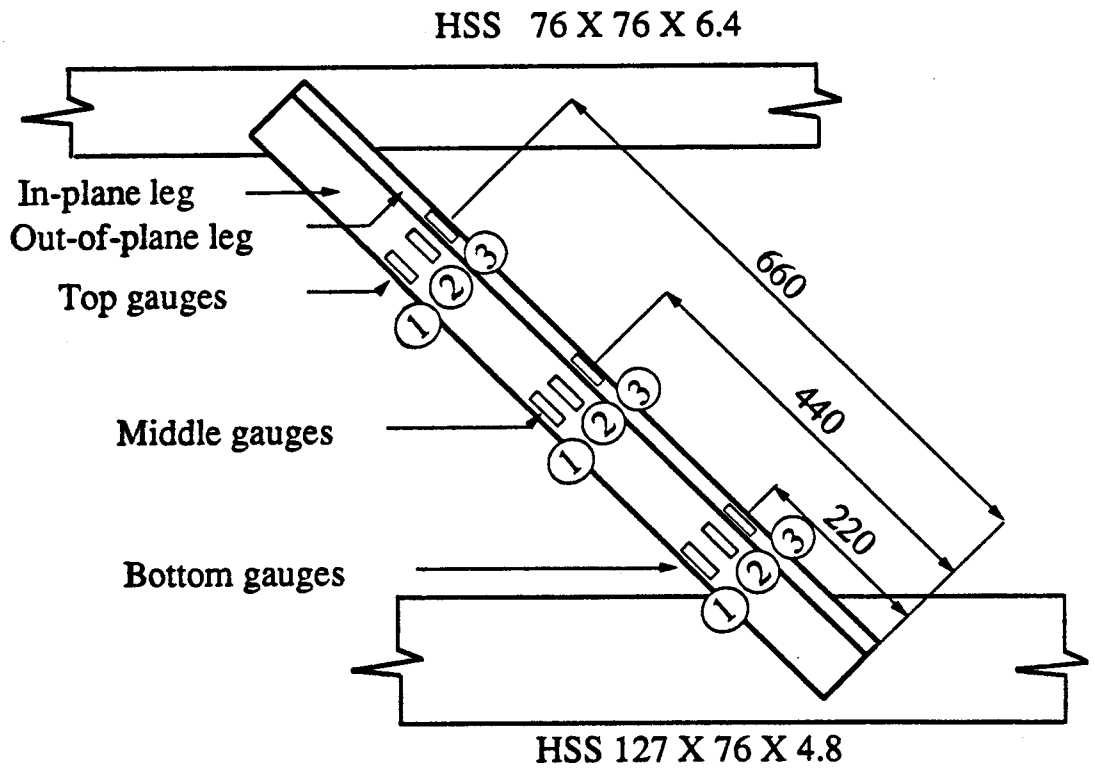

Figure 2.6 Typical strain gauge locations on an angle section

CHAPTER 3

ANALYSES OF WEB MEMBER BEHAVIOUR

3.1 General

Two types of analyses were made to study the behaviour of the web members.

Analyses of the entire truss under a given loading condition using a plane-frame-truss (PFT) computer program gives the member forces in the truss elements due to in-plane behaviour. Out-of-plane behaviour is not assessed. Three levels of detail were used to model the truss.

In the first, the truss was modelled as a series of pin-jointed members with the web members extending from the mid-depth of the bottom chord to the mid-thickness of the cover slab even though the web members are connected to the steel top chord and the extension upward into the cover slab is notional. This analysis generates only axial forces in the truss members.

In the second, the same web member configuration was used but the web members were considered to be rigidly connected to the steel bottom chord and the concrete cover slab. This analysis gives the axial forces in the truss members and the secondary moments that develop due to joint rotations.

The third analysis had the greatest sophistication. All steel members were considered to be rigidly connected with in-plane joint eccentricities measured along the chord axes as discussed in section 2.3. As well, when the centroid of the connecting welds did not lie on the axis of the member, the resulting connection eccentricity moment

equal to the axial force in the member multiplied by the distance perpendicular to the axis of the member between the centroid of the weld and that of the member was applied as a concentrated moment to the node under consideration. The steel top chord was connected to the concrete cover slab with elements to model the behaviour of the studs in shear and tension. The third analysis generates axial forces, joint eccentricity moments and secondary moments due to joint rotations.

Analyses of the strain data obtained for selected web members can provide information on their in-plane and out-of-plane behaviour. Two types of multiple regression analyses were performed. In the first, the strain data obtained from the six strain gauges at a given level were analyzed to determine the axial forces at that level. Analyses of these data provide a means to assess the reliability of the strain gauge data because the axial force determined at each level should of course be the same. In the second, the 18 strain readings at three levels were analyzed to determine the unique value of the axial force in the member and bending moments about the principal axes at the three levels. These data were then used to assess the in-plane and out-of-plane behaviour.

3.2 Plane Frame Truss Analyses

3.2.1. Truss analysis

Because the web members were positioned such that their lines of action of adjacent members would intersect at mid-depth of the cover slab, and because the joint eccentricities on the bottom chord

were only as large as that required for placing the welds, it was considered appropriate to carry out an analysis assuming that the web members were pinned at the top and bottom. Moreover CSA Standard S16.1-M89 in Clause 17.9.2 (CSA 1989) neglects the area of the steel top chord in analyzing the composite truss for the ultimate limit state. The results of the pin-jointed analysis also serve as a basis for comparison with other analytical models and test results. The results of this simplified analysis and the other analyses are reported in Tables 3.1 and 3.2 for selected web members for five different load steps for composite trusses 1 and 2 respectively. In these and subsequent tables compressive forces are indicated by a negative value. The web members selected are those that were strain gauged as discussed in section 2.7 and shown in Figures 2.3 and 2.4 with the exception that results are not reported for web members W9 and W10 of truss 1. These members, were the truss perfectly symmetric and symmetrically loaded, would be zero force members. The small axial forces generated in these members due to slight asymmetry of loading and due to joint fixity were not further considered. Based on this, web members 9 and 10 of truss 2 were not strain gauged. Hence, results are reported for web members W11, W14 and W15 of truss 1 and web members W2, W4, W13, W14 and W15 of truss 2. For each load step the average load applied to each of the four jacks is also reported.

The five load steps selected for any web member were representative of the range of loads within which the member behaved elastically. In this selection an allowance of 0.3 of the yield strain was made for the residual strains due to the manufacturing

process based on the work of Nuttal and Adams (1970) and Al-Sayed and Bjorhovde (1989). The loads on the trusses at the highest load steps used were about equal to those at which flaking of the whitewash at the ends of some of the selected members was first noticed corroborating the selection based on the maximum strain readings.

3.2.2 Frame analysis

Tables 3.1 and 3.2 also list the results of the simplified frame analysis. In this analysis (i) the member ends are considered to be fixed rather than pinned as was the case in the simplified pin-jointed truss analysis and (ii) no joint eccentricities were considered to exist. The ratio of member forces generated in the frame analysis and pin-jointed analysis range from 0.975 to 0.993. The mean value of the ratio of the member forces from the frame and pin-jointed analyses for the two trusses is 0.987 with a coefficient of variation of 0.005. This indicates, as expected, that a truss carries loads primarily as axial forces in the members and that frame action contributes little to the overall strength.

3.2.3 Detailed frame analysis

In this analysis the actual physical characteristics of the web members were modelled, i.e. the members were considered to be rigidly connected to the steel top and bottom chords and the actual joint eccentricities, i.e. the eccentricities that exist because the centerline of the members at a joint do not intersect at a common point, were used. Figure 3.1 also shows that the joint eccentricities at

the lower chord level (about 60 mm on this figure but ranging between 55 and 60 mm) are much smaller than those at the steel top chord level of about 260 mm.

In addition, the connection eccentricity that results because the centroid of a weld group may not lie on the axis of the member, was considered by applying at the appropriate node a concentrated moment equal to the axial force in the member multiplied by this connection eccentricity as discussed in section 3.1. As may be seen from Figure 3.1 the space available for welds results in relatively small connection eccentricities at the upper end because a major portion of the longitudinal weld is placed along the heel of the angle. At the lower end the connection eccentricities are relatively large because the major longitudinal fillet weld lies at the toe of the web angle.

Because the concrete cover slab provides the compressive force for the internal resisting couple, the studs connecting the cover slab to the steel top chord, also had to be modelled. The modelled stud extended from the mid-depth of the top chord to the mid-thickness of the cover slab and was considered fixed at its lower end and free to rotate at its top end. The axial stiffness of the modelled stud was determined using a model area,

$$[3.1] \qquad A_m = A_p \frac{L_m}{L_p}$$

in order that the elongation of the longer modelled stud was the same as that of the prototype. Similarly the moment of inertia of the model stud was increased by

[3.2] $$I_m = I_p \left(\frac{L_m}{L_p}\right)^3$$

to give the same relative cantilever deflection of the top of the stud. The prototype flexural stiffness was determined from load-slip curve for push-out tests of studs of truss 2. Although the studs behave inelastically at high loads and allow significant redistribution of loads from one stud to another, for the purpose of this analysis the behaviour was considered to be linearly elastic corresponding to a cantilever tip deflection of 0.9 mm at a load of 50 kN. The maximum load carried by a stud in a push-out test was 64 kN, and in only a few cases did the analysis indicate that the stud load exceeded a value of 50 kN. For truss 1, the analysis showed that two of the 19 studs exceeded the 50 kN load at load step 10 and of course at load step 11. At load step 11, one stud exceeded the maximum push-out value of 64 kN. For truss 2, two of the studs exceeded a load of 50 kN at load steps 20 and up, and one of these two studs exceeded the 64 kN limitation at these load steps. In all of these cases, however, when the load on the most highly loaded stud was averaged with that of its neighbour or neighbours the average maximum load was well within the capacity of a single stud and, furthermore, did not require significant inelastic action. Therefore, this model for the studs is considered appropriate.

In modelling the concrete slab the full width of the slab was considered to be effective because the strain distribution across the slab both at the mid span and one-fifth points was relatively uniform as established by Brattland and Kennedy (1992). The modulus of

elasticity of the concrete was taken as the secant value at a stress of 0.4 of the strength at the time of testing. Figure 3.2 is an elevation of one half of the truss model showing node and member numbers. In fact, because the truss was not perfectly symmetrical about the centerline, the full truss was modelled. It is noted from Figure 3.2 that the loads were considered to be applied to the steel top chord at the nodes where the web members intersect it. Analysis with loads applied to the concrete slab did not result in a significant difference in the member forces and moments.

In an attempt to get better correspondence between the results of the detailed frame analysis and results of the strain analyses as discussed subsequently various modifications of the stiffness of the web and chord members in the vicinity of the joints were made. These included:

(i) a decreased web member stiffness at the ends to account for the distortion in the welds based on load-deflection curves for the welds developed by Lesik and Kennedy (1990),

(ii) an increased web member stiffness at the ends to account for the increased stiffness within the dimensions of the joints. Within the joint, the web members in particular may have a significantly larger stiffness because of the extent of the chords to which they are connected. Stiffnesses upto 100 times those of the web members were used.

(iii) a decreased stiffness of the bottom chord , as little as 1/100 of its actual value between adjacent web members to account for possible inelastic action within these short links.

(iv) the centroid of the transformed area of the concrete cover slab and the steel top chord was first established. With the web members considered to extend to this level the joint eccentricities on the top chord are considerably reduced compared to the model of Figure 3.2.

None of these modifications proved fruitful. If the postulated decreased web member stiffness and the increased web member stiffness at the end existed, they appear to have counteracted each other. Inelastic action of the bottom chord in the short links between adjacent web members apparently did not occur. The action of the concrete cover slab and the steel top chord with shear connectors was apparently better modelled with these elements considered separately rather than to attempt to lump them together. Therefore, the original model with rigidly connected prismatic members extending from node to node and with modelling of both the connection and joint eccentricities as discussed previously was used.

The axial forces determined from the detailed frame analysis are given in Table 3.1 for the three web members of truss 1 that were analyzed and in Table 3.2 for the five web members of truss 2. The axial forces from the detailed analysis vary from 0.940 to 1.011 of those obtained from the simplified pin-jointed analysis. The mean ratio is 0.976 with a coefficient of variation of 0.019. The close correspondence between the detailed analysis, taking into account the actual physical conditions, and the pin-jointed analysis, substantiates the validity of the approach of positioning the web members such that their lines of action intersect at the mid-depth of the cover slab. It is also noted that the maximum differences between the two analyses occur for the more lightly loaded web

members and that for the highly loaded end compression diagonals, members W2 and W15 in the two trusses, the mean value of the axial load for the two analyses is 0.971 with a coefficient of variation of 0.010.

Of the three structural analysis performed of the trusses, the detailed analysis modelling all the members of the truss including the studs, and taking into account the joint eccentricities and the connection eccentricity moments is considered to be the most valid. Physical realities of the truss are modelled. This analysis is therefore used in subsequent comparisons with the strain analyses.

3.3 Strain analyses

3.3.1 Regression analyses

Regression analyses are appropriate when the number of data available is greater than the minimum required to define all the unknowns. A multiple regression analysis using a least square fit applies when there is more than one independent variable. Considering that the welded connection of the angle web members to relatively rigid chord members prevented any substantial twisting of the angle sections and, moreover, that the warping constant for an angle is approximately zero and, therefore, that warping normal stresses are very small, it is deemed satisfactory to consider that the normal strains as measured by strain gauges, arise solely from the axial forces and bending moments.

3.3.2 Planar analysis

In the first multiple regression analysis, the "Planar analysis", the strain data obtained from the six strain gauges at a given level of a member were analyzed to determine the axial forces at that level. This was done by simply finding the best fit plane to the strain data based on the assumption that plane sections remain plane after bending. The axial force is then determined by integrating the strains multiplied by the measured modulus of elasticity over the cross-section. Tables 3.3 and 3.4 for the web members of trusses 1 and 2 respectively, give the axial forces at the three gauge levels and their average for a number of load steps for each gauged web member. It is seen from the tables that the ratio of the maximum axial load to the minimum does not exceed about 1.106. This ratio with a mean value of 1.037 with a coefficient of variation of 0.029 is indicative of the relative reliability of the strain gauges.

3.3.3 Overall multiple regression analyses

Based on the assumption that the warping strains are negligible, equations can be written for the strain at any location on a cross-section in terms of the axial load and the bending moments about the two principal axes. With six strain gauges at each of the three levels there are eighteen strain equations available to establish the seven unknowns consisting of the axial load and the two moments about the principal axes at each level. The multiple regression analysis is performed on eighteen equations with seven unknowns and eleven degrees of freedom.

Multiple regression analyses were performed for each of five load steps for truss members W11, W14 and W15 of truss 1 and W2, W4, W13, W14 and W15 of truss 2. The coefficients of determination, R^2, for these forty analyses ranged from 0.9891 to 0.9998 with a mean value of 0.9979 indicative of very good statistical correlation. (Mendenhall and Sincich 1988)

The axial forces determined from the overall multiple regression analysis are given in Tables 3.3 and 3.4 for composite truss 1 and composite truss 2 respectively together with the results of the detailed structural analysis and planar analysis. With the exception of web member 2 of truss 2 where differences between the mean axial force from planar analysis and the overall multiple regression analysis of up to 2.5% exist, (load step 20), the two strain analyses are generally within 0.4%.

Excluding one outlier as determined using Chauvenet's criterion (Kennedy and Neville 1980),(web member W11 of truss 1 load step 3 for which the strains were only about 150$\mu\varepsilon$ on the average) the ratio of the axial force determined by the overall multiple regression analysis divided by that determined by the detailed structural analysis, given in Tables 3.3 and 3.4 ranges from 0.951 to 1.190 with a mean value of 1.050 and a coefficient of variation of 0.058. This ratio can also be called the test-to-predicted ratio as the multiple regression analysis has an experimental basis in the strain readings while the structural analysis predicts the axial force in the members from the known loads and geometry. On the average therefore the two analyses agree within 5%. This is considered to be very good as all the analytical assumptions and experimental errors are

encompassed in these statistical figures. To reiterate, the analytical assumptions are that:

(i) the members are prismatic extending from node to node,

(ii) the shear connectors are modelled as discussed previously,

(iii) the full width and thickness of the cover slab is considered effective,

(iv) connection eccentricities are incorporated based on the eccentricity of the weld group with respect to the axis of the web member,

(v) joint eccentricities are included.

Experimental errors affecting one or another of the analyses may include errors in:

(i) load cell readings,

(ii) strain gauge readings,

(iii) co-ordinate geometry of the truss,

(iv) strain gauge locations on the cross-section and along the length of a member, and

(v) the modulus of elasticity.

3.4 Moments, deflections and eccentricities

3.4.1 About principal axes

The web members are obviously subjected to both in-plane and out-of-plane end eccentricities giving rise to moments about the principal axes as were determined from the overall multiple regression analyses. Consider the member shown in Figure 3.3 subjected to an axial force P with end eccentricities parallel to a

principal (v) axis of e_b at the bottom end and e_t at the top end resulting in end moments M_b and M_t respectively. The equation for the deflected shape as a function of the distance z along the member (Roark 1943) is

$$[3.3] \qquad v = \frac{1}{P}\left[M_b + (M_t - M_b)\frac{z}{L} - (M_t - M_b\cos u)\frac{\sin\frac{z}{j}}{\sin u} - M_b\cos\frac{z}{j}\right]$$

$$[3.3a] \qquad v = \left[e_b + (e_t - e_b)\frac{z}{L} - (e_t - e_b\cos u)\frac{\sin\frac{z}{j}}{\sin u} - e_b\cos\frac{z}{j}\right]$$

where

P = axial compressive force

M_b = moment at bottom end

M_t = moment at top end

e_b = eccentricity at bottom end

e_t = eccentricity at top end

$j = \sqrt{\frac{EI}{P}}$

EI = the flexural stiffness about the axis of bending

$u = \frac{L}{j}$

Thus at a distance z from the bottom end the moment is

$$[3.4] \qquad M_u = P(e + v) = P\left[\left(\frac{(L-z)}{L}\right)e_b + \frac{z}{L}e_t + v\right]$$

or

$$[3.4a] \qquad e_v = (e + v) = \left[\frac{(L-z)}{L}e_b + \frac{z}{L}e_t + v\right]$$

and substituting v from [3.3a] gives

$$[3.4b] \qquad e_v = \left[(e_t - e_b \cos u)\frac{\sin\frac{z}{j}}{\sin u} + e_b \cos\frac{z}{j} \right]$$

Thus, having determined the moments and hence eccentricities about both principal axes at three locations along the length of the member, three simultaneous equations can be written in terms of the two unknown end eccentricities e_b and e_t. With these end eccentricities determined by the regression analysis the deflected shape is established from [3.3a] and, of course, if the coefficient of determination, R^2, were equal to 1, would pass through the three points determined from the multiple regression analysis.

Figures 3.4 to 3.35 show the deflected shape and eccentricities with respect to the u and v axis for two load steps for the eight web members of trusses 1 and 2 that were instrumented. The deflected shape determined for the member with an axial force and end moments equal to the axial force multiplied by the end eccentricities is drawn with respect to the zero reference line. The thrust line joins the calculated bottom and top eccentricities. The eccentricities, determined from the multiple regression analysis are measured from the thrust line. These test eccentricities lie close to the deflected shape.

3.4.2 About x and y axes.

For the orientation of axes used as shown in Figure 3.36, the moments and eccentricities about the x and y axes can be determined from those computed for the principal axes as:

[3.5a] $M_x = (M_u - M_v)\cos 45^0$

[3.5b] $M_y = (M_u + M_v)\sin 45^0$

and

[3.6a] $e_y = (e_u + e_v)\sin 45^0$

[3.6b] $e_x = (e_u - e_v)\cos 45^0$

where the eccentricities are simply equal to the moment divided by the axial force.

The moments, M_x, and eccentricities, e_y, are out-of-plane moments and eccentricities respectively, while the moments, M_y, and eccentricities, e_x, are the in-plane moments and eccentricities respectively.

3.4.2.1 Out-of-plane eccentricities

Out-of-plane eccentricities were calculated for five load steps for each of the eight web members gauged from [3.6a]. Sixteen of these 40 eccentricities are plotted in Figures 3.37 to 3.52. On each figure is also plotted the deflected shape in the y direction and as well the eccentricities in this direction, measured from the thrust line, for the three strain gauge levels. Both the deflected shape ordinates and the eccentricities have been computed from an equation paralleling [3.6a]. The three points representing the eccentricities lie close to the deflected shape.

For all the compression members, with the exception of web member W11T1, the out-of-plane end eccentricities at both the top and bottom ends are negative. The negative values result from the fact that the connections between the chord and the web members

lie in the negative y direction as shown in Figure 3.36. The anomaly of a positive end eccentricity at the top end of web member 11 has not been resolved. The compression members all show positive y direction deflections as would be expected with negative end eccentricities as shown in the appropriate figures in the range from Figures 3.37 to 3.52. The tension web member W14 of the two trusses, as shown in Figures 3.39, 3.40, 3.49 and 3.50 all have relatively small end eccentricities that in general are positive as would be expected. The action of the eccentric tensile force is to reduce the eccentricities along the length of the member.

The end eccentricities calculated from [3.6a] can be normalized by dividing by the centroidal distance from the back of the angle. These normalized end eccentricities for the bottom and top end are given in Tables 3.5 and 3.6. The mean value of the normalized end eccentricities at the bottom and top ends for the compression members for the two trusses are 0.43 and 0.23 with corresponding coefficients of variations of 0.123 and 0.480 respectively. (The end eccentricity at the top end of web member W11 whose behaviour was anomalous as discussed previously is not included in the statistical analysis). These normalized end eccentricities indicate that couple moments are developed in the end connection effectively reducing the end moment Py as shown in Figure 3.53. The couple moments consist of a compressive force between the angles and the chords near the extreme ends of the angle and a tensile force developed in the welds further away from the ends of the angles. This phenomenon is further illustrated schematically in Figure 3.54 where the extreme ends of the web members push the side walls of

the HSS chords inward. The resulting end moments acting on the web member are therefore

[3.7a] $M_b = Py - M_{cb}$

[3.7b] $M_t = Py - M_{ct}$

That the reduction in the end moment is greater at the top end than at the bottom is attributed to the relatively greater flexural stiffness of the side wall of the HSS at the top end where the depth of the section is 76 mm and the wall thickness is 6.4 mm as compared to the depth of the section of 127 mm and a wall thickness of 4.8 mm at the bottom end. This phenomenon is illustrated schematically in Figure 3.54.

It is also noted that the end eccentricity at the bottom end of the tension web members W14 is much less than the compression members at the same location. This could be attributed to the relative flexible side wall allowing the tension member to draw in and reduce the end eccentricity. At the top end with a stiffer side wall this does not occur to such an extent.

It is concluded therefore that the moments developed in the end connection reduce markedly the end eccentricity of the axial load. The effective end eccentricity is only about 1/5 to 2/5 of the centroidal distance and decreases as the stiffness of the member to which the web member is connected increases. It is anticipated for example for web members welded to opposite sides of the stem of a T-shaped chord that the effective end eccentricity would be less than 1/5 of the centroidal distance and could in fact approach zero. For

angle web members connected to HSS chords a reasonable estimate of the effective end eccentricity is 1/3 of the centroidal distance of the angle.

3.4.2.2 In-plane eccentricities

In-plane eccentricities were calculated for five load steps for each of the eight web members gauged from [3.6b]. Sixteen of these 40 results are plotted in Figures 3.55 to 3.70. On each figure is also plotted the deflected shape in the x direction together with the eccentricities in the x direction for the three strain gauge levels measured from the thrust line. Both the deflected shape ordinates and the eccentricities have been computed from an equation paralleling [3.6b]. Not unexpectedly, the plotted eccentricities lie close to the deflected shape.

With the exception of member W4T2 all the web members are bent in double curvature. Member W4T2 has a relatively small eccentricity at its lower end as shown in Figures 3.63 and 3.64 while its mirror image W13T2 (see Figures 3.65 and 3.66) has a small eccentricity but of the opposite sign as compared to W4T2. Member W13T2 is therefore bent in double curvature. Other things being equal, the differences in eccentricities at the bottom end of members 4 and 13 are indicative of the degree of precision of the end eccentricities determined from the multiple regression analysis. For example, at load step 6 the difference between the eccentricities at the bottom end of the two members is only about 1.5mm.

It is considered that the end eccentricities arise from a combination of the joint eccentricities when the centroidal

longitudinal axes of the members at a joint do not intersect at a common point and connection eccentricities when the centroid of the connecting weldments do not coincide with the centroidal axis of the member together with eccentricities due to secondary moments that develop at the fixed joints when the truss deforms.

The end eccentricities as determined from the detailed frame analysis given in section 3.2.3 and the thrust line joining them are plotted on Figures 3.55 to 3.70 as dash-dot lines. The detailed frame analysis certainly displays the same behaviour and trends as the overall multiple regression analysis and can be said to be in reasonable agreement with it. As discussed in section 3.3.3 all the analytical assumptions and experimental errors listed there can contribute to differences between the results of the experimental and the purely analytical approach. Two methods of assessing the compatibility of the experimental and theoretical results follow, keeping in mind that the in-plane eccentricities examined are relatively small.

Tables 3.7 and 3.8 give the ratios of the in-plane end eccentricities determined from the overall multiple regression analysis, the test values, divided by those determined from the detailed frame analysis, the predicted values, for the bottom and top ends, for each of the five load steps for the eight web members that were strain gauged.

When Chauvenet's criterion is applied to the bottom end eccentricity ratios and when the five observations for a web member are treated as a block, those for W11T1 become outliers. The resulting mean value of the bottom end eccentricity ratio is 0.610

with a coefficient of variation of 0.670. Although not justified by Chauvenet's criterion, the behaviour of the bottom end of web members W4T2 and W13T2 as discussed previously is somewhat peculiar. Excluding these observation from the set, results in a mean value of the bottom end eccentricity ratio of 0.846 with a standard deviation of 0.173 and a coefficient of variation of 0.204.

At the top end, applying Chauvenet's criterion to the block of results for a web member again results in the exclusion of those for web member W11T1 as outliers. The mean value of the remainder of the results is 1.164 with a standard deviation of 0.177 and a coefficient of variation of 0.152. It is concluded, therefore, that the test eccentricities determined from the multiple regression analysis of the strain gauge readings are in reasonable agreement with those based on the detailed frame analysis.

The second method of assessing the degree of agreement between the experimental and theoretical results is simply to determine the absolute value of the differences between the test eccentricities and the predicted eccentricities. These are given in Tables 3.7 and 3.8. The mean difference at both the bottom and top ends is about 2mm as given in the tables when the top end of member W11T1 and the bottom ends of members W4T2 and W13T2 are excluded. This is indicative of reasonable agreement between the experimental and theoretical results. Differences in extreme cases for the aforementioned members range up to 7mm. These sets of observations for members W11T1, W4T2 and W13T2 all lie close to being classified as outliers based on Chauvenet's criterion. It is

therefore concluded that the test and predicted eccentricities are in reasonable agreement.

Table 3.1 Axial forces in web members of composite truss 1 from three structural analyses

			Structural analysis		
Web member	Load step	Applied load/Jack kN	Truss analysis kN	Frame analysis kN	Detailed analysis kN
W11	3	16.14	-10.84	-10.57	-10.19
	5	31.79	-21.49	-20.96	-20.55
	6	40.02	-27.13	-26.45	-25.51
	8	55.54	-37.81	-36.87	-35.56
	10	71.47	-48.84	-47.62	-45.93
W14	3	16.14	10.84	10.71	10.68
	5	31.79	21.49	21.23	21.55
	6	40.02	27.13	26.79	26.73
	8	55.54	37.81	37.34	37.26
	10	71.47	48.84	48.23	48.12
W15	4	24.58	-33.54	-33.05	-32.67
	6	40.02	-54.59	-53.80	-55.18
	8	55.54	-75.83	-74.74	-73.87
	10	71.47	-97.66	-96.26	-95.14
	11	80.04	-109.42	-107.85	-106.59

Table 3.2 Axial forces in web members of composite truss 2 from three structural analyses

			Structural analysis		
Web member	Load step	Applied load/Jack kN	Truss analysis kN	Frame analysis kN	Detailed analysis kN
W2	6	24.68	-33.62	-33.17	-32.59
	10	40.39	-55.08	-54.34	-53.39
	12	47.99	-65.45	-64.57	-63.43
	16	63.08	-85.98	-84.82	-83.33
	20	80.35	-109.51	-108.04	-106.13
W4	6	24.68	-16.72	-16.60	-16.63
	10	40.39	-27.39	-27.18	-27.24
	15	54.78	-37.26	-36.98	-37.06
	23	84.54	-57.51	-57.08	-57.19
	33	92.60	-63.09	-62.62	-62.75
W13	6	24.68	-16.86	-16.73	-16.82
	10	40.39	-27.62	-27.41	-27.56
	15	54.78	-37.58	-37.30	-37.49
	23	84.54	-58.22	-57.77	-58.07
	33	92.60	-63.88	-63.39	-63.72
W14	6	24.68	16.86	16.64	16.27
	10	40.39	27.62	27.26	26.66
	15	54.78	37.58	37.09	36.27
	23	84.54	58.22	57.46	56.19
	33	92.60	63.88	63.05	61.65
W15	6	24.68	-33.78	-33.33	-32.66
	10	40.39	-55.23	-54.49	-53.41
	12	47.99	-65.64	-64.76	-63.46
	16	63.08	-86.32	-85.16	-83.46
	20	80.35	-109.95	-108.48	-106.31

Table 3.3 Axial forces in web members of composite truss 1

Web member	Load step	Detailed structural analysis	Planar analysis						Overall multiple regression analysis kN	M.R.A. Detailed analysis
			Gauge locations							
			Top kN	Middle kN	Bottom kN	Mean kN	Extreme / Mean	Max / Min		
W11	3	-10.19	-14.16	-13.86	-13.92	-13.98	0.991 - 1.013	1.022	-14.00	1.318*
	5	-20.55	-24.27	-24.04	-24.16	-24.16	0.995 - 1.005	1.010	-24.19	1.154
	6	-25.51	-29.45	-29.11	-29.19	-29.25	0.995 - 1.007	1.012	-29.29	1.107
	8	-35.56	-39.11	-38.59	-38.70	-38.80	0.995 - 1.008	1.013	-38.85	1.053
	10	-45.93	-48.45	-47.59	-47.90	-47.98	0.992 - 1.010	1.018	-47.96	1.007
W14	3	10.68	12.74	12.70	12.63	12.69	0.995 - 1.004	1.009	12.70	1.190
	5	21.55	24.60	24.38	24.23	24.40	0.993 - 1.008	1.015	24.42	1.154
	6	26.73	30.88	30.51	30.00	30.46	0.985 - 1.014	1.017	30.49	1.142
	8	37.26	42.48	41.82	41.46	41.92	0.989 - 1.013	1.025	41.95	1.123
	10	48.12	53.93	53.54	53.18	53.55	0.993 - 1.007	1.014	53.57	1.119
W15	4	-32.67	-34.65	-33.60	-33.45	-33.90	0.987 - 1.022	1.036	-33.87	1.025
	6	-55.18	-56.29	-54.04	-53.22	-54.52	0.976 - 1.032	1.058	-54.49	1.013
	8	-73.87	-77.65	-74.28	-73.71	-75.21	0.980 - 1.032	1.053	-75.20	1.006
	10	-95.14	-99.85	-94.84	-99.10	-97.93	0.968 - 1.020	1.053	-97.91	1.017
	11	-106.59	-111.36	-108.72	-101.93	-107.34	0.950 - 1.037	1.093	-107.36	0.996

Note: * rejected as outlier

Table 3.4 Axial forces in web members of composite truss 2

Web member	Load step	Detailed structural analysis	Planar analysis						Overall multiple regression analysis kN	M.R.A Detailed analysis
			Gauge locations							
			Top kN	Middle kN	Bottom kN	Mean kN	Extreme Mean	Max Min		
W2	6	-32.59	-35.20	-33.90	-33.80	-34.30	0.985 - 1.026	1.041	-33.94	1.041
	10	-53.39	-58.90	-55.23	-54.76	-56.30	0.973 - 1.046	1.075	-55.17	1.033
	12	-63.43	-68.93	-65.40	-64.65	-66.33	0.975 - 1.039	1.066	-65.29	1.029
	16	-83.33	-91.15	-85.20	-84.10	-86.82	0.969 - 1.050	1.084	-85.05	1.021
	20	-106.13	-116.95	-107.27	-105.72	-109.98	0.961 - 1.063	1.106	-107.27	1.011
W4	6	-16.63	-17.88	-17.79	-17.88	-17.85	0.997 - 1.002	1.005	-17.86	1.074
	10	-27.24	-28.61	-28.57	-28.51	-28.56	0.998 - 1.002	1.004	-28.60	1.050
	15	-37.06	-38.63	-38.50	-38.37	-38.50	0.997 - 1.003	1.007	-38.55	1.040
	23	-57.19	-58.88	-58.18	-58.31	-58.46	0.997 - 1.007	1.010	-58.48	1.023
	33	-62.75	-64.02	-63.08	-62.90	-63.33	0.993 - 1.011	1.018	-63.42	1.011
W13	6	-16.82	-16.81	-17.84	-17.19	-17.28	0.973 - 1.032	1.061	-17.33	1.030
	10	-27.56	-26.02	-28.46	-27.57	-27.35	0.951 - 1.041	1.094	-27.47	0.997
	15	-37.49	-35.10	-37.86	-36.55	-36.50	0.962 - 1.037	1.080	-36.64	0.977
	23	-58.07	-53.36	-57.57	-55.83	-55.59	0.960 - 1.036	1.080	-55.81	0.961
	33	-63.72	-58.02	-62.48	-60.61	-60.37	0.961 - 1.035	1.077	-60.62	0.951

Table 3.4 (cont'd) Axial forces in web members of composite truss 2

Web member	Load step	Detailed structural analysis	Planar analysis						Overall multiple regression analysis kN	M.R.A Detailed analysis
			Gauge locations							
			Top kN	Middle kN	Bottom kN	Mean kN	Extreme Mean	Max Min		
W14	6	16.27	19.09	18.88	19.09	19.02	0.993 - 1.004	1.011	19.03	1.170
	10	26.66	30.54	30.24	30.58	30.46	0.993 - 1.004	1.011	30.47	1.143
	15	36.27	40.71	40.28	40.77	40.59	0.992 - 1.004	1.015	40.60	1.119
	23	56.19	60.03	59.44	60.05	59.84	0.993 - 1.004	1.010	59.88	1.066
	33	61.65	65.21	64.57	65.41	65.06	0.992 - 1.005	1.013	65.11	1.056
W15	6	-32.66	-33.51	-33.29	-32.67	-33.16	0.985 - 1.011	1.026	-33.13	1.014
	10	-53.41	-54.92	-54.18	-54.30	-54.13	1.001 - 1.015	1.014	-54.09	1.013
	12	-63.46	-65.19	-64.21	-63.12	-64.17	0.984 - 1.016	1.033	-64.12	1.010
	16	-83.46	-85.30	-83.69	-82.13	-83.71	0.981 - 1.019	1.039	-83.65	1.002
	20	-106.31	-107.91	-105.75	-103.70	-105.79	0.980 - 1.020	1.041	-105.74	0.995
μ								1.037		
V								0.029		

Table 3.5 Normalized out-of-plane eccentricities of web members of composite truss 1

Web member	Load step	Centroidal distance mm	Bottom $\frac{e_b}{y}$	Top $\frac{e_t}{y}$
W11	3	15.06	0.333	-0.232
	5		0.331	-0.155
	6		0.370	-0.164
	8		0.429	-0.178
	10		0.477	-0.204
W14	3	11.94	0.018	0.245
	5		0.033	0.262
	6		0.097	0.296
	8		0.036	0.198
	10		0.131	0.223
W15	4	19.24	0.301	0.295
	6		0.394	0.302
	8		0.458	0.313
	10		0.415	0.357
	11		0.535	0.313

Table 3.6 Normalized out-of-plane eccentricities of web members of composite truss 2

Web member	Load step	Centroidal distance mm	Bottom $\frac{e_b}{y}$	Top $\frac{e_t}{y}$
W2	6	19.24	0.427	0.261
	10		0.389	0.273
	12		0.401	0.280
	16		0.427	0.289
	20		0.450	0.302
W4	6	15.06	0.440	0.116
	10		0.399	0.134
	15		0.433	0.134
	23		0.493	0.150
	33		0.473	0.170
W13	6	15.06	0.442	0.070
	10		0.406	0.063
	15		0.430	0.071
	23		0.504	0.061
	33		0.505	0.072
W14	6	11.94	0.026	0.285
	10		0.007	0.314
	15		0.059	0.263
	23		0.024	0.280
	33		0.039	0.268
W15	6	19.24	0.438	0.304
	10		0.398	0.310
	12		0.483	0.375
	16		0.415	0.331
	20		0.428	0.342
For all values in Tables 3.5 and 3.6		μ	0.430	0.230
		V	0.123	0.480

Table 3.7 Comparison of test-to-predicted in-plane end eccentricities of web members of composite truss 1

Web member	Load step	In-plane eccentricity			
		Test eccentricity / Predicted eccentricity		Difference between test and predicted eccentricity	
		Bottom	Top	Bottom	Top
W11	3	2.30	24.25	2.49	7.05
	5	1.77	15.55	1.45	4.44
	6	1.70	14.30	1.32	4.06
	8	1.75	13.05	1.43	3.68
	10	1.56	12.00	1.05	3.36
W14	3	0.84	0.98	1.05	0.11
	5	0.81	0.98	0.75	0.12
	6	0.99	1.00	0.07	0.02
	8	0.57	1.35	1.63	1.79
	10	0.63	1.38	1.43	1.96
W15	4	0.86	1.14	1.28	1.56
	6	0.80	1.20	1.87	2.27
	8	0.79	1.28	1.95	3.11
	10	0.87	1.37	1.21	4.13
	11	0.78	1.37	0.92	4.11

Table 3.8 Comparison of test-to-predicted in-plane end eccentricities of web members of composite truss 2

Web member	Load step	In-plane eccentricity			
		Test eccentricity / Predicted eccentricity		Difference between test and predicted eccentricity	
		Bottom	Top	Bottom	Top
W2	6	0.75	1.07	2.14	0.87
	10	0.76	1.09	2.01	1.05
	12	0.78	1.14	1.83	1.61
	16	0.81	1.22	1.56	2.48
	20	0.83	1.29	1.40	3.24
W4	6	-0.14	0.95	5.17	0.27
	10	-0.05	1.01	4.76	0.01
	15	-0.07	1.10	4.84	0.35
	23	-0.16	1.36	5.27	1.38
	33	-0.06	1.49	4.78	1.92
W13	6	0.15	0.92	4.90	0.41
	10	0.15	0.82	4.94	0.91
	15	0.21	0.98	4.59	0.13
	23	0.06	1.06	5.45	0.23
	33	0.11	1.16	5.14	0.73
W14	6	0.82	0.95	0.77	0.25
	10	0.93	0.92	0.32	0.42
	15	0.71	1.19	1.20	1.03
	23	0.65	1.18	1.46	0.98
	33	0.61	1.14	1.60	0.77
W15	6	0.95	1.19	0.29	1.88
	10	1.00	1.20	0.02	1.99
	12	1.24	1.49	1.20	4.70
	16	1.14	1.36	0.72	3.44
	20	1.22	1.42	0.29	4.00
μ		0.846	1.164		
V		0.204	0.152		

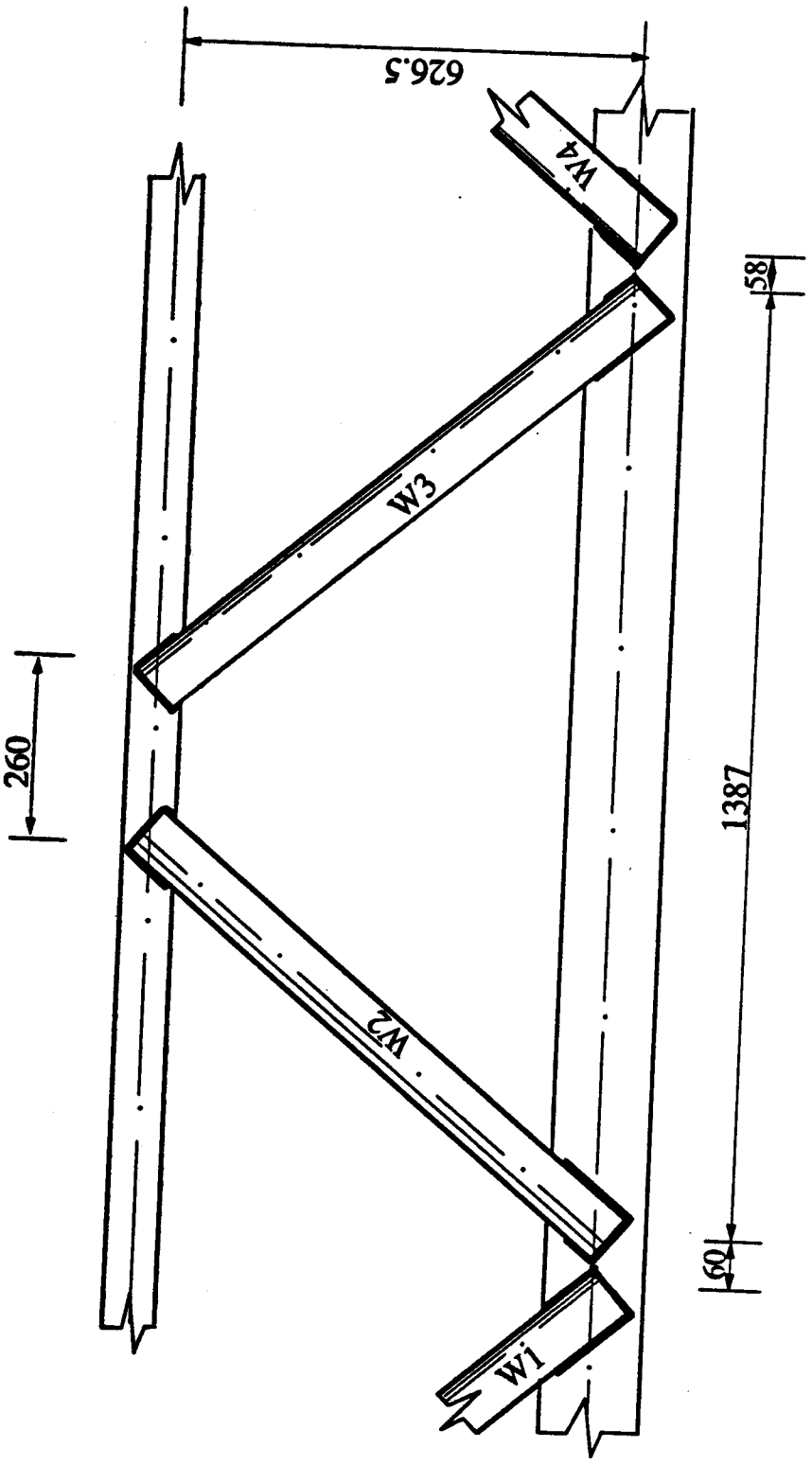

Figure 3.1 Joint eccentricities and placement of fillet welds

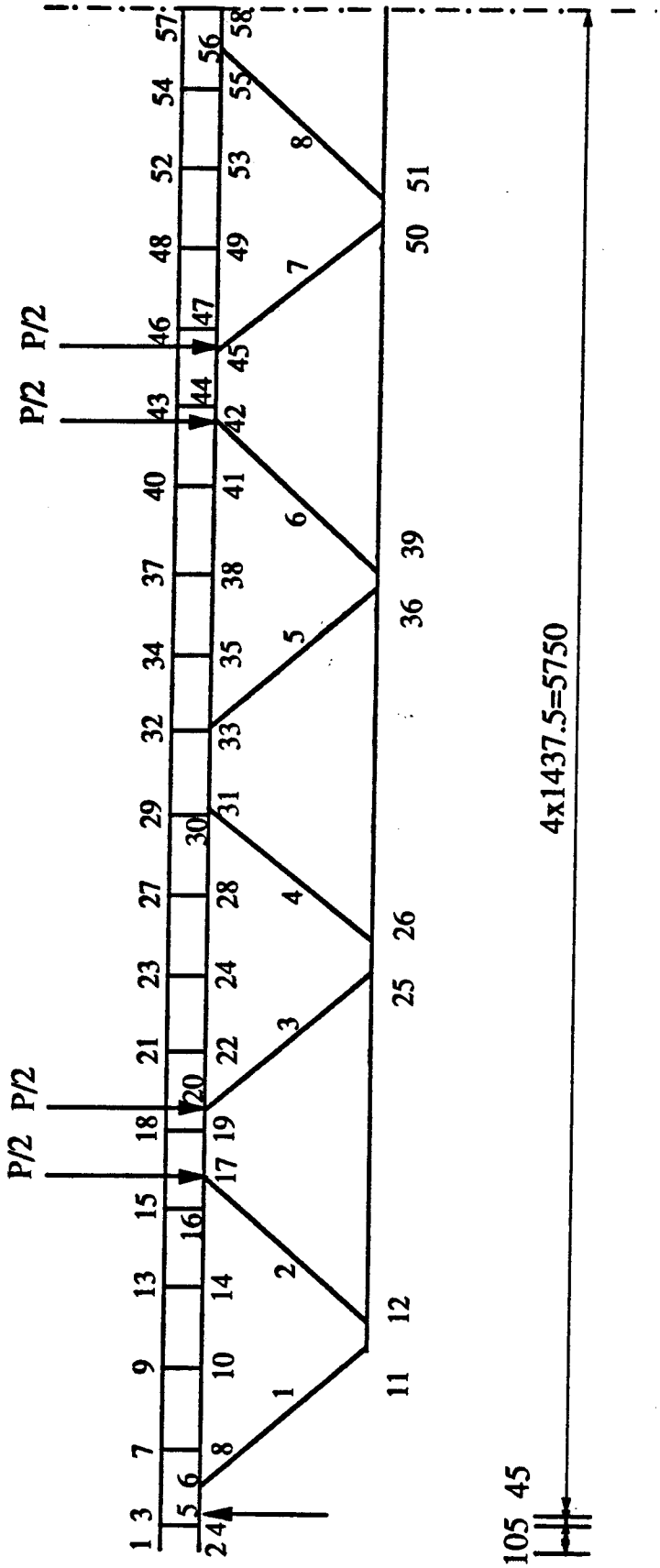

Figure 3.2 Detail of half a composite truss model

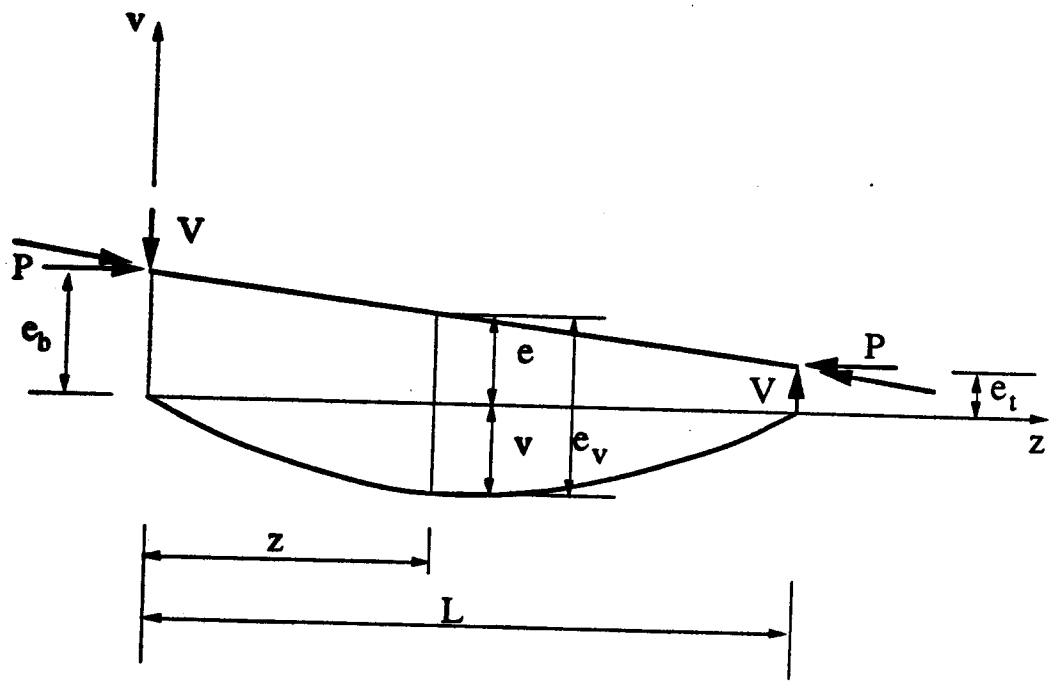

Figure 3.3 Diagram of member loaded with end eccentricity moments and axial force

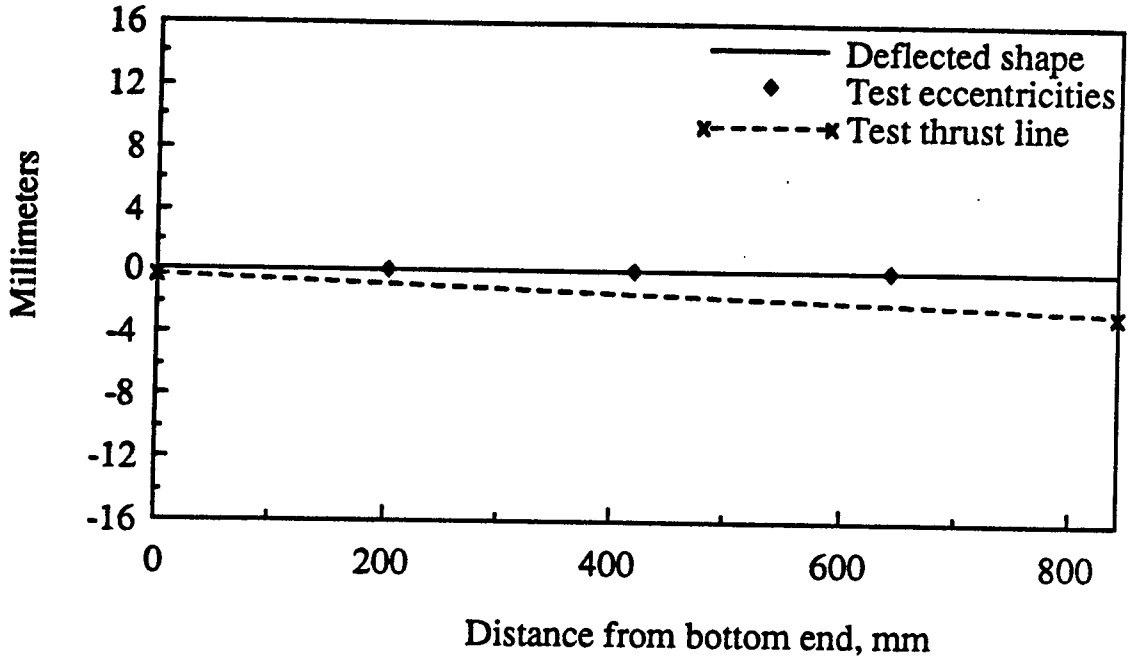

Figure 3.4 Deflected shape and eccentricities, u, member W11T1 - Load step 3

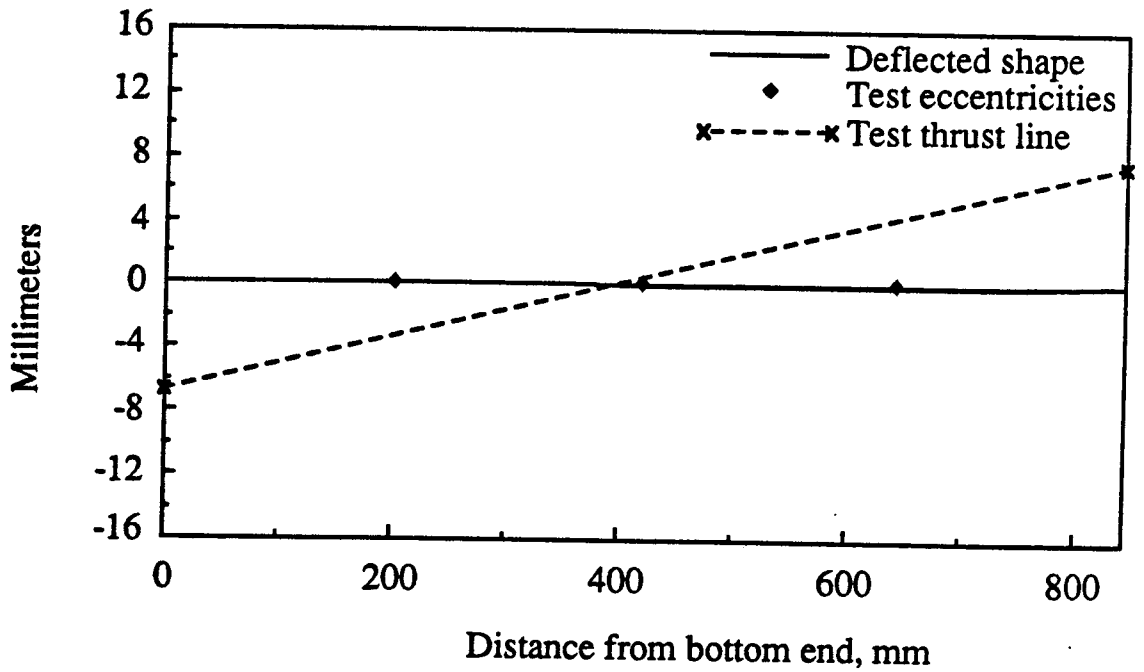

Figure 3.5 Deflected shape and eccentricities, v, member W11T1 - Load step 3

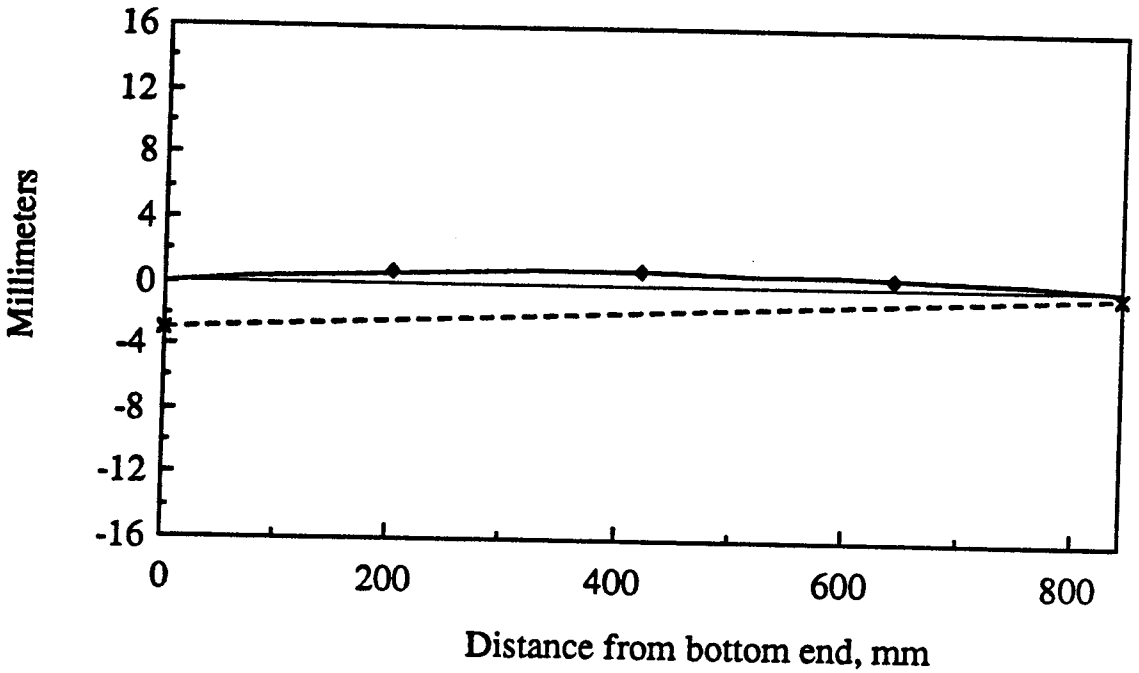

Figure 3.6 Deflected shape and eccentricities, u,
member W11T1 - Load step 10

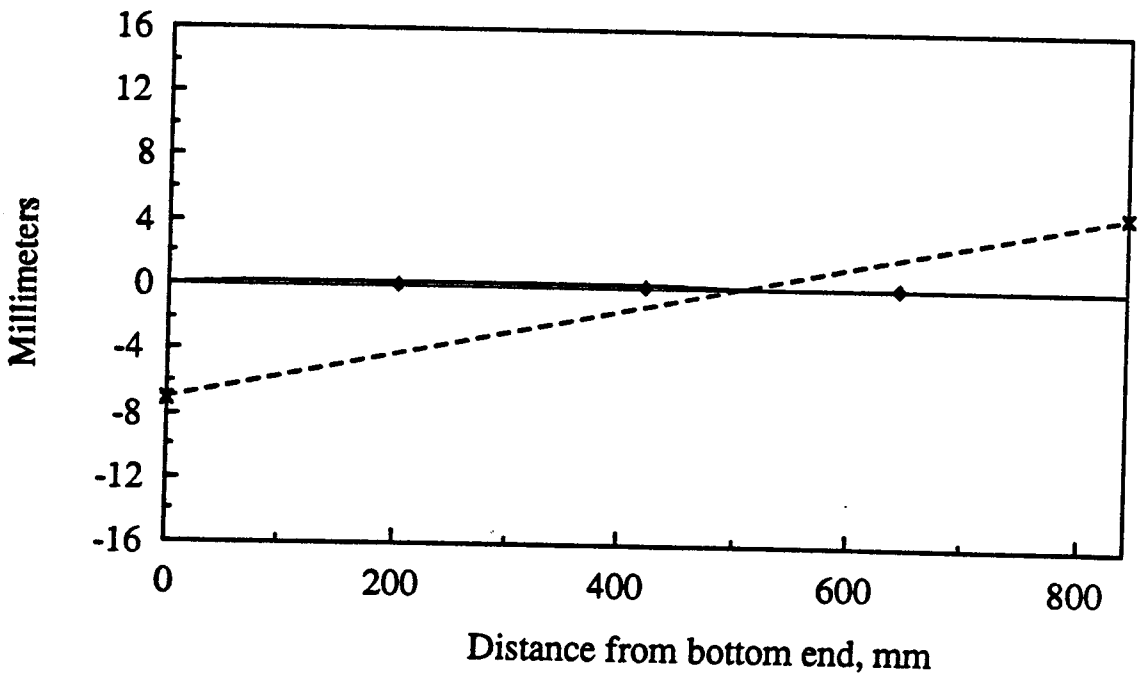

Figure 3.7 Deflected shape and eccentricities, v,
member W11T1 - Load step 10

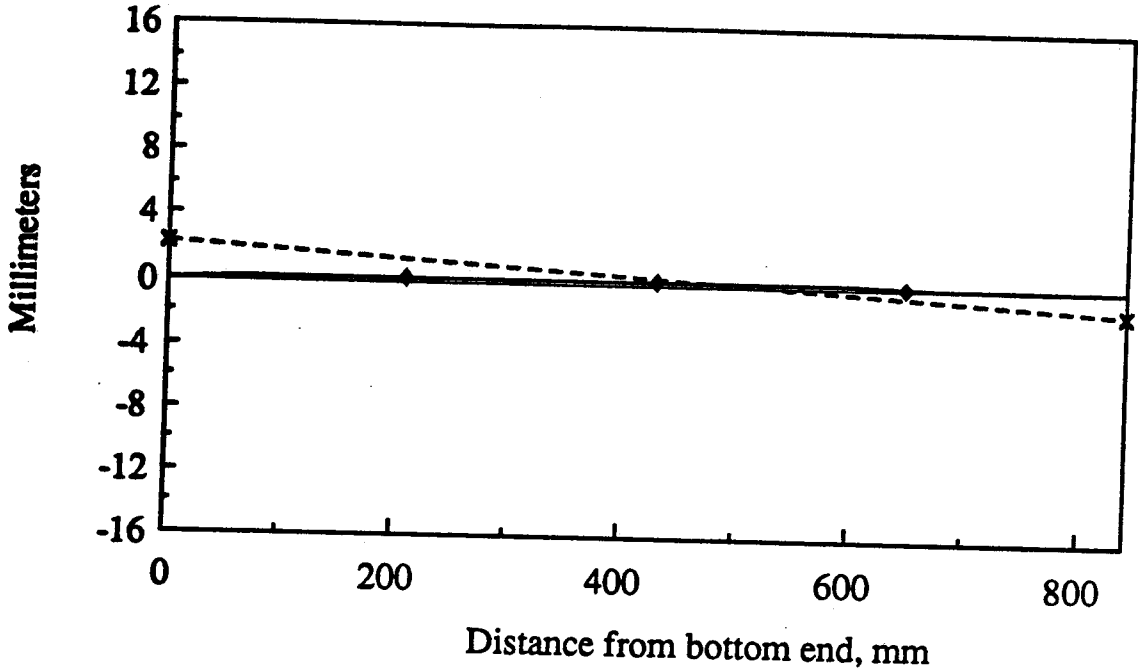

Figure 3.8 Deflected shape and eccentricities, u, member W14T1 - Load step 3

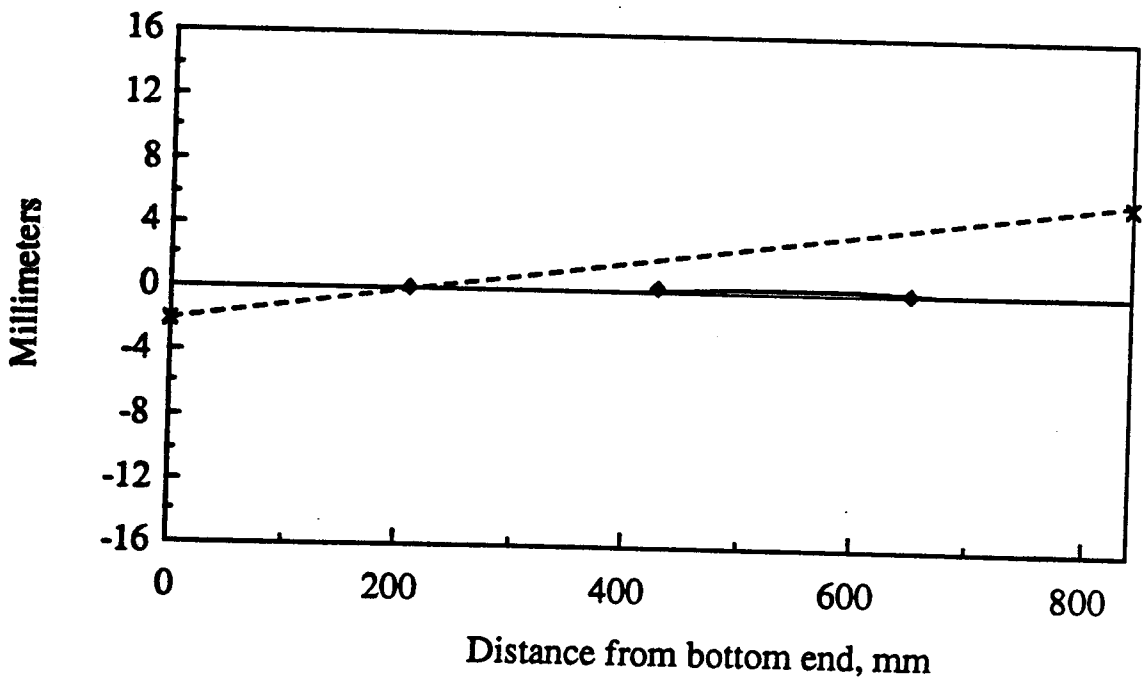

Figure 3.9 Deflected shape and eccentricities, v, member W14T1 - Load step 3

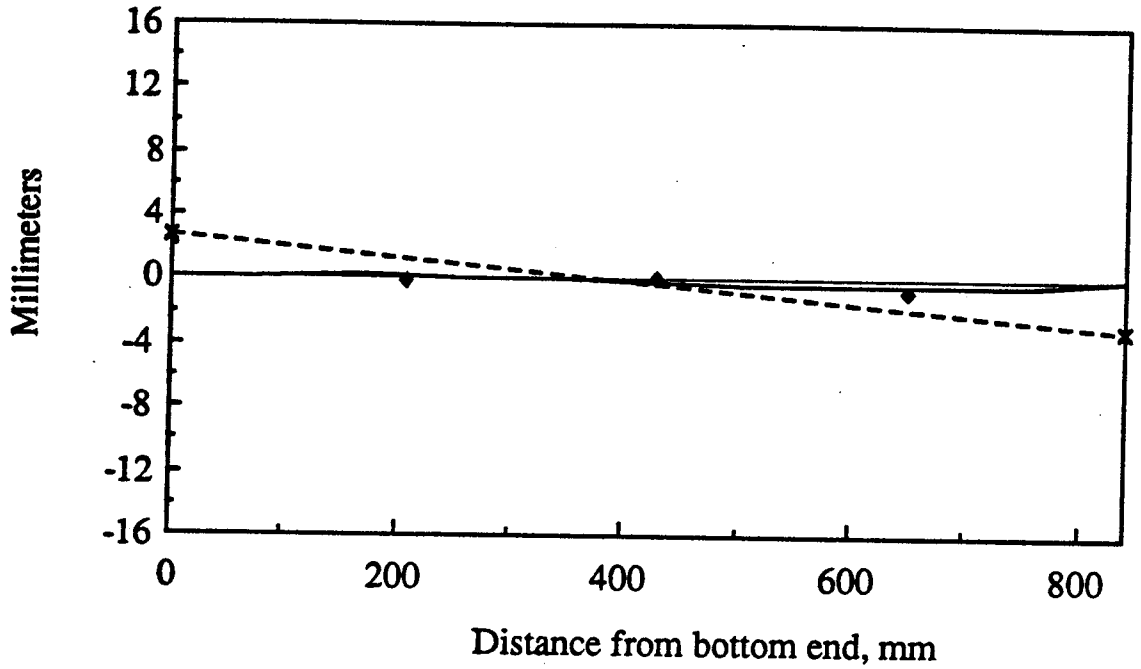

Figure 3.10 Deflected shape and eccentricities, u,
member W14T1 - Load step 10

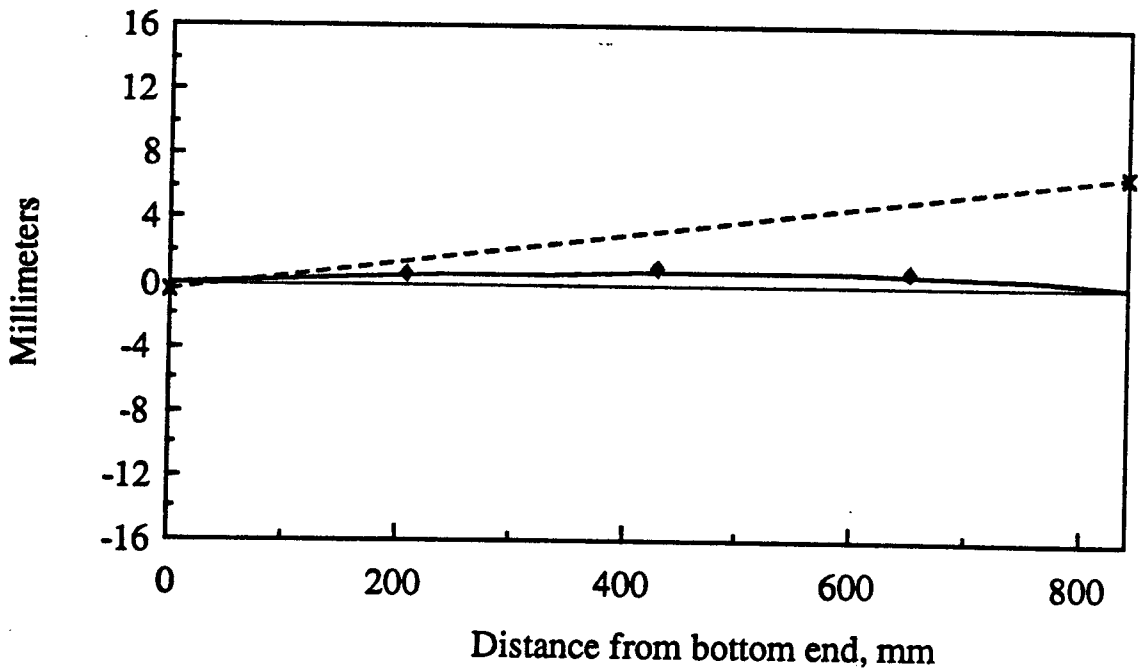

Figure 3.11 Deflected shape and eccentricities, v,
member W14T1 - Load step 10

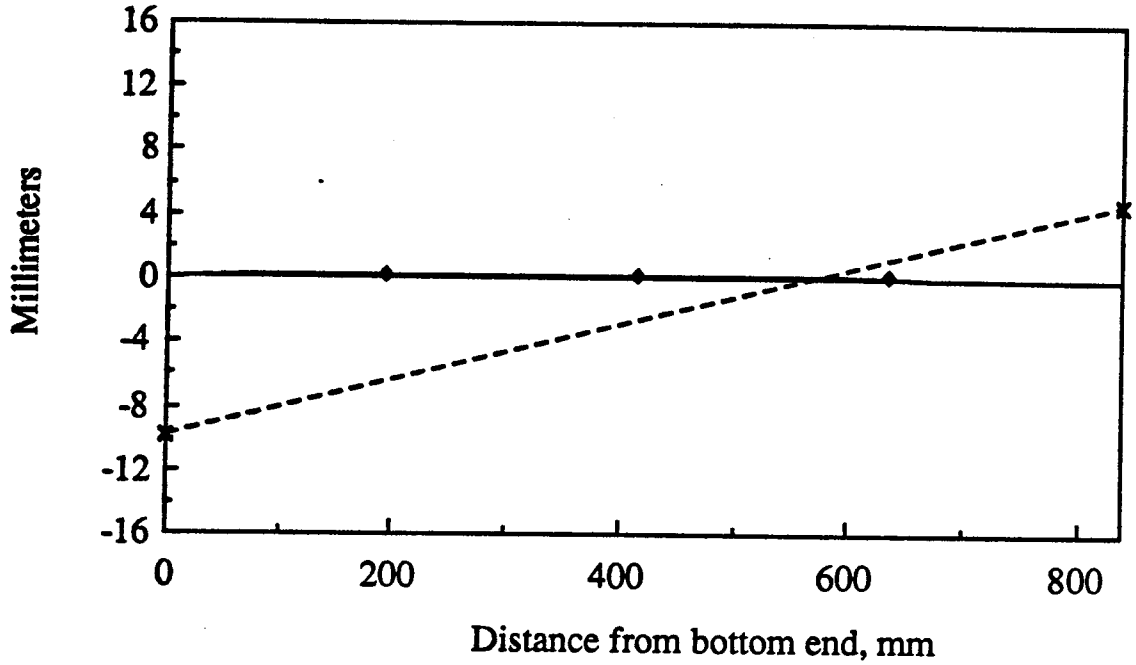

Figure 3.12 Deflected shape and eccentricities, u, member W15T1 - Load step 4

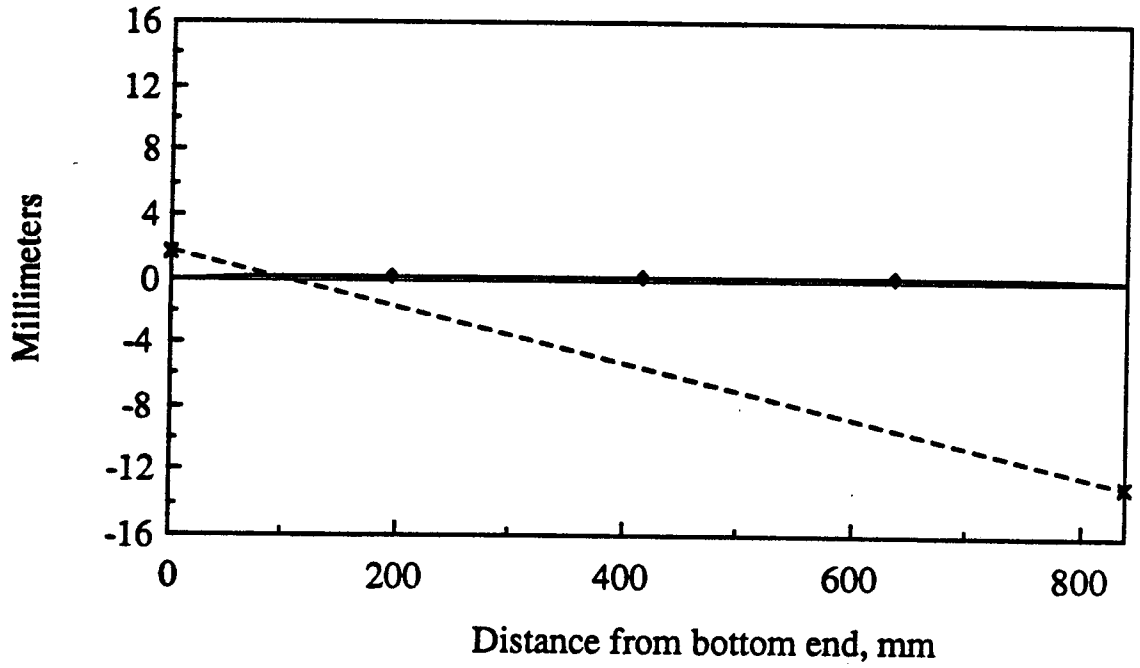

Figure 3.13 Deflected shape and eccentricities, v, member W15T1 - Load step 4

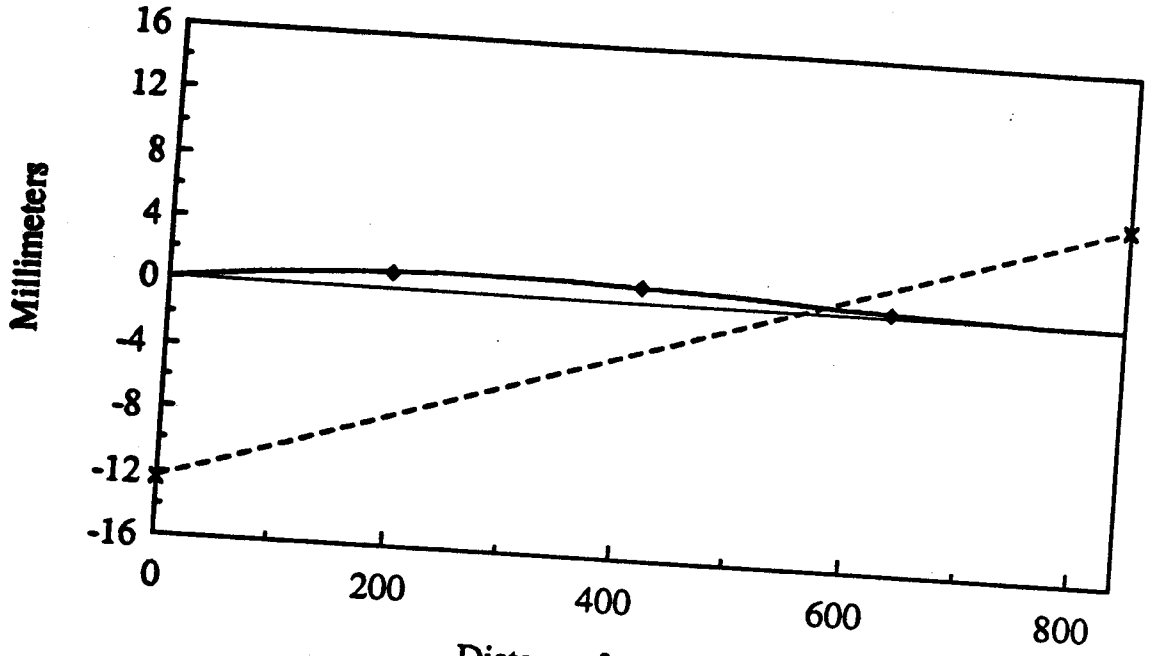

Figure 3.14 Deflected shape and eccentricities, u, member W15T1 - Load step 11

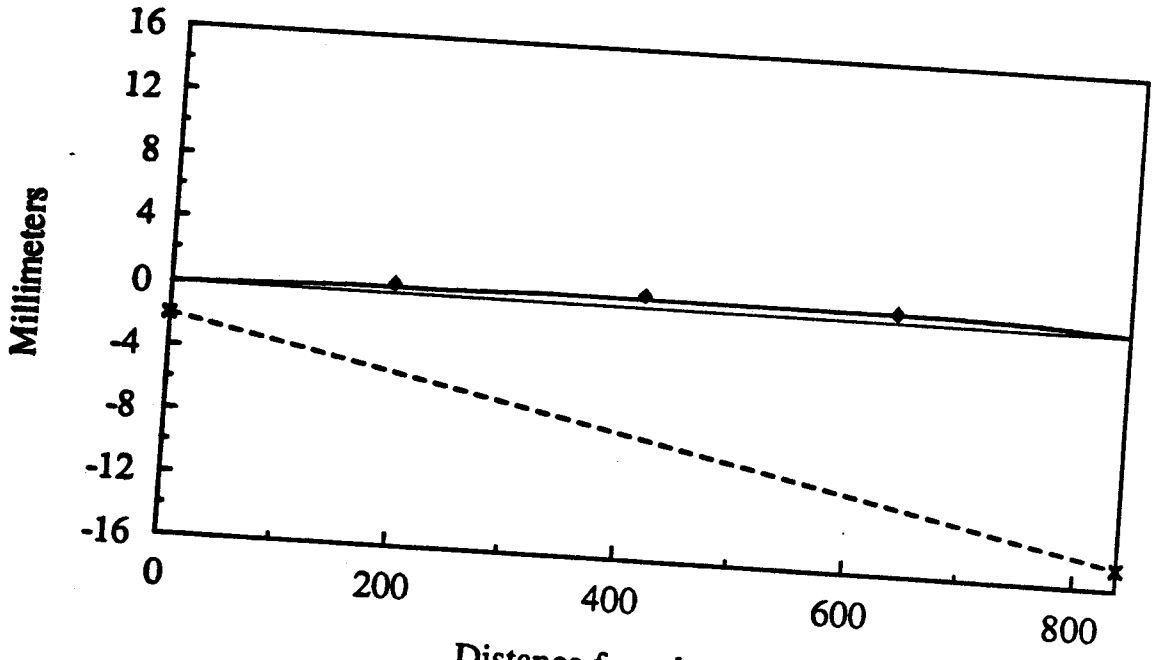

Figure 3.15 Deflected shape and eccentricities, v, member W15T1 - Load step 11

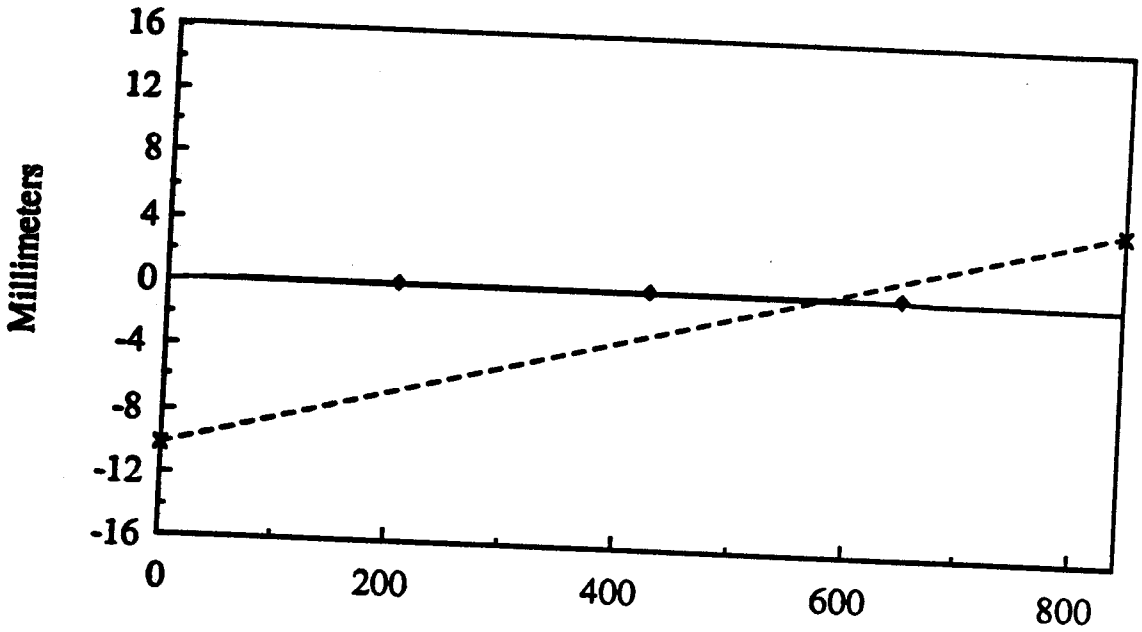

Figure 3.16 Deflected shape and eccentricities, u, member W2T2 - Load step 6

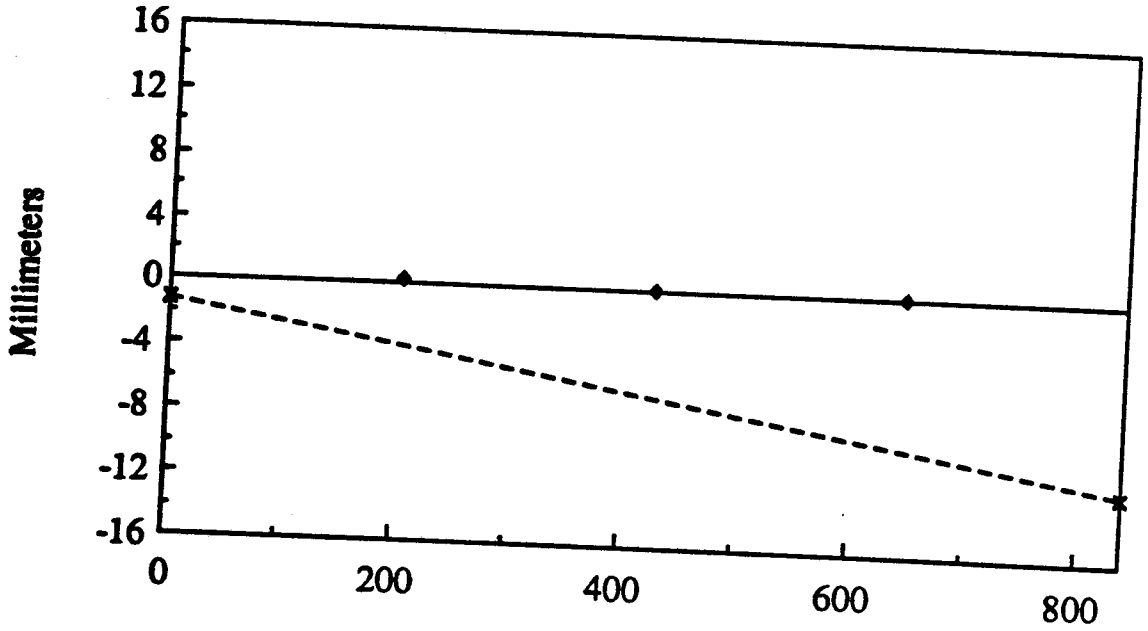

Figure 3.17 Deflected shape and eccentricities, v, member W2T2 - Load step 6

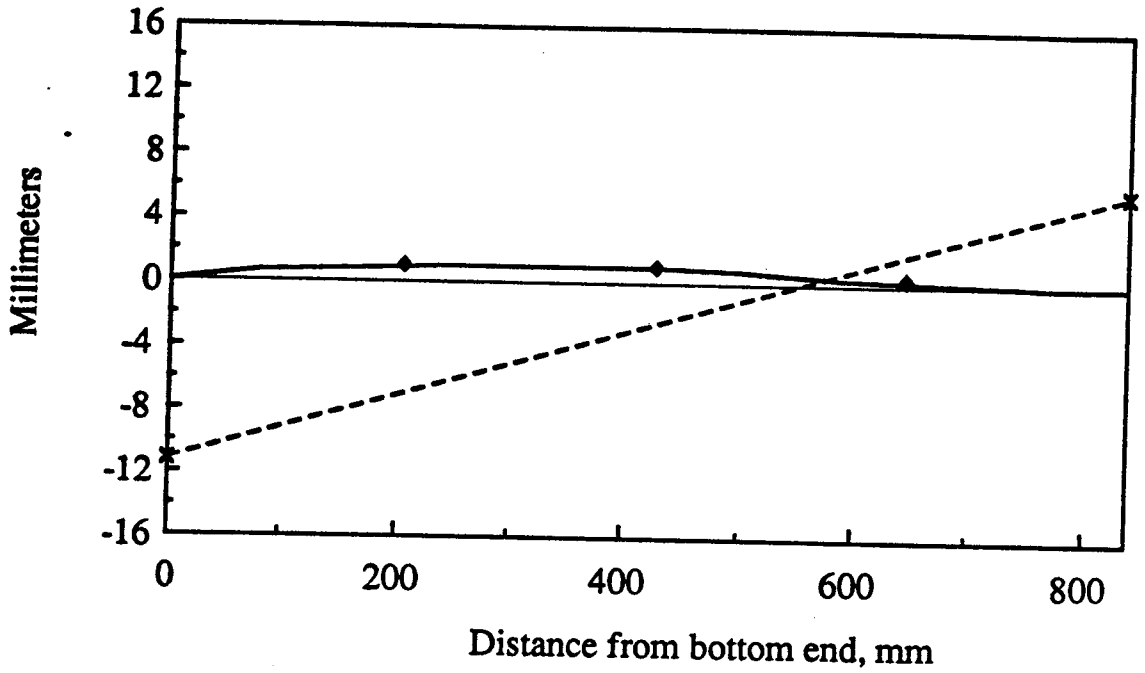

Figure 3.18 Deflected shape and eccentricities, u, member W2T2 - Load step 20

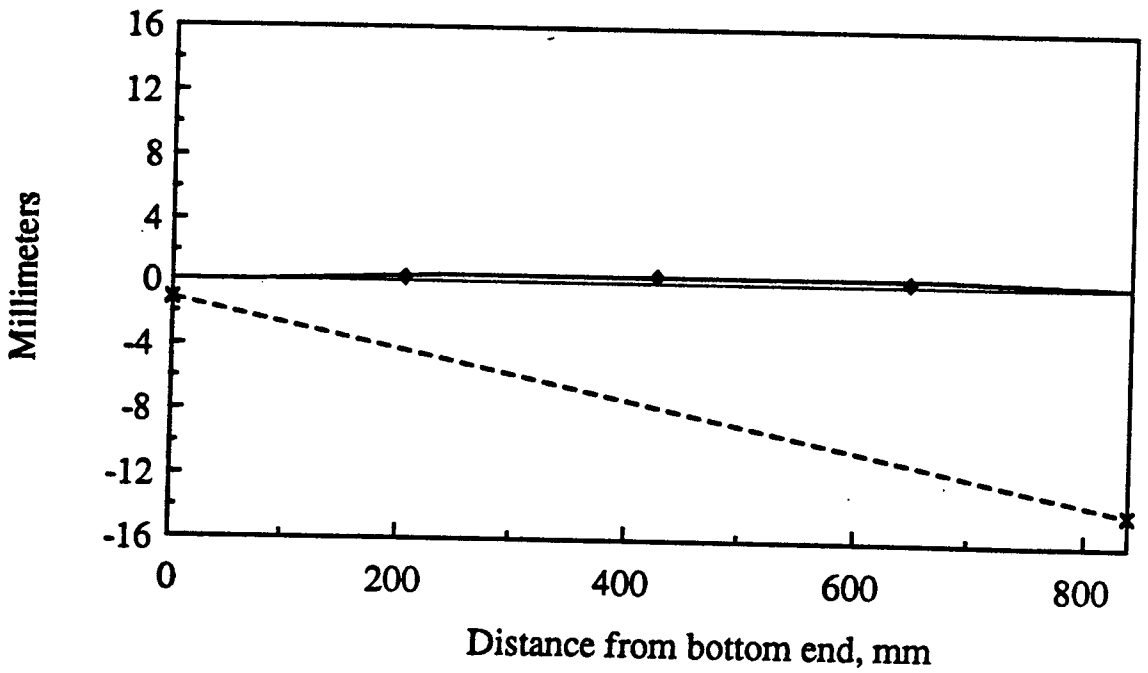

Figure 3.19 Deflected shape and eccentricities, v, member W2T2 - Load step 20

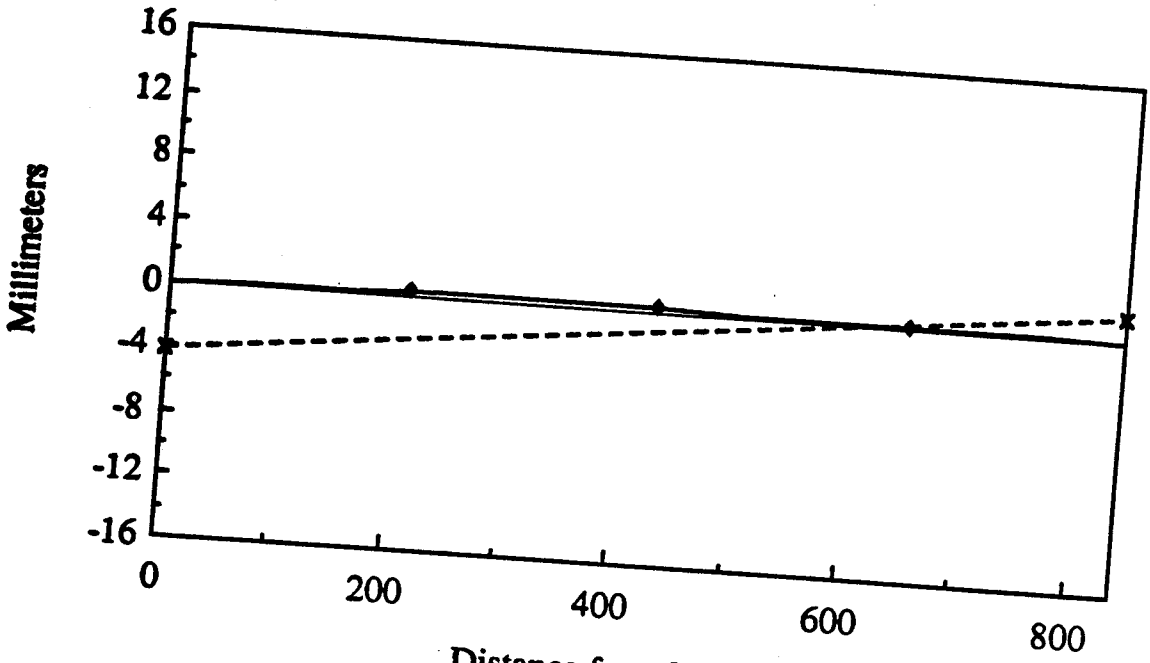

Figure 3.20 Deflected shape and eccentricities, u, member W4T2 - Load step 6

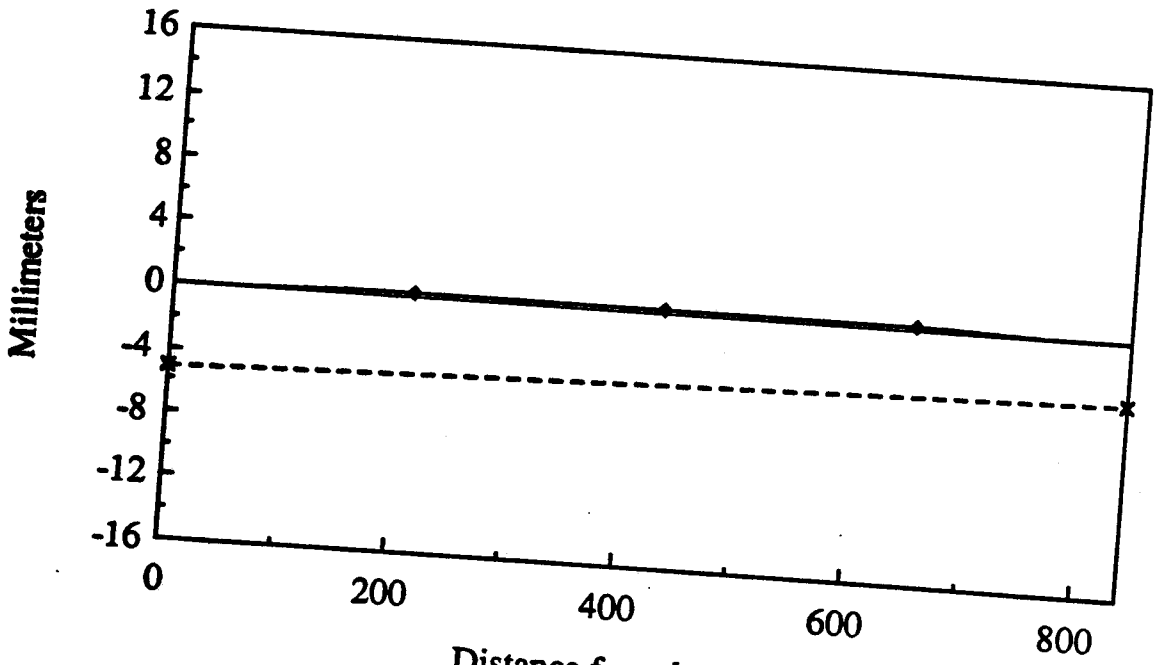

Figure 3.21 Deflected shape and eccentricities, v, member W4T2 - Load step 6

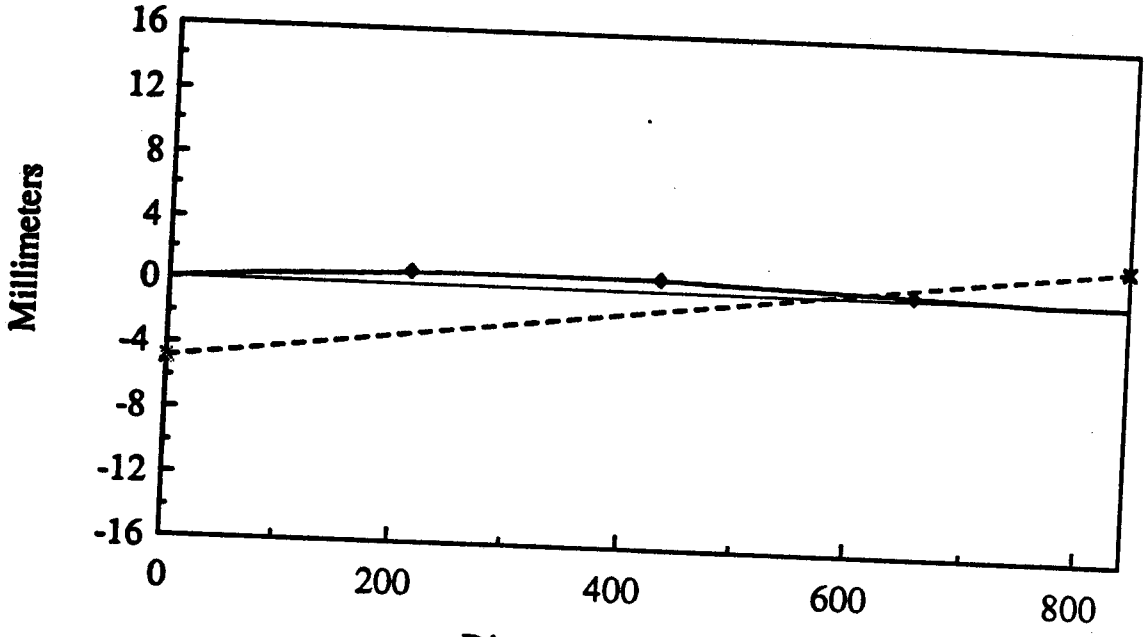

Figure 3.22 Deflected shape and eccentricities, u, member W4T2 - Load step 33

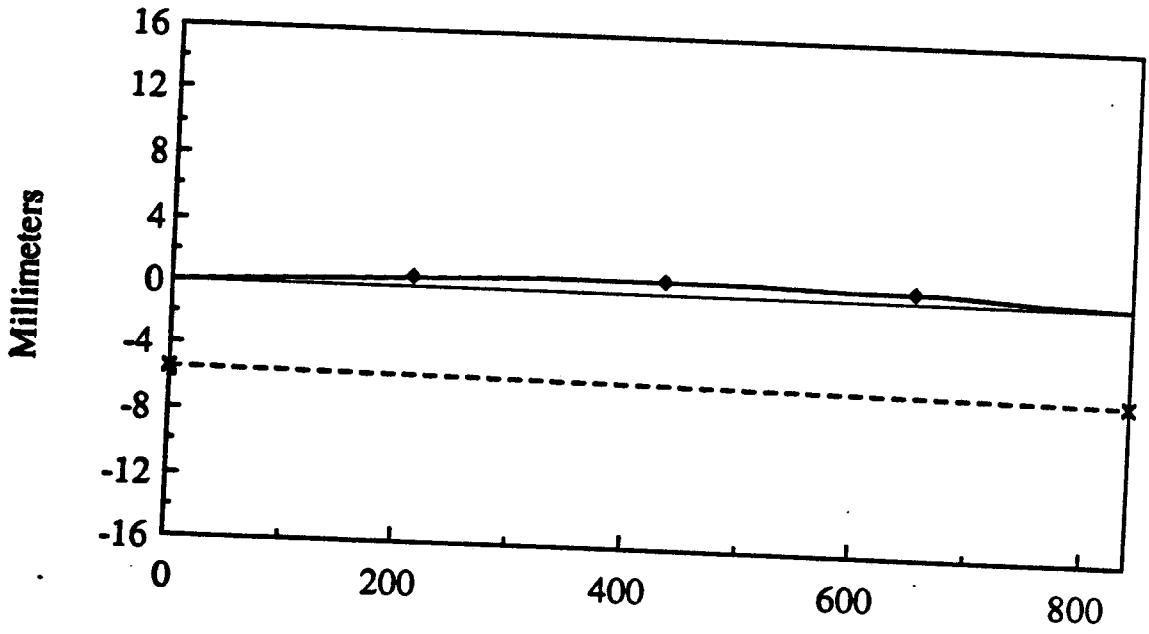

Figure 3.23 Deflected shape and eccentricities, v, member W4T2 - Load step 33

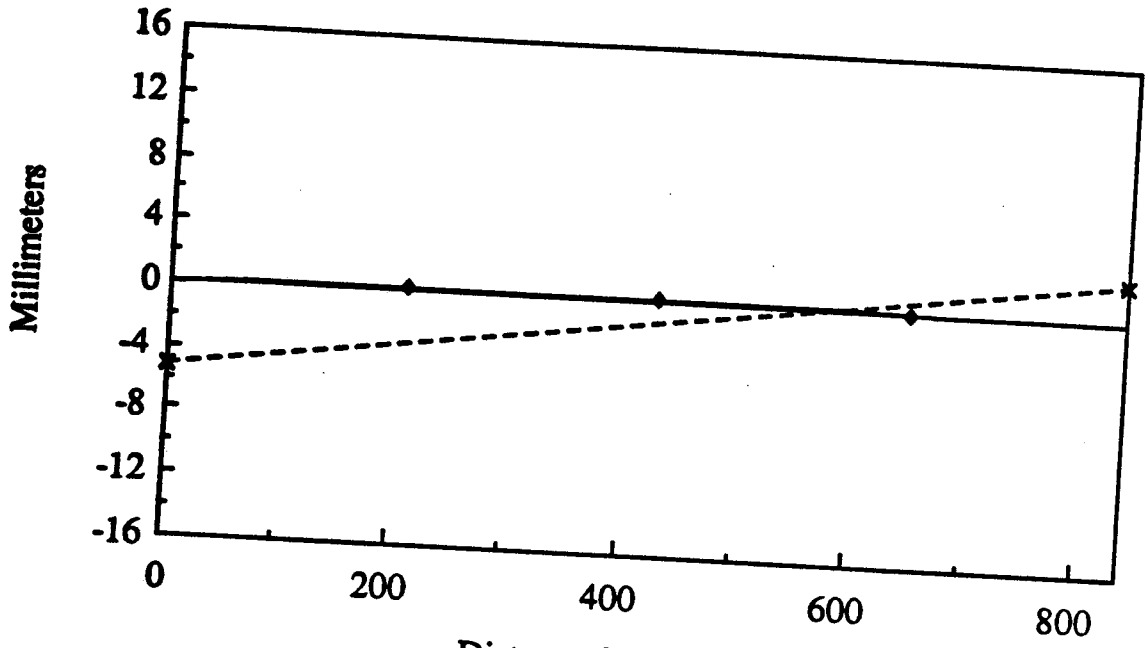

Figure 3.24 Deflected shape and eccentricities, u, member W13T2 - Load step 6

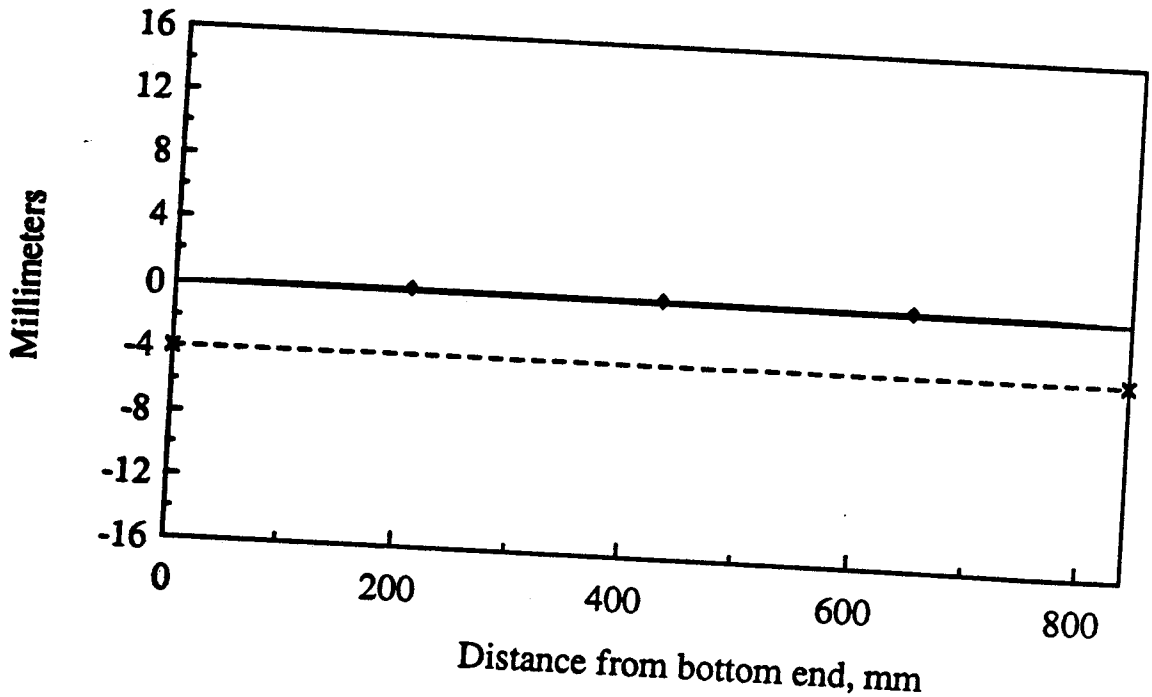

Figure 3.25 Deflected shape and eccentricities, v, member W13T2 - Load step 6

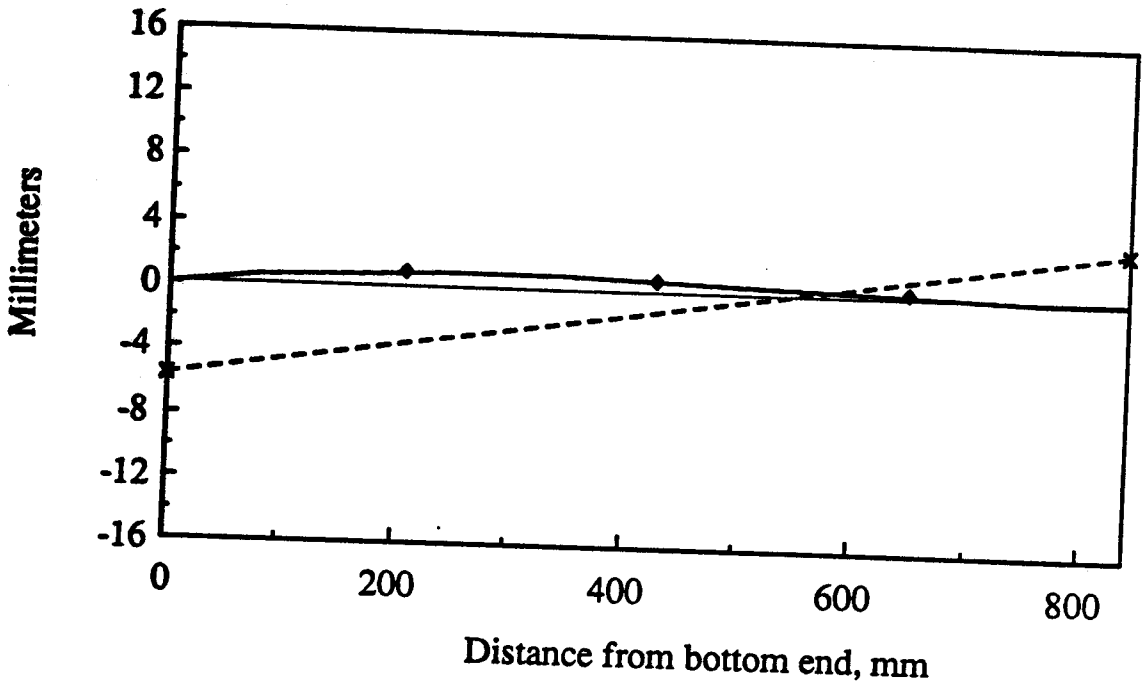

Figure 3.26 Deflected shape and eccentricities, u, member W13T2 - Load step 33

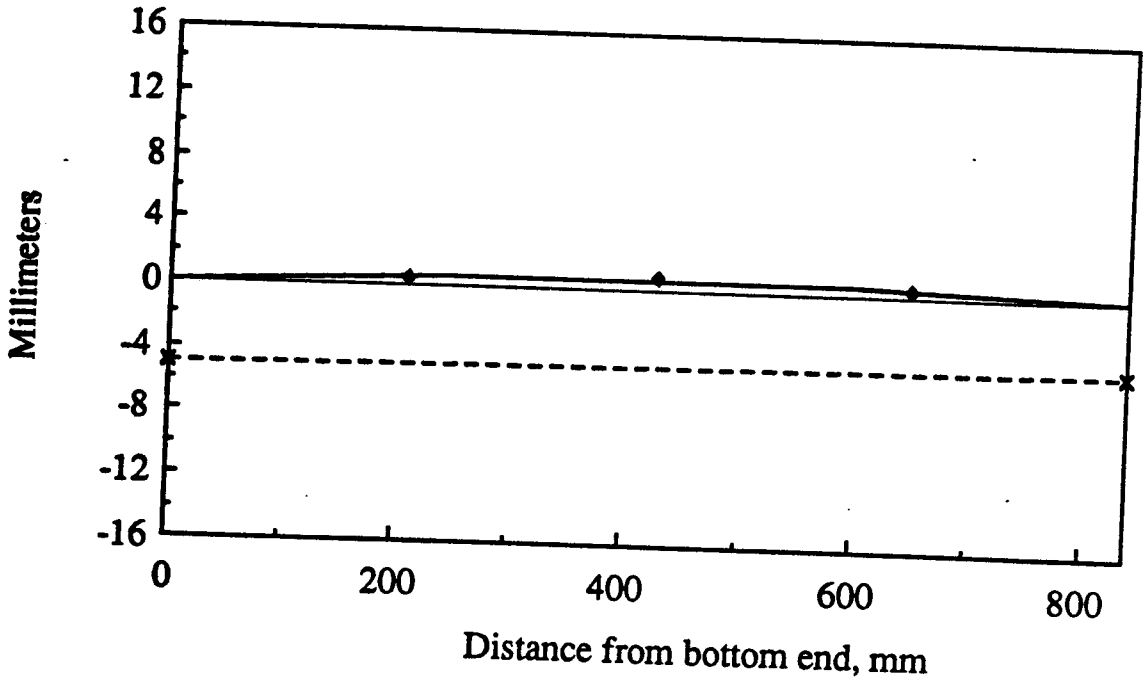

Figure 3.27 Deflected shape and eccentricities, v, member W13T2 - Load step 33

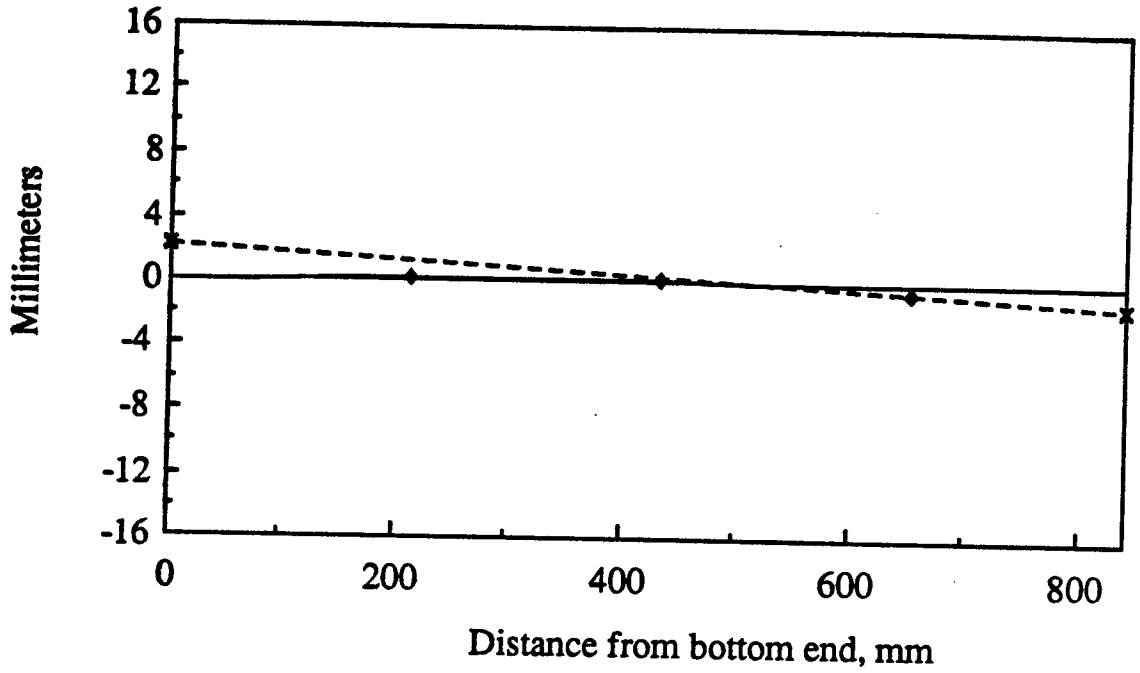

Figure 3.28 Deflected shape and eccentricities, u, member W14T2 - Load step 6

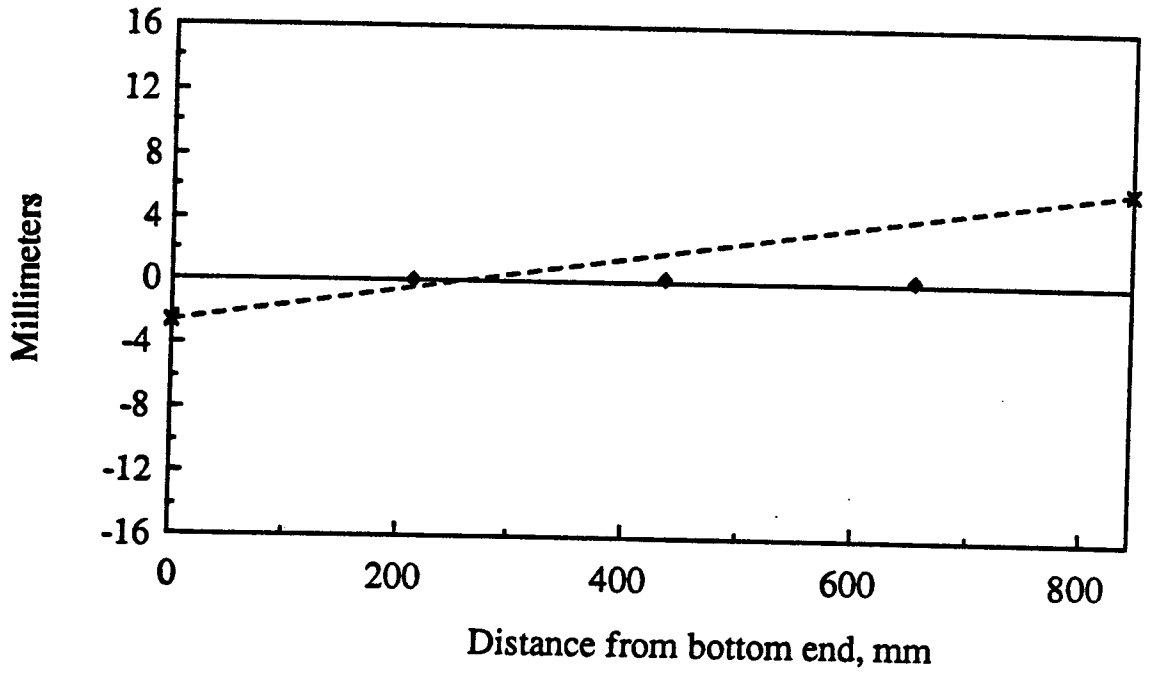

Figure 3.29 Deflected shape and eccentricities, v, member W14T2 - Load step 6

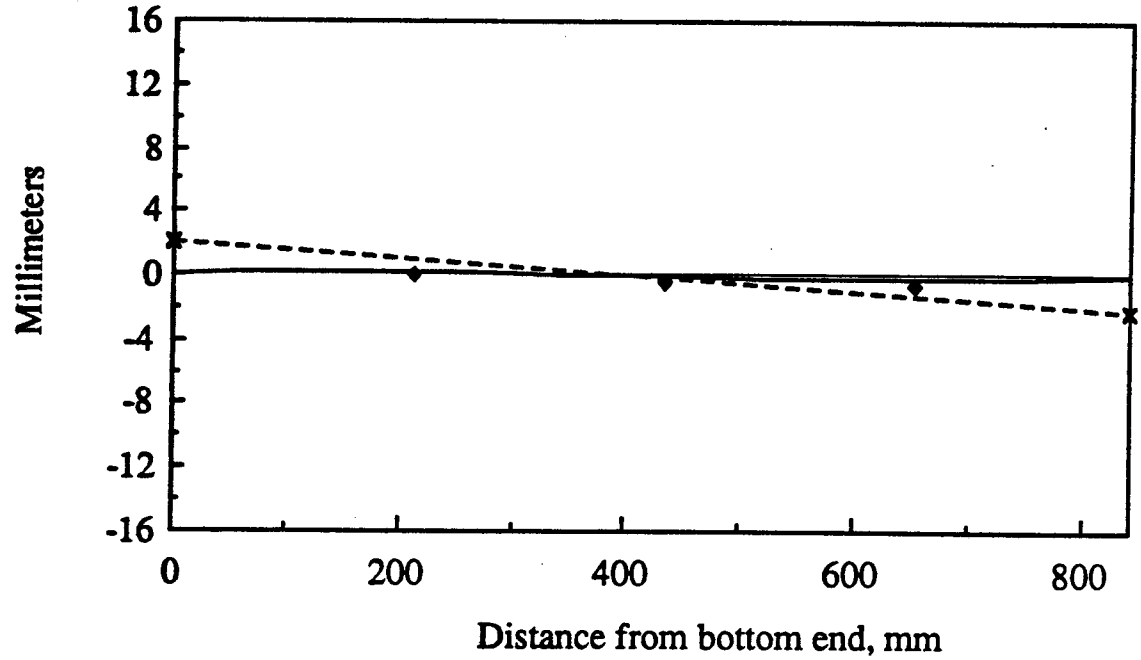

Figure 3.30 Deflected shape and eccentricities, u, member W14T2 - Load step 33

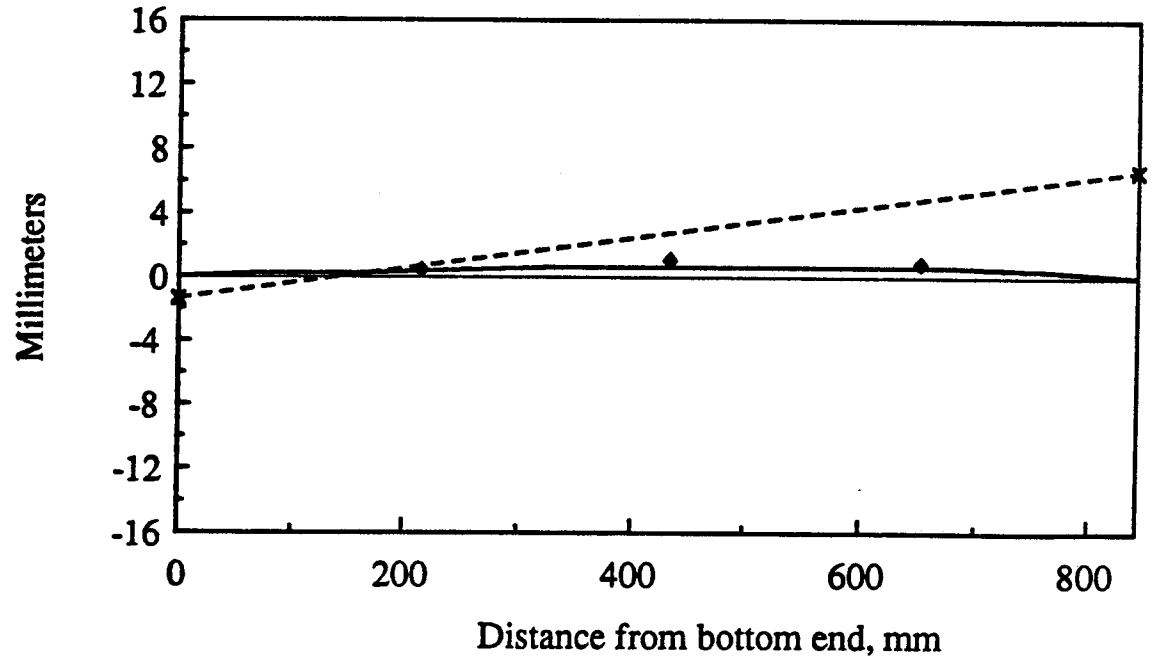

Figure 3.31 Deflected shape and eccentricities, v, member W14T2 - Load step 33

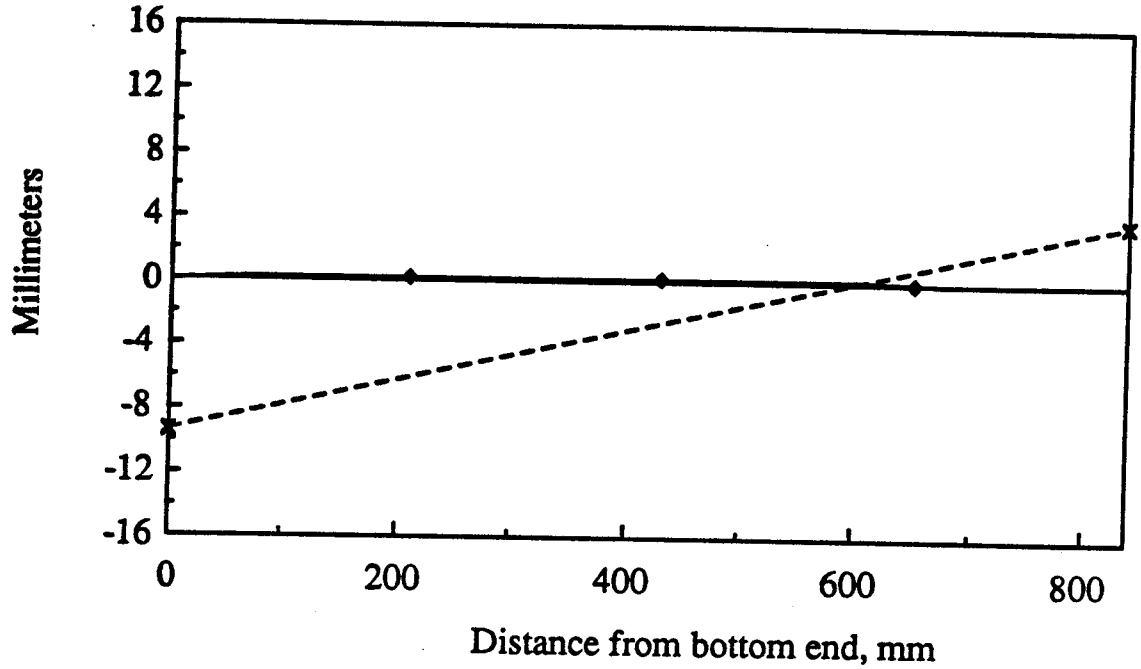

Figure 3.32 Deflected shape and eccentricities, u, member W15T2 - Load step 6

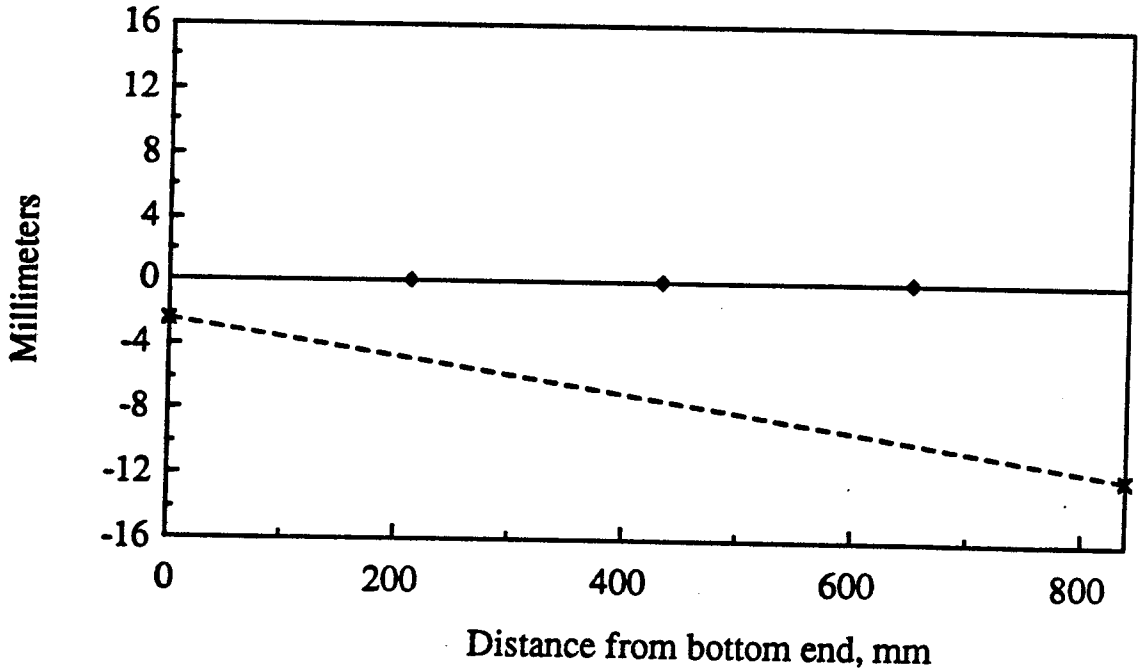

Figure 3.33 Deflected shape and eccentricities, v, member W15T2 - Load step 6

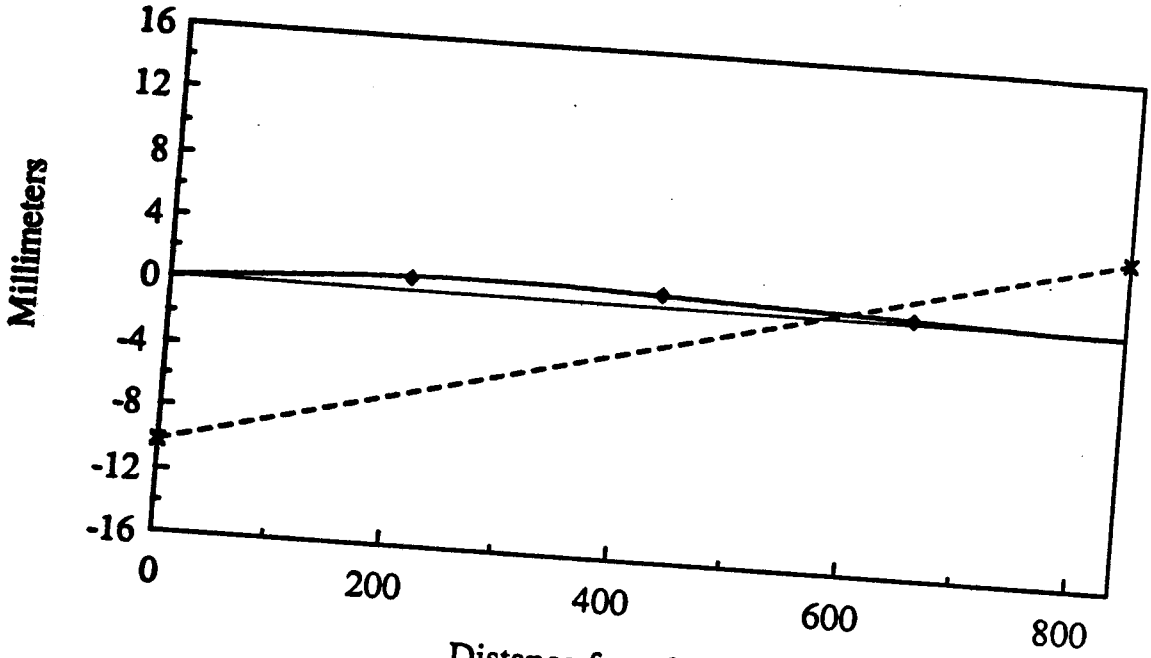

Figure 3.34 Deflected shape and eccentricities, u, member W15T2 - Load step 20

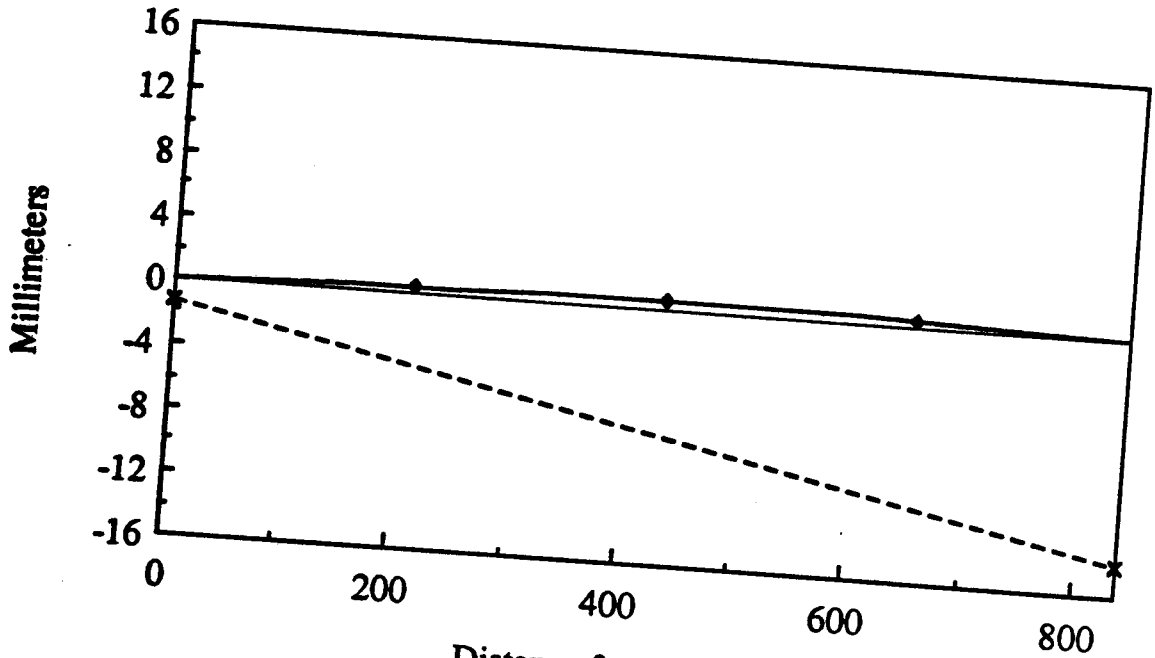

Figure 3.35 Deflected shape and eccentricities, v, member W15T2 - Load step 20

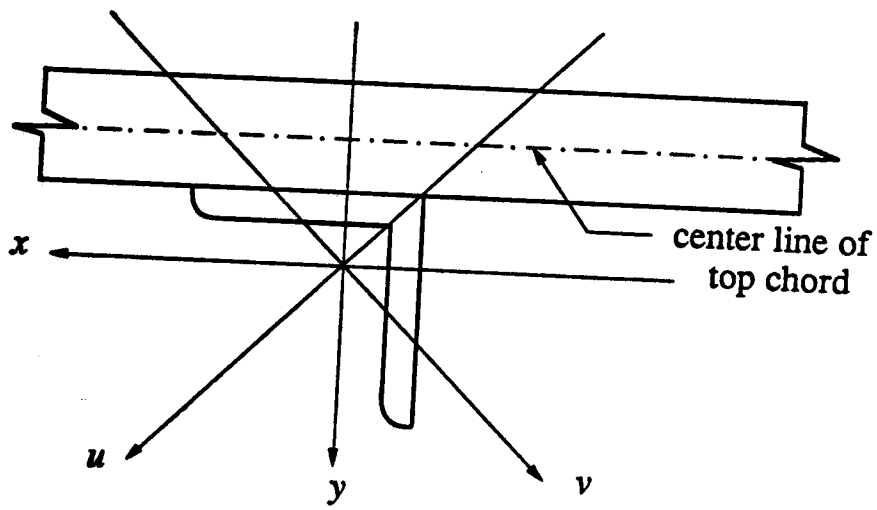

Figure 3.36 Orientation of the centroidal axes of a web member.

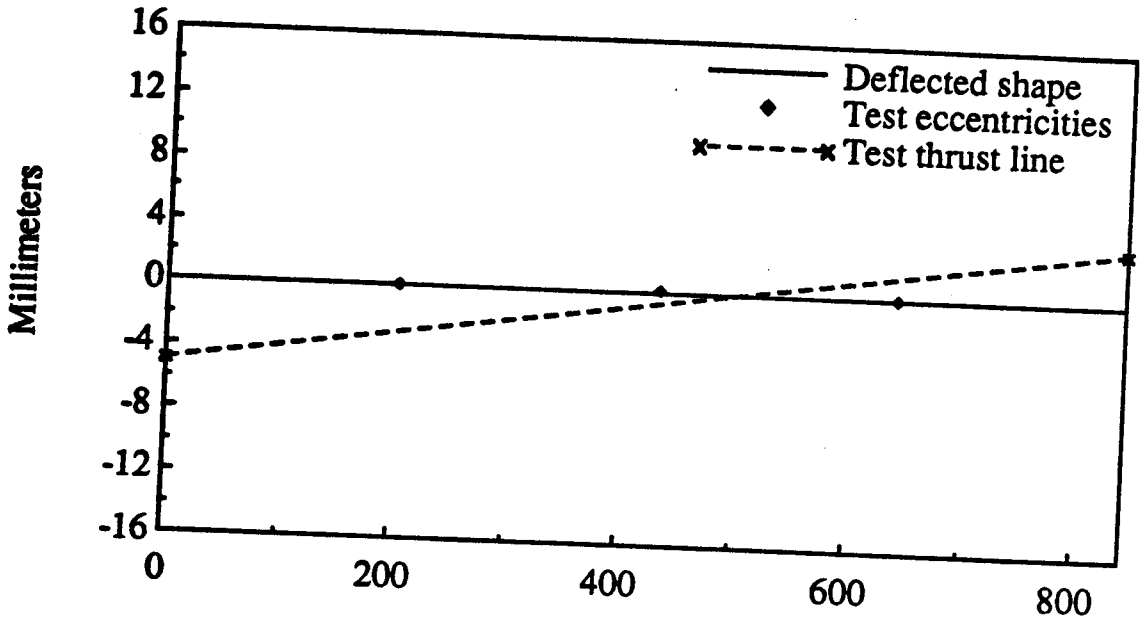

Figure 3.37 Deflected shape and eccentricities, y, member W11T1 - Load step 3

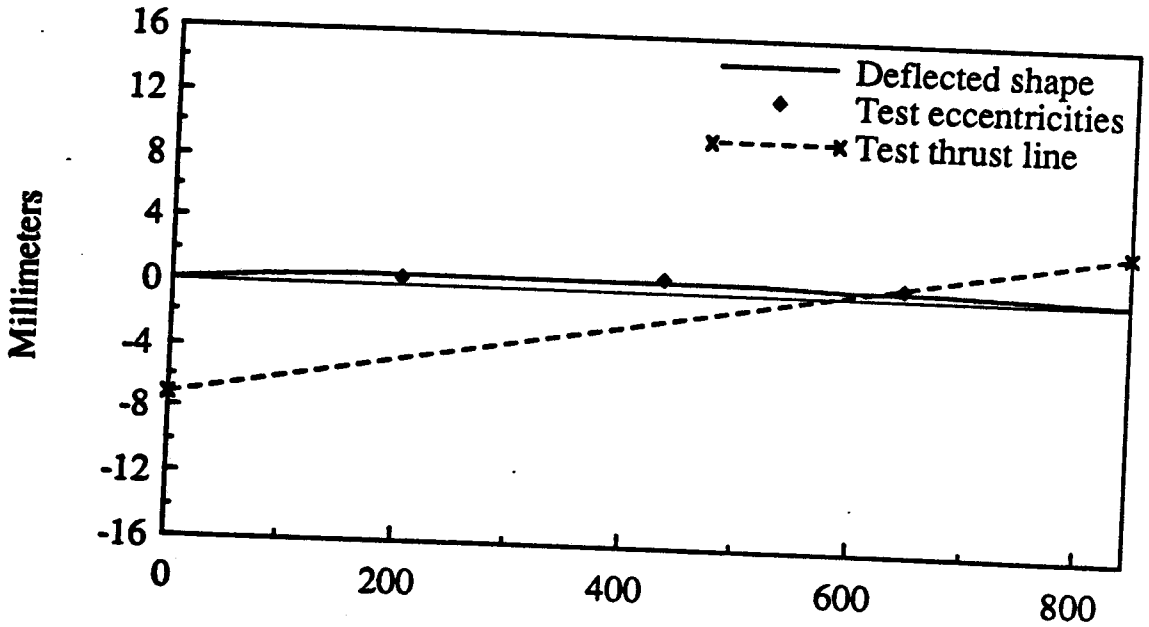

Figure 3.38 Deflected shape and eccentricities, y, member W11T1 - Load step 10

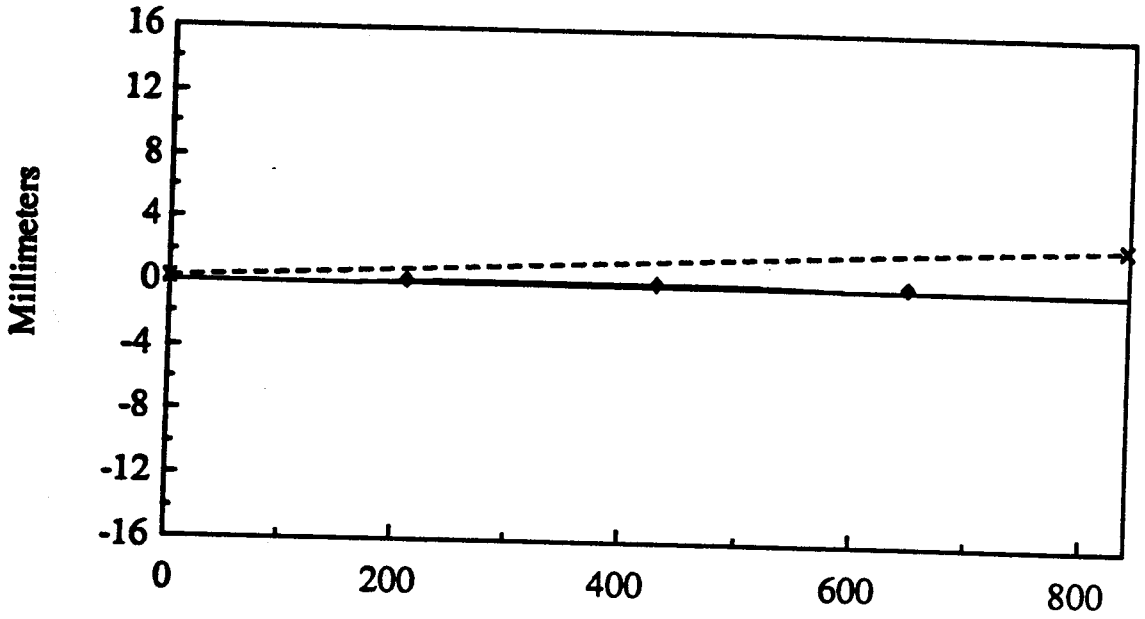

Figure 3.39 Deflected shape and eccentricities, y, member W14T1 - Load step 3

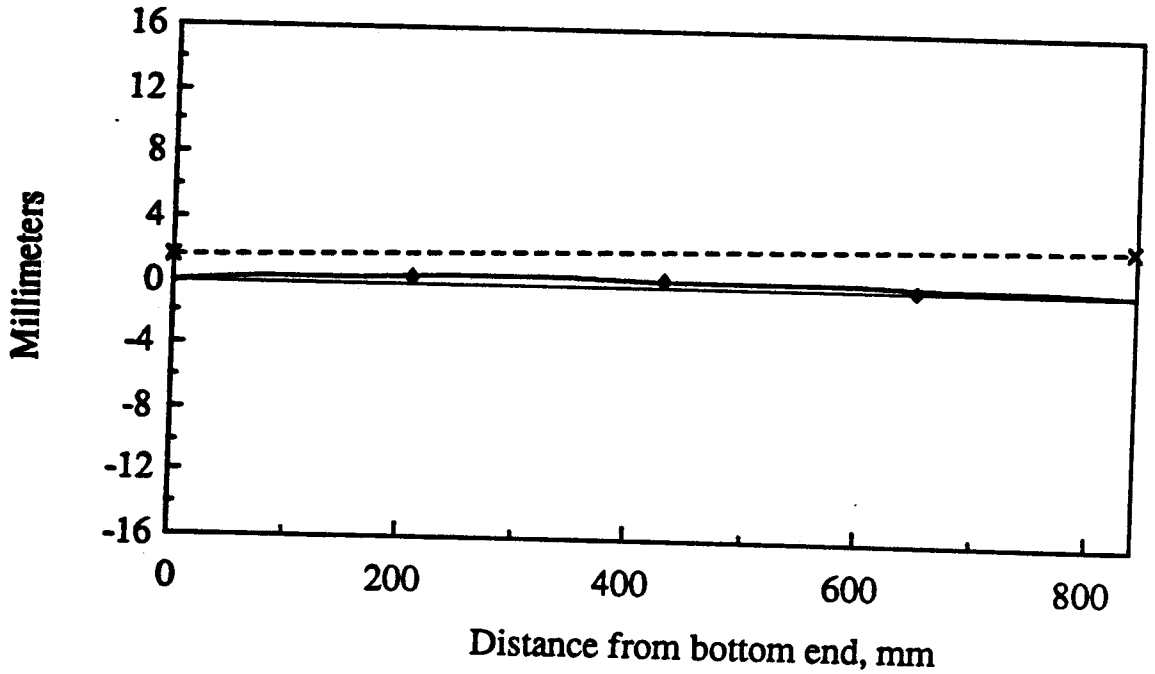

Figure 3.40 Deflected shape and eccentricities, y, member W14T1 - Load step 10

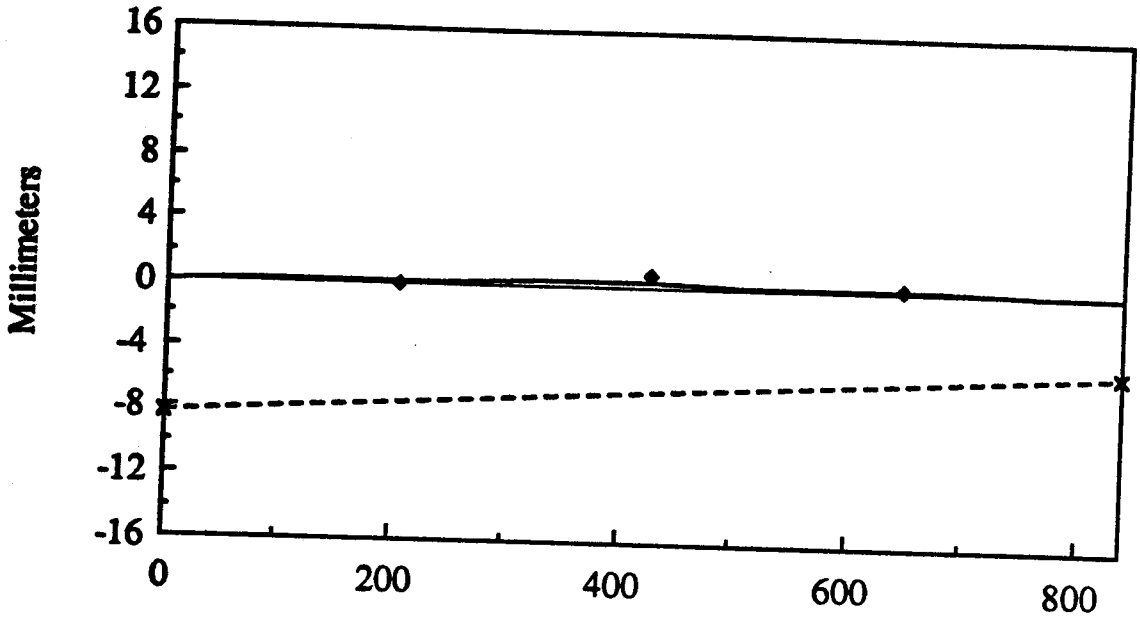

Figure 3.43 Deflected shape and eccentricities, y, member W2T2 - Load step 6

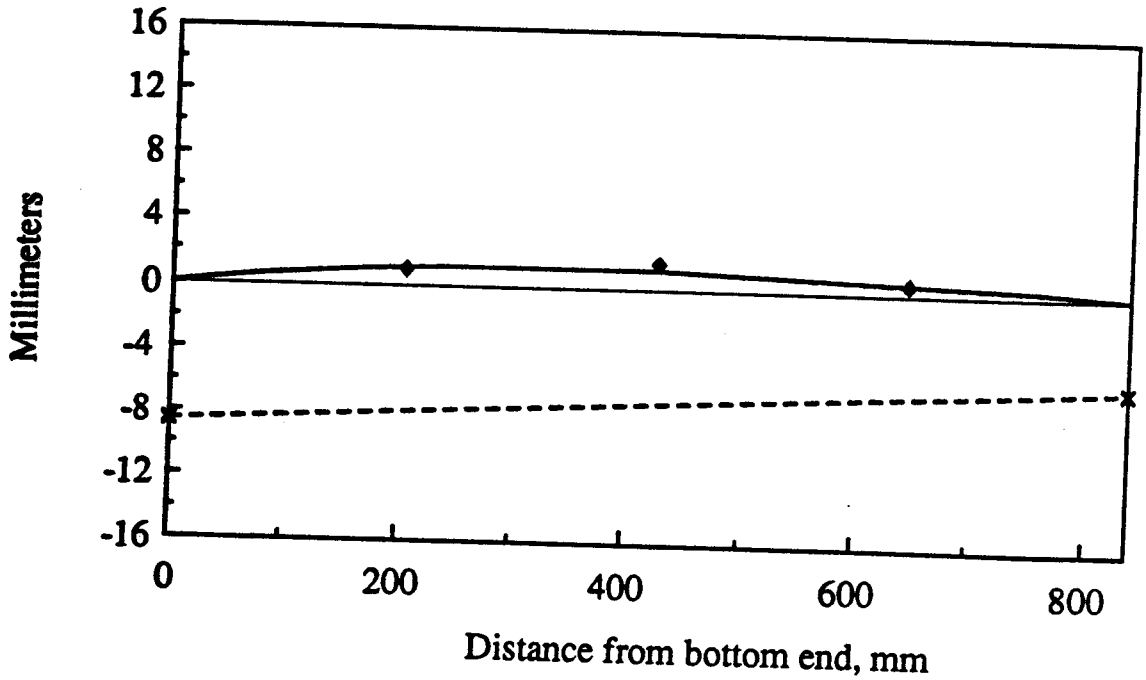

Figure 3.44 Deflected shape and eccentricities, y, member W2T2 - Load step 20

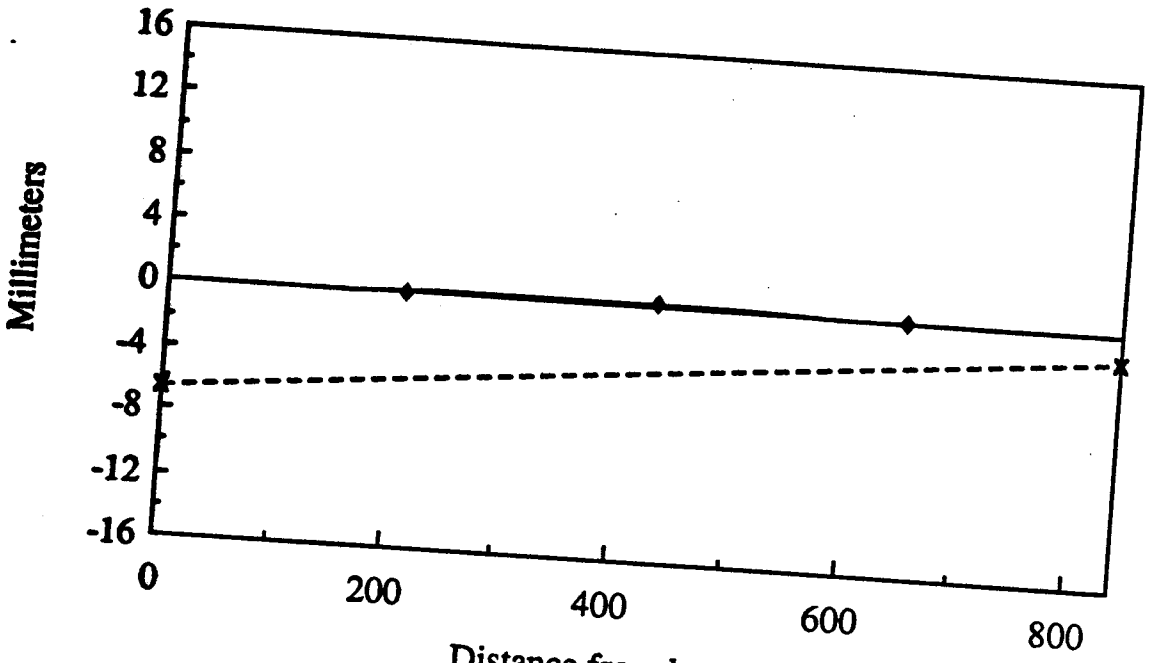

Figure 3.45 Deflected shape and eccentricities, y, member W4T2 - Load step 6

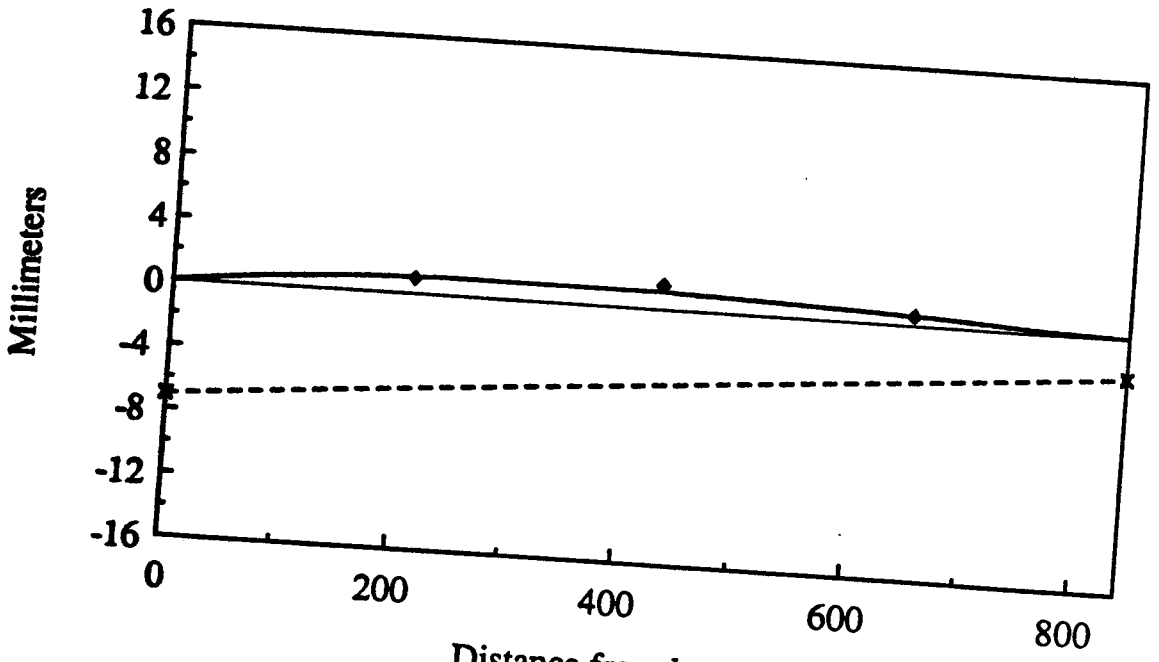

Figure 3.46 Deflected shape and eccentricities, y, member W4T2 - Load step 33

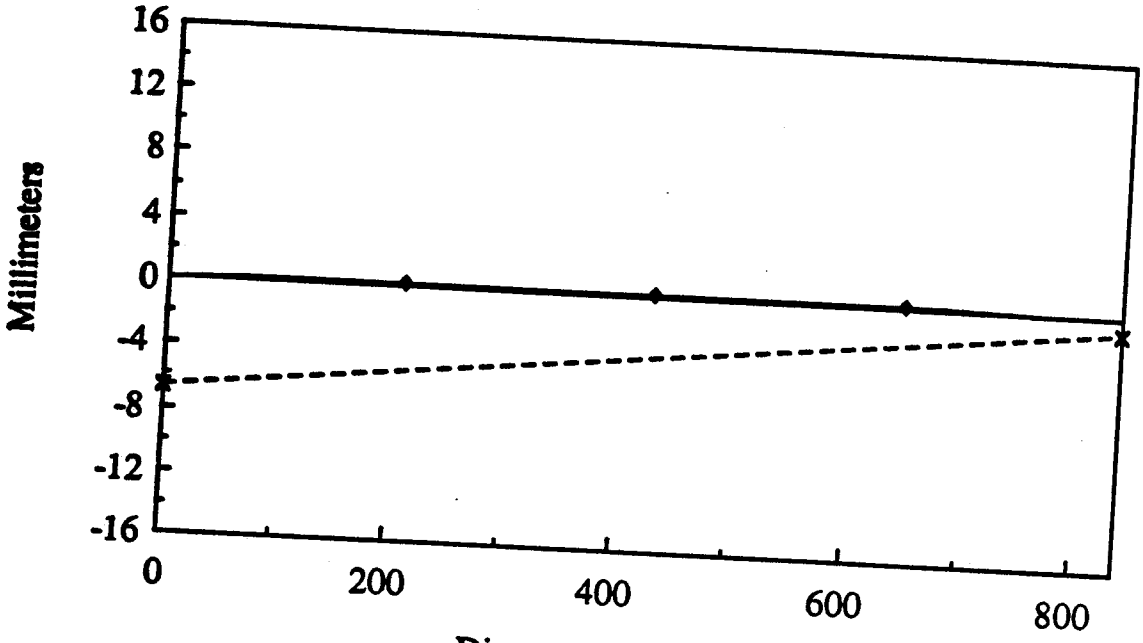

Figure 3.47 Deflected shape and eccentricities, y, member W13T2 - Load step 6

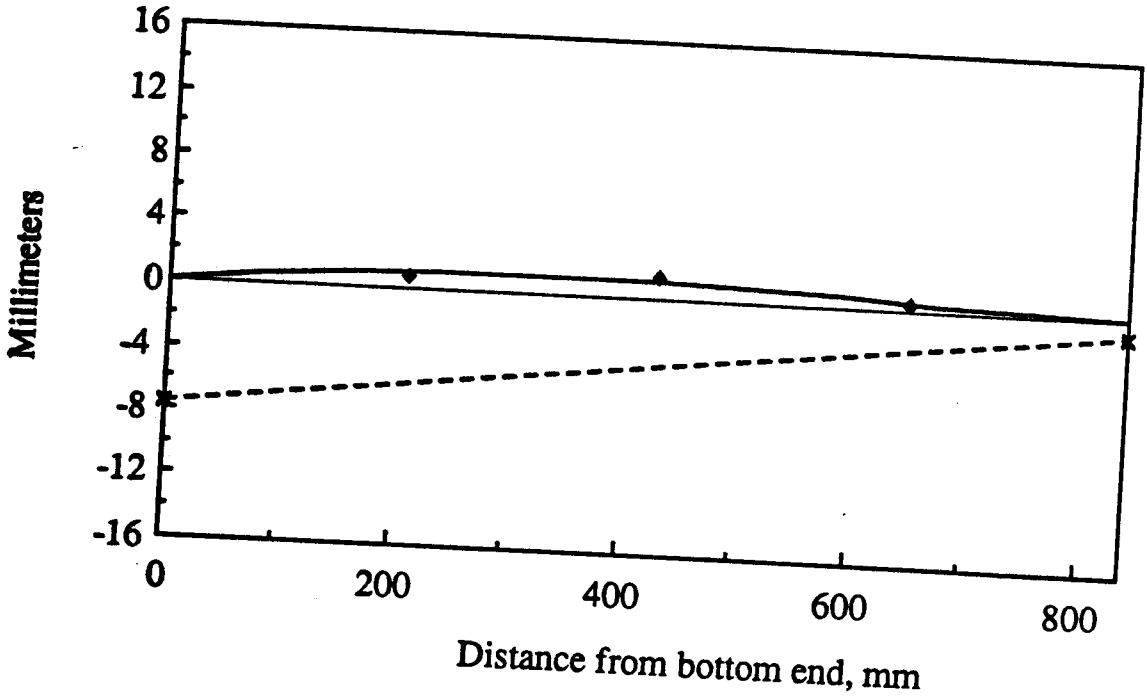

Figure 3.48 Deflected shape and eccentricities, y, member W13T2 - Load step 33

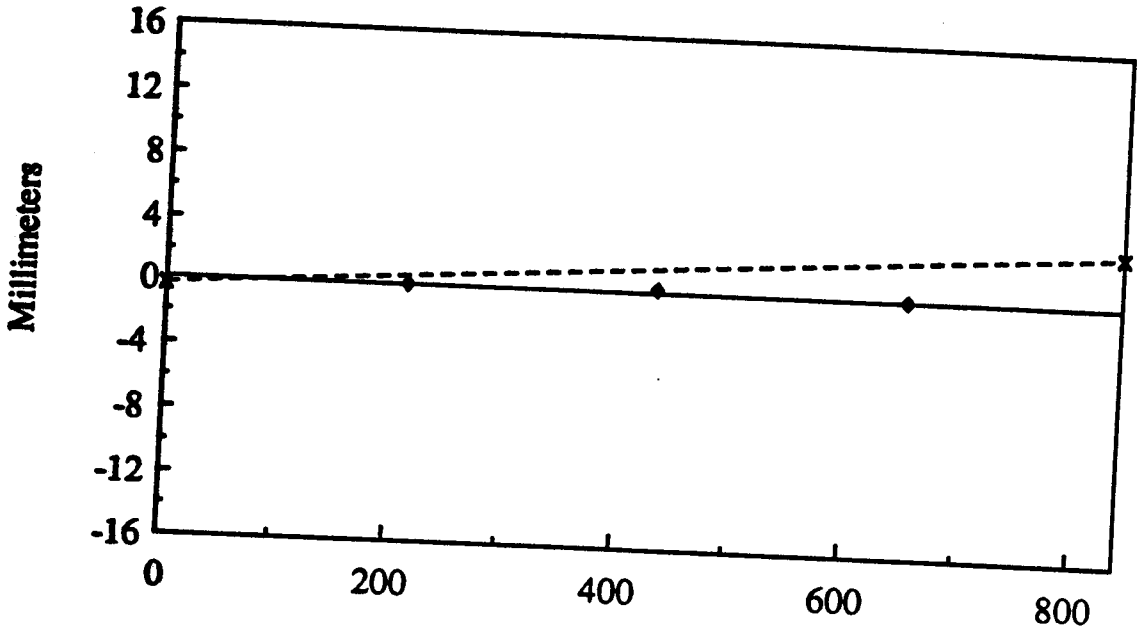

Figure 3.49 Deflected shape and eccentricities, y, member W14T2 - Load step 6

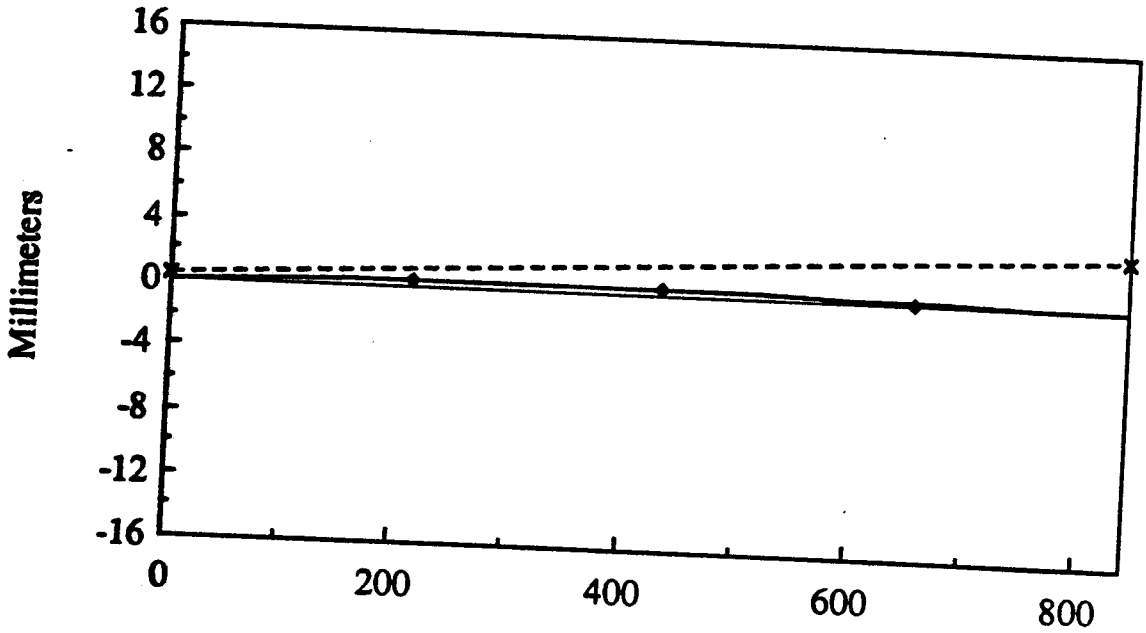

Figure 3.50 Deflected shape and eccentricities, y, member W14T2 - Load step 33

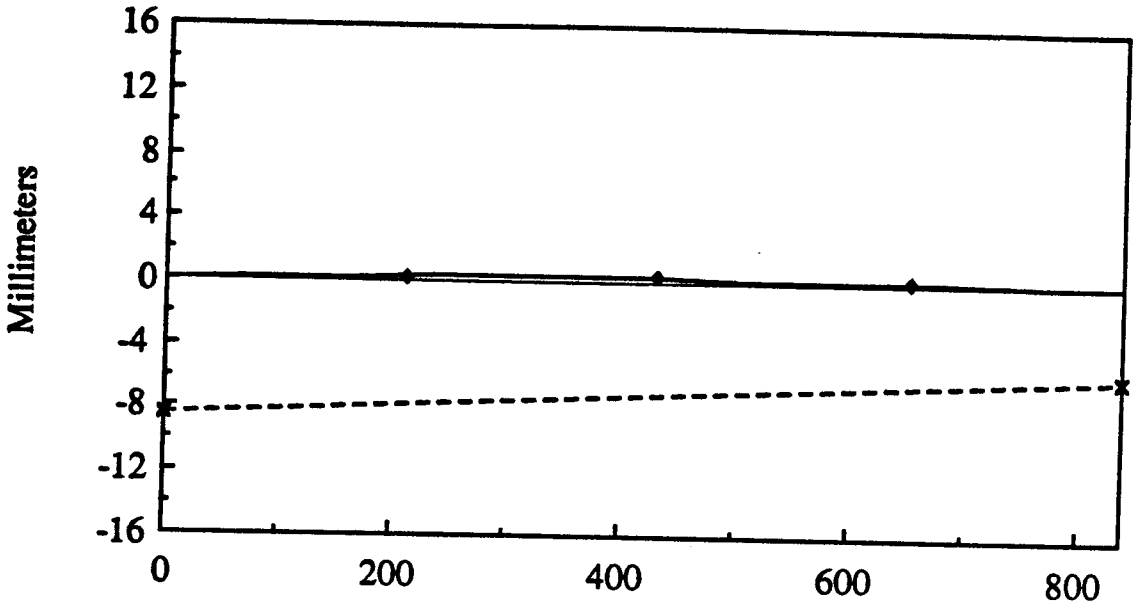

Figure 3.51 Deflected shape and eccentricities, y, member W15T2 - Load step 6

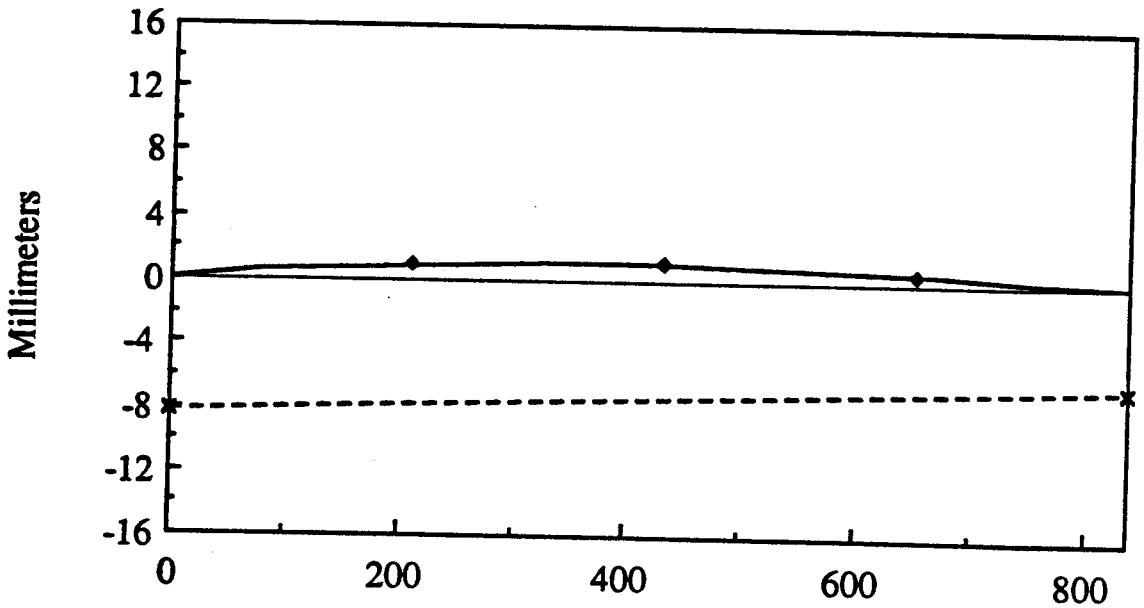

Figure 3.52 Deflected shape and eccentricities, y, member W15T2 - Load step 20

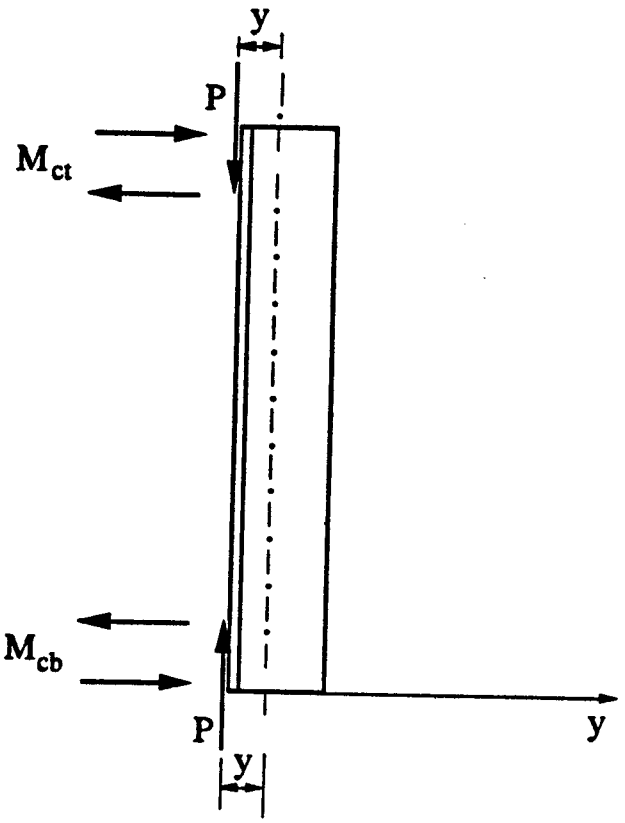

Figure 3.53 Eccentrically loaded web member

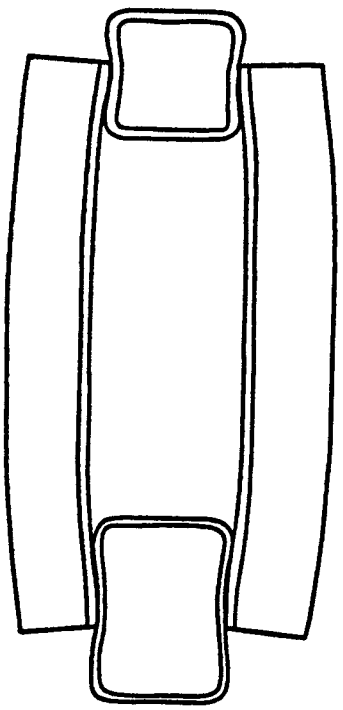

Figure 3.54 Distortion of chord walls and angles

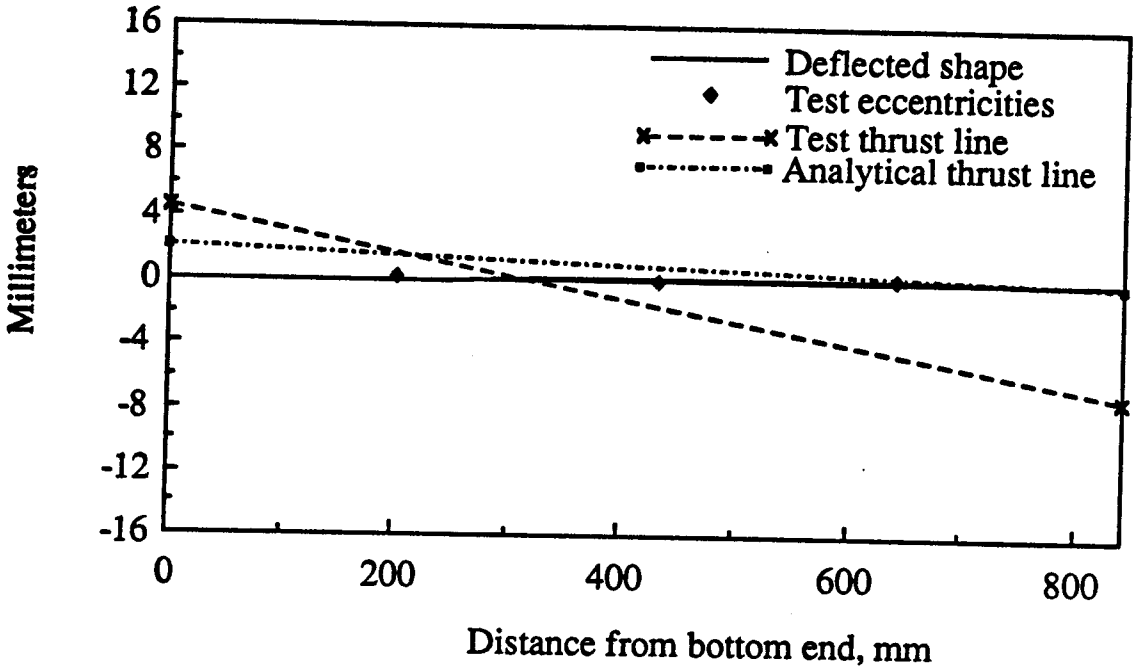

Figure 3.55 Deflected shape and eccentricities, x, member W11T1 - Load step 3

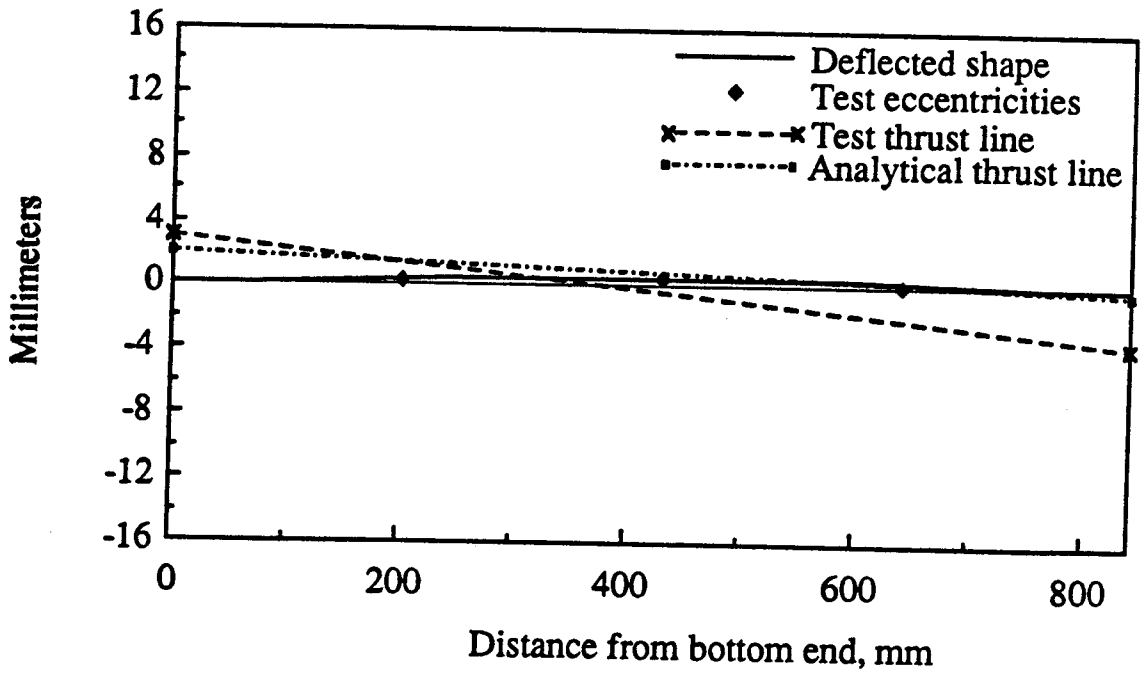

Figure 3.56 Deflected shape and eccentricities, x, member W11T1 - Load step 10

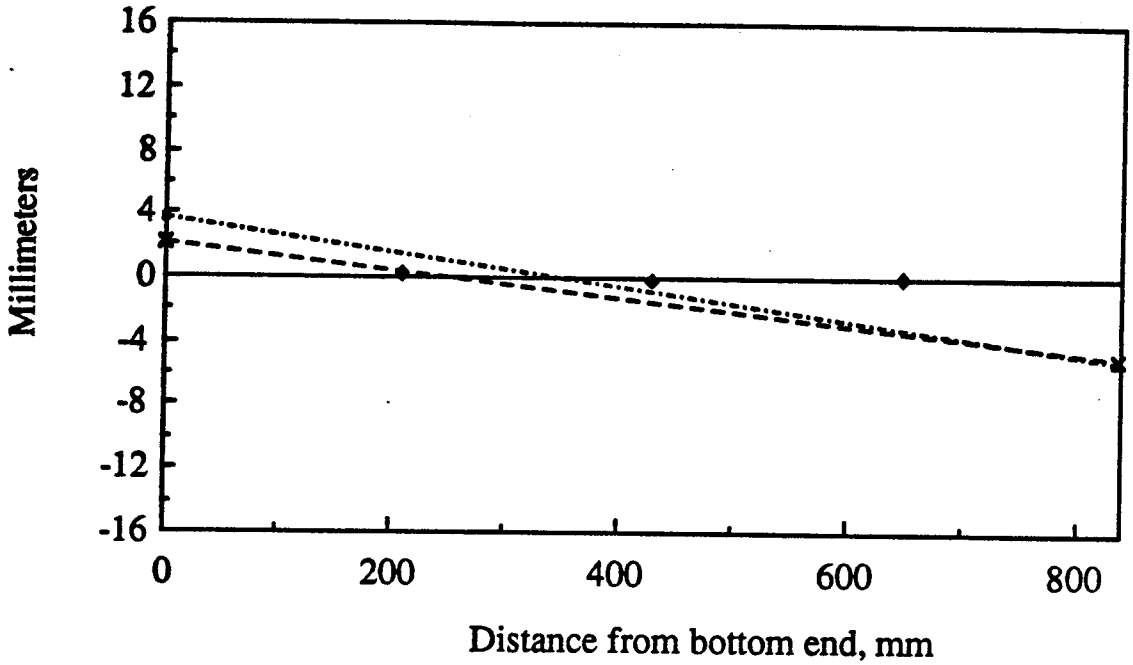

Figure 3.57 Deflected shape and eccentricities, x, member W14T1 - Load step 3

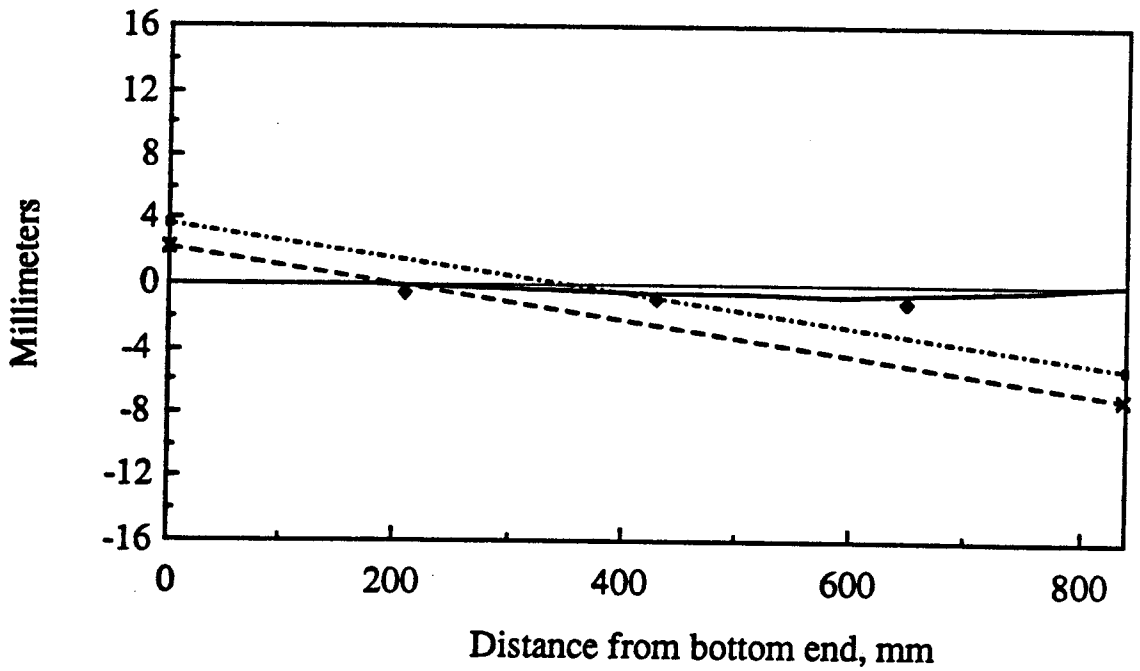

Figure 3.58 Deflected shape and eccentricities, x, member W14T1 - Load step 10

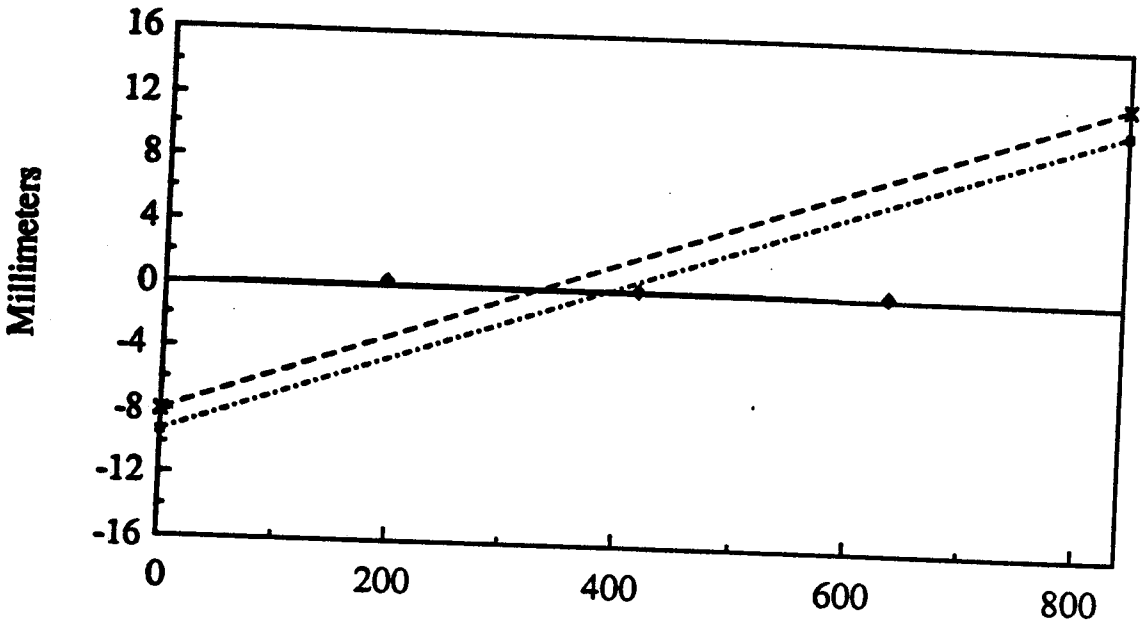

Figure 3.59 Deflected shape and eccentricities, x, member W15T1 - Load step 4

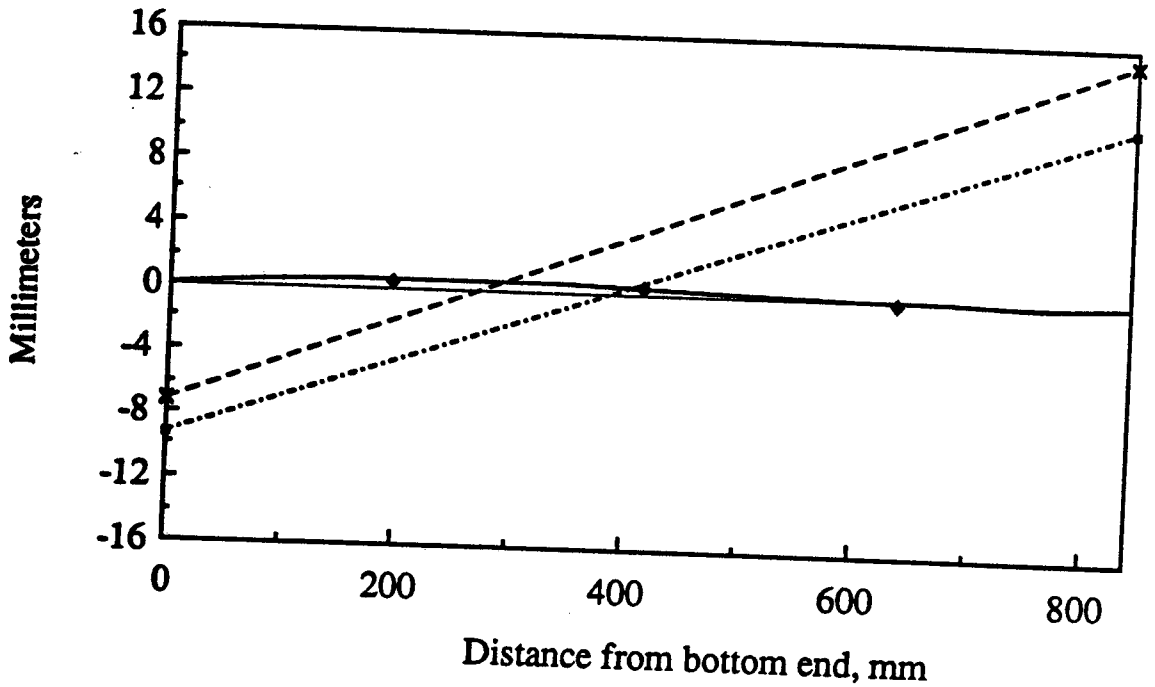

Figure 3.60 Deflected shape and eccentricities, x, member W15T1 - Load step 11

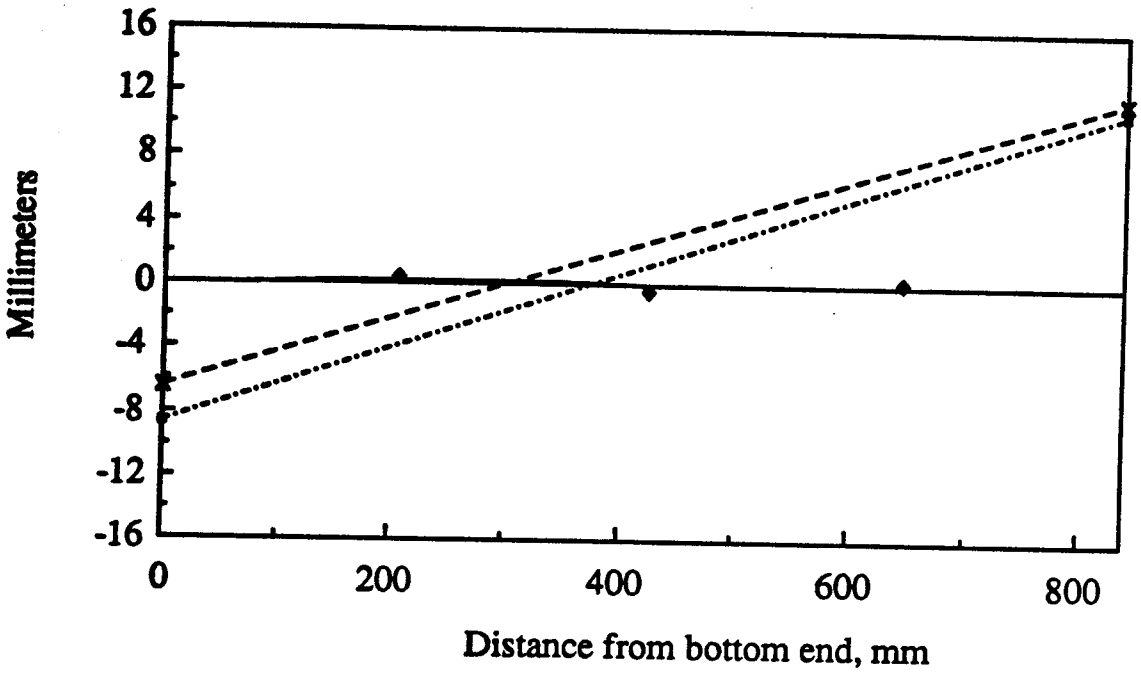

Figure 3.61 Deflected shape and eccentricities, x, member W2T2 - Load step 6

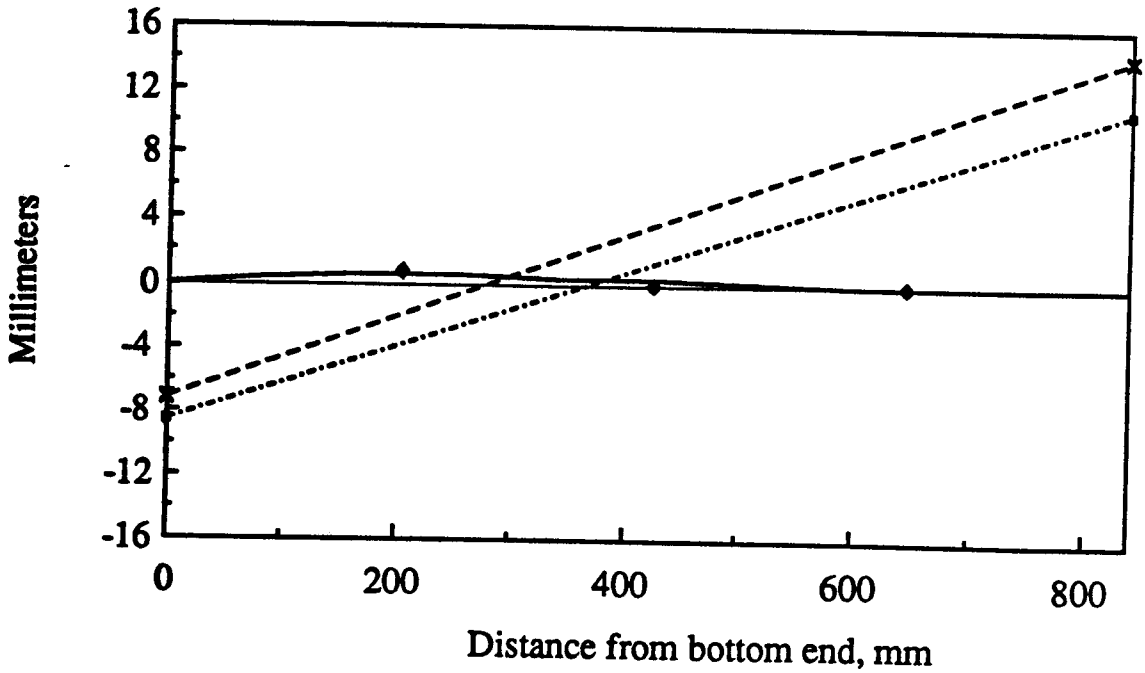

Figure 3.62 Deflected shape and eccentricities, x, member W2T2 - Load step 20

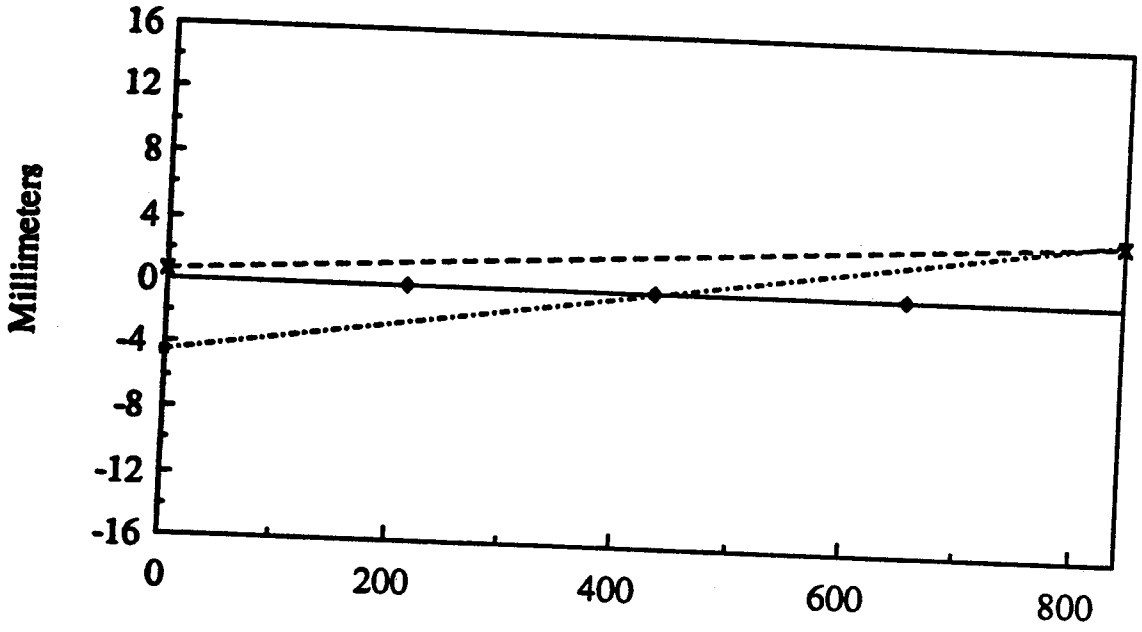

Figure 3.63 Deflected shape and eccentricities, x, member W4T2 - Load step 6

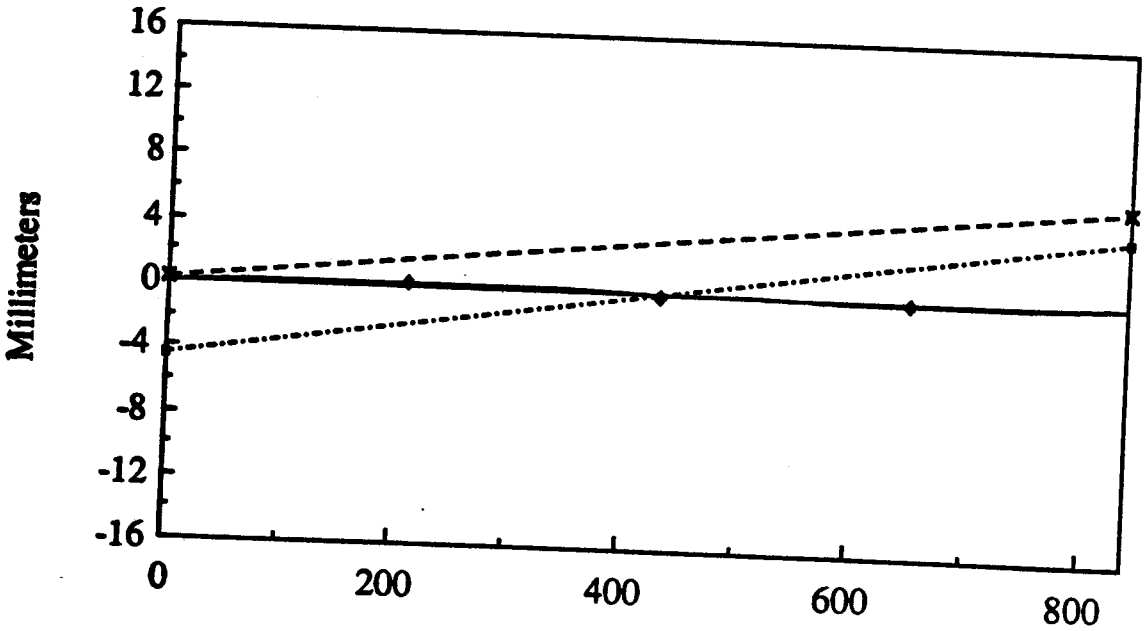

Figure 3.64 Deflected shape and eccentricities, x, member W4T2 - Load step 33

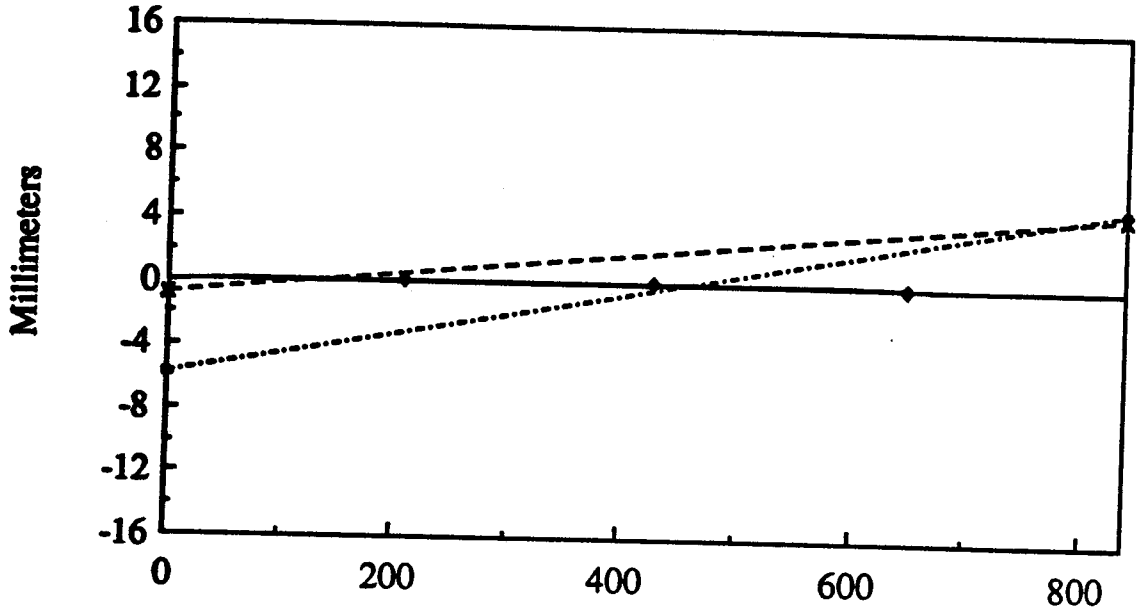

Figure 3.65 Deflected shape and eccentricities, x, member W13T2 - Load step 6

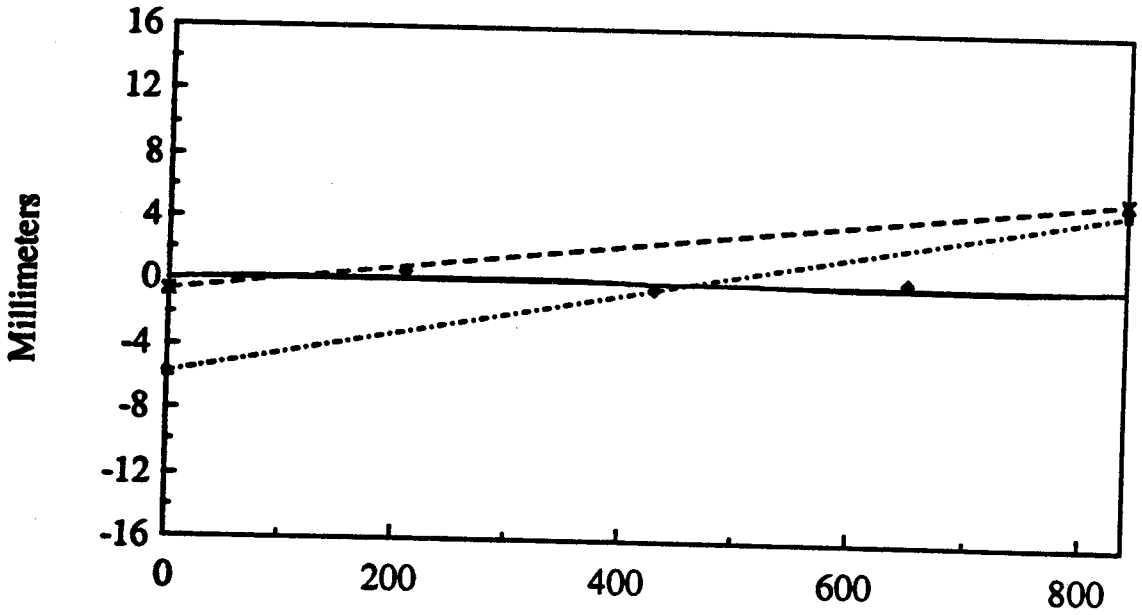

Figure 3.66 Deflected shape and eccentricities, x, member W13T2 - Load step 33

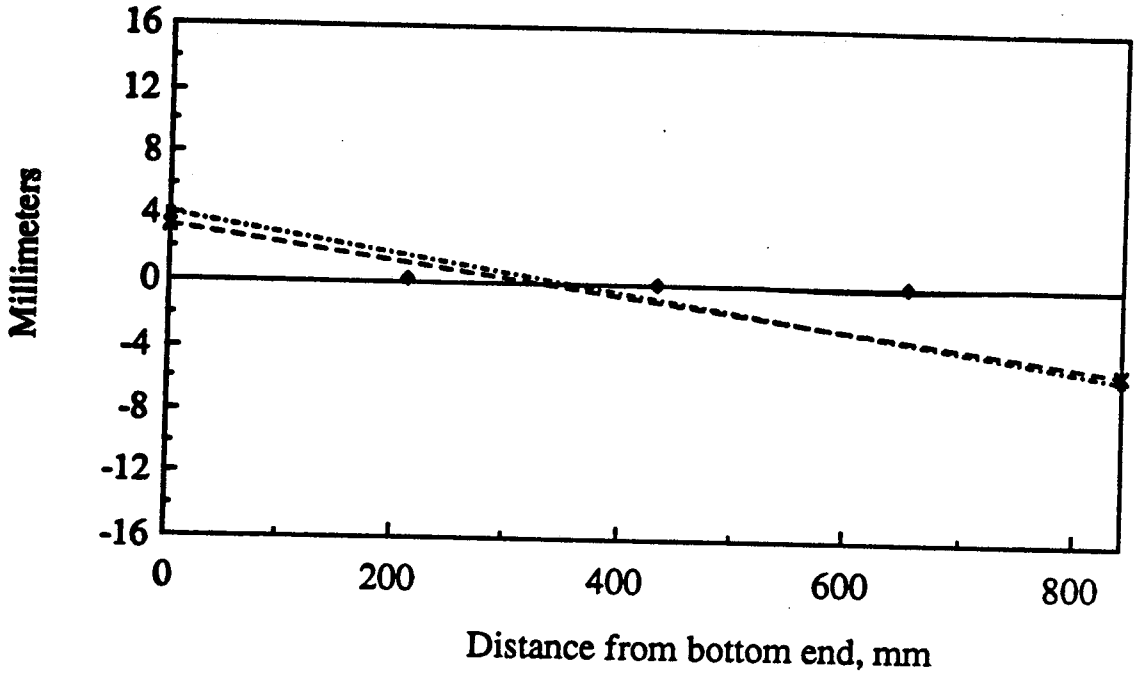

Figure 3.67 Deflected shape and eccentricities, x, member W14T2 - Load step 6

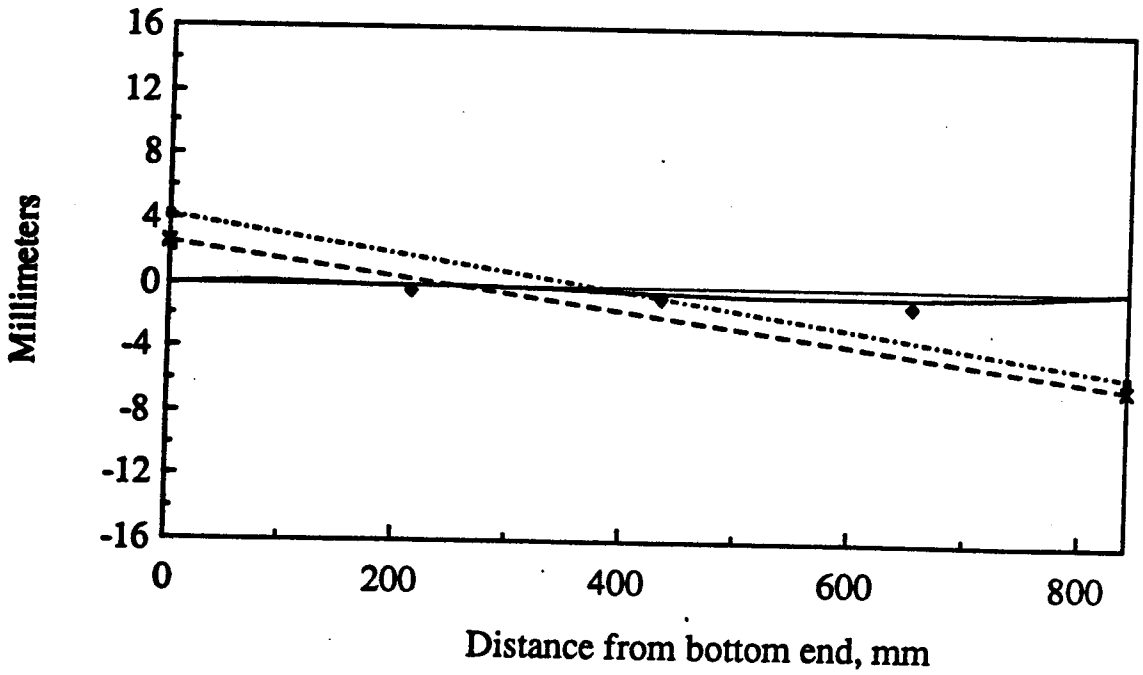

Figure 3.68 Deflected shape and eccentricities, x, member W14T2 - Load step 33

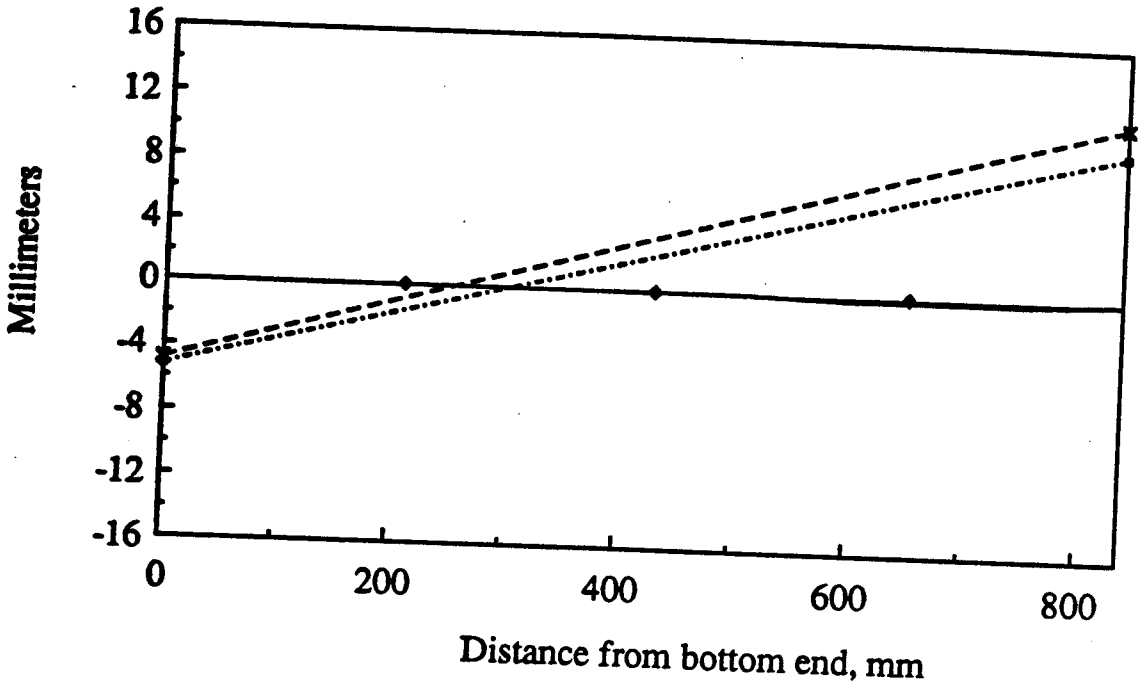

Figure 3.69 Deflected shape and eccentricities, x, member W15T2 - Load step 6

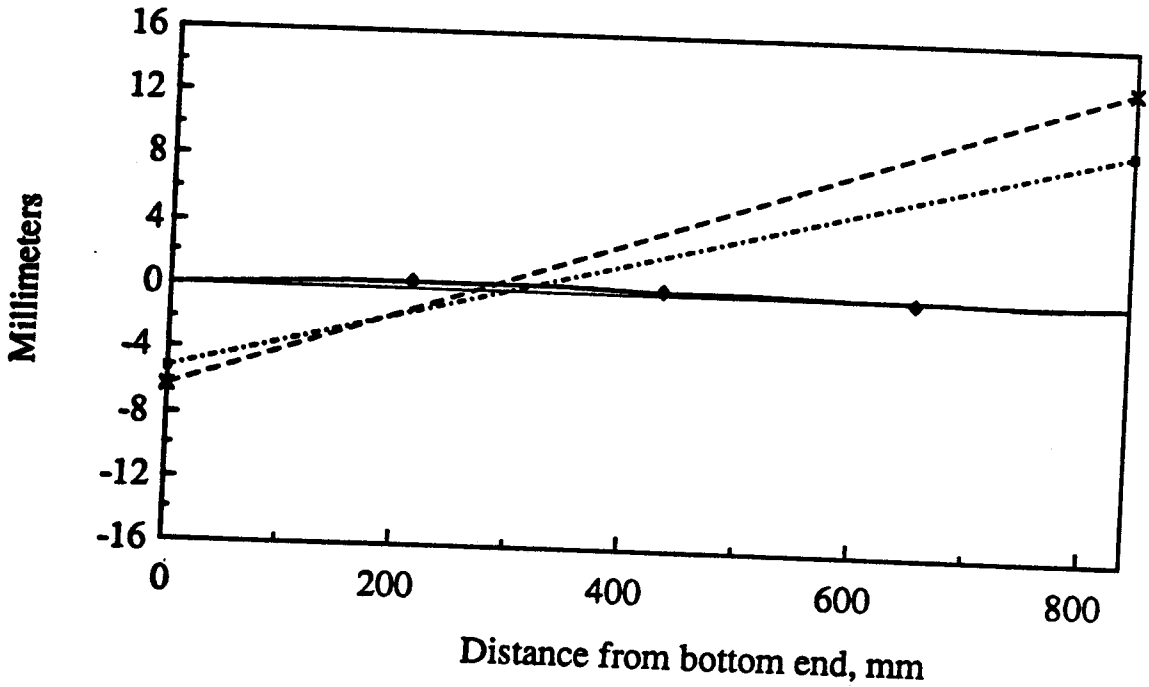

Figure 3.70 Deflected shape and eccentricities, x, member W15T2 - Load step 20

CHAPTER 4
VIBRATION TESTS

4.1. General

A total of 20 heel-drop tests (Lenzen,1966) were conducted on each of the two steel and two composite trusses to determine their vibration characteristics. The trusses were simply supported on puck bearings which allow free end rotations.

In a heel-drop test a person with a mass of approximately 77 kg raises himself on the balls of his feet and then allows his weight to strike the floor. The impulse imparted is closely approximated by a force of 2700 N decreasing linearly to zero in 0.05 seconds (I=67.5 N.sec) (Lenzen and Murray, 1969). The heel-impact was imparted to a truss within about 80 mm of the accelerometers taped to the top of the truss at mid span. The output from a Brüel and Kjaer model 8036 accelerometer was amplified in a Brüel and Kjaer model 2635 charge amplifier and recorded on a magnetic tape. Subsequently the tape records were analyzed on a Hewlett Packard model 39660A Dynamic Analyzer. From these analyses, the fundamental frequencies and the variation of acceleration with time can be determined. In turn, from the acceleration-time plot the initial peak acceleration, a_0, and the damping ratio, ß, as well as the frequency, if a separate frequency plot is not available, are established. In the first analyses of the magnetic tape the first three fundamental frequencies were determined for the composite trusses at the frequencies where the output peaked. In the next series of analyses the higher frequencies

were filtered so that the initial peak acceleration due to the first fundamental frequency was better defined.

The first fundamental frequency in cycles per second (Hz) of a simply supported beam (Clough and Penzien 1975) is given by

[4.1] $$f=\frac{\pi}{2L^2}\sqrt{\frac{EI}{m}}$$

where

L = is the span, m

EI = the flexural stiffness, Nm^2

$\bar{m}$ = the mass per unit length, Kg/m

The effective moment of inertia of steel trusses is commonly based on the moment of inertia of the truss chords reduced by 10% to account for the increased flexibility due to the open web system. For the composite trusses the 10% reduction factor would be applied to the transformed moment of inertia of the cross-section consisting of the steel chords and the concrete slab. This moment of inertia is further reduced to account for the flexibility of the shear connectors and interfacial slip. Brattland and Kennedy (1992) give

[4.2] $$I_e = I_s + 0.77\ p^{0.25}\ (I_t - I_s)$$

where

I_e = effective moment of inertia, mm^4

p = the decimal fraction of shear connection (here p=1.0)

and both I_s and I_t are reduced by the ratio 1/1.10 to account for the flexibility of the open web system. Thus to calculate the first

fundamental frequency for the steel trusses from [4.1] the effective moment of inertia of the steel trusses is used and for the composite trusses the effective moment of inertia determined from [4.2] including the reduction due to the flexibility of the open web system is used.

Clough and Penzien (1975) show, during the loading interval of phase I, for a single degree of freedom system, as the trusses are here modelled, when subjected to a triangular impulse with the force decreasing from P_0 to zero in time t_1, that the displacement is given by

$$v(t) = \frac{P_0}{k}\left(\frac{\sin\omega t}{\omega t} - \cos\omega t - \frac{t}{t_1} + 1\right) \qquad [4.3]$$

where

ω = natural circular frequency, rad/sec

k = spring constant, N/mm

P_0 = 2700 N for these tests

Evaluating [4.3] and its derivative at the end of phase I ($t=t_1$) gives

$$v(t_1) = \frac{P_0}{k}\left(\frac{\sin\omega t_1}{\omega t_1} - \cos\omega t_1\right) \qquad [4.4]$$

$$\dot{v}(t_1) = \frac{P_0\,\omega}{k}\left(\frac{\cos\omega t_1}{\omega t_1} + \sin\omega t_1 - \frac{1}{\omega t_1}\right) \qquad [4.5]$$

which can be substituted into

[4.6] $$v(\bar{t}) = [\frac{\dot{v}(t_1)}{\omega} \sin\omega\bar{t} + v(t_1) \cos\omega\bar{t}\ ]$$

where

$$\bar{t} = (t-t_1) > 0$$

to obtain the free vibration response in phase II after the impulse has ended.

The maximum values of displacement and acceleration are found for the times of zero velocity. Clough and Penzien state that for loading of very short duration with $t_1/T < 0.4$ the maximum response occurs during the free vibrations of phase II. For longer duration of loading the maximum response occurs during the loading interval of phase I.

Because the maximum response to an impulsive load is reached in a short time before the damping forces can absorb much energy from the structure Clough and Penzien consider it valid to determine the undamped response to impulsive loads as given above.

The damping ratio, based on measurements, is determined from the first mode (Allen and Rainer 1976) as

[4.7] $$\beta = \frac{1}{2\pi(n-1)} \ln\frac{a_1}{a_n}$$

where a_1 and a_n are peak accelerations (n-1) cycles apart provided that the damping does not exceed about 20% of the critical value.

4.2 Test results

4.2.1 Steel trusses

Figures 4.1 and 4.2 give examples of the output from the dynamic analyzer for a heel-drop test on steel truss 1 and Figures 4.3 and 4.4 for steel truss 2. For steel truss 1 the first fundamental frequency from Figure 4.1 is 15.12 Hz and the initial peak acceleration is 12.01 m/sec^2. The corresponding figures for truss 2 from Figures 4.3 and 4.4 are 15.12 Hz and 11.10 m/sec^2. From Figure 4.2 for truss 1 for four complete cycles the acceleration has decreased from 12.01 m/sec^2 to 1.06 m/sec^2 giving a damping ratio of 0.091. Correspondingly for steel truss 2 from Figure 4.4 the damping ratio is 0.080.

The mean value, standard deviation and coefficient of variation for the first fundamental frequency, initial peak acceleration and damping ratio as determined from the 20 tests for each truss are given in Table 4.1. The initial peak acceleration is given both in absolute terms and as a decimal fraction of the acceleration due to gravity, g.

4.2.2 Composite Trusses

Figures 4.5 and 4.6 present the dynamic analyzer output for one heel-drop test on composite truss 1. From Figure 4.5 the first fundamental frequency is 5.90 Hz. These figures give the variation of frequency and acceleration when the higher modes are filtered. From Figure 4.6 the initial peak acceleration is 0.98 m/sec^2. In 15 cycles the acceleration decreased from 0.98 m/sec^2 to 0.26 m/sec^2 (see Figure 4.7) to give a damping ratio for the composite truss of 0.015.

The higher frequencies have been filtered from the frequency and acceleration plot for composite truss 2 are given in Figure 4.8 and 4.9 for one test. From these figures the first fundamental frequency, the initial peak acceleration and the damping ratio are determined to be 6.00 Hz, 1.00 m/sec^2 and 0.017 respectively.

The data for all 20 tests on each of the composite trusses 1 and 2 are given, in the same manner as for the steel trusses, in Table 4.1.

4.3 Discussion

The coefficients of variations of the frequency observations range from 0.006 to 0.015 thereby indicating a high degree of precision. The test to predicted ratios for the steel and composite trusses, in the range of 1.00 to 1.04, are indicative of excellent agreement.

The initial peak acceleration for the steel trusses determined from the heel-drop tests exhibit relatively small scatter with coefficient of variation 0.066 and 0.048 for trusses 1 and 2 respectively. The test-predicted ratios for the two trusses show excellent correlation with values of 0.95 and 0.99. For the composite trusses the variation in the initial peak acceleration is greater than for the steel trusses with a coefficient of variation of 0.089 for truss 1 and 0.070 for truss 2. The calculated values of the initial peak acceleration are significantly less than the measured values resulting in test-predicted ratios for the two trusses 1.61 and 1.79 respectively. This range of test to predicted ratios is certainly within the range reported for 42 tests by Allen and Rainer (1976) where

test to predicted ratios varying from 0.33 to 2.5 are reported. The correlation between the test or measured initial peak acceleration would appear to deteriorate when its mean value is small. The initial peak acceleration may be sensitive to the mass of the person conducting the test and the manner in which his heels hit the floor. Pernica and Allen (1982) report test-to-predicted ratios of 0.9 to 1.8 and suggest that varying heel impact and the use of an average impulse as possible reasons for this variation.

While the mean value of the damping ratios for the two steel trusses are about the same at 0.078 and 0.080 respectively, these values are unrealistic and reflect the fact that the mass of the test individual is a considerable portion of the mass of the bare steel trusses, amounting to about 17%. In fact the individual is damping the vibration as well and the coefficient of variation of the damping ratios 0.13 and 0.14 are also large.

The damping ratios for the composite trusses 1 and 2 were measured as 0.015 and 0.017 respectively. These are relatively low values but are comparable to values reported by others (Allen and Rainer 1976). Based on Appendix G of CSA Standard S16.1-M89 (CSA1989) the composite trusses with the first fundamental frequency of 6 Hz and an initial peak acceleration of about 10% g and a damping ratio of 0.016 of critical would exceed the annoyance threshold criterion given there. A composite truss, as part of a structure, would likely exhibit considerably more damping because of the presence of carpeting, partitions and other furnishings as well as the effects of the actual structural connections as opposed to the

simple support of the puck bearing, and the continuity with the remainder of the structure.

Table 4.1 Frequency and acceleration comparison of predicted and measured values

Quantity	Steel trusses		Composite trusses	
	1	2	1	2
Test frequency, f , Hz				
μ	15.03	15.30	5.92	6.02
σ	0.209	0.226	0.034	0.084
V	0.014	0.015	0.006	0.014
n	20	20	20	20
Predicted frequency, Hz	15.00	15.00	5.810	5.770
Test/predicted ratio	1.002	1.020	1.019	1.043
Initial peak acceleration, m / sec^2				
μ	11.71	12.19	1.025	1.122
σ	0.774	0.589	0.091	0.078
V	0.066	0.048	0.089	0.070
μ / g	1.194	1.243	0.104	0.114
σ/ g	0.079	0.060	0.009	0.008
Predicted a, m / sec^2	12.36	12.36	0.636	0.635
Test/predicted	0.947	0.986	1.612	1.787
Damping Ratio , β				
μ	0.078	0.080	0.015	0.017
σ	1.024	1.135	0.139	0.134
V	0.132	0.142	0.095	0.079

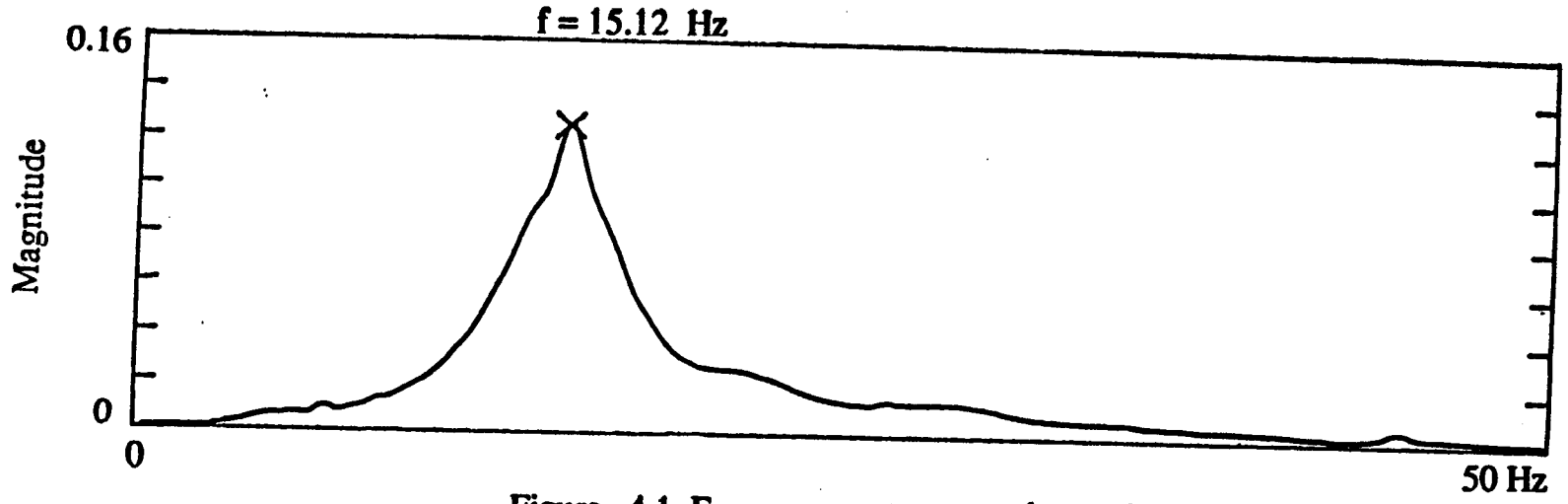

Figure 4.1 Frequency output, steel truss 1

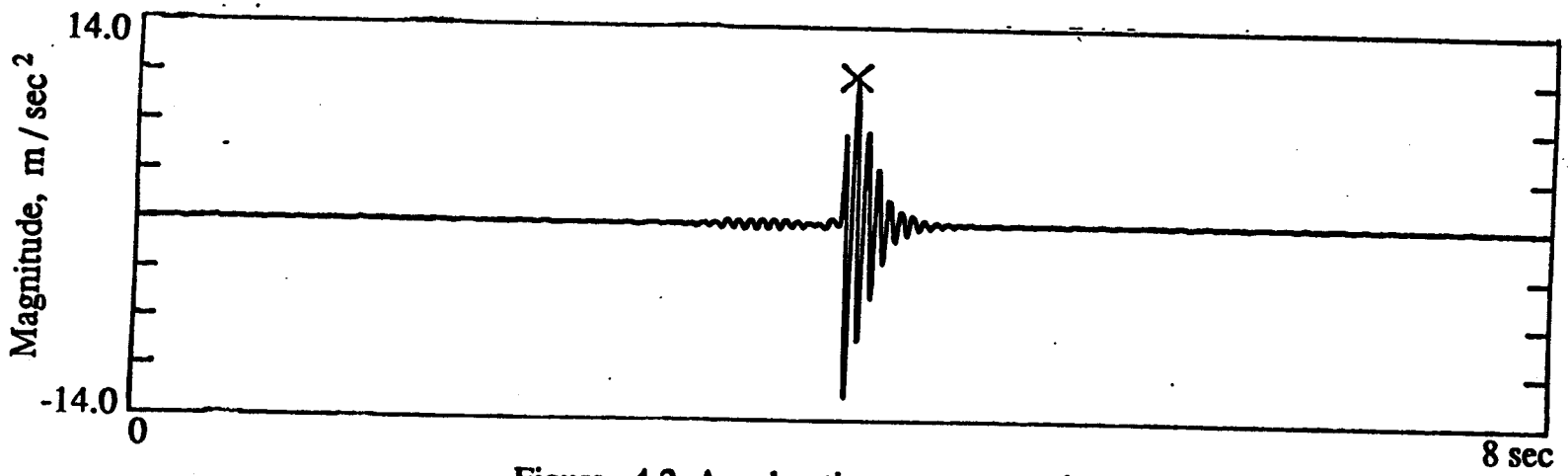

Figure 4.2 Acceleration output, steel truss 1

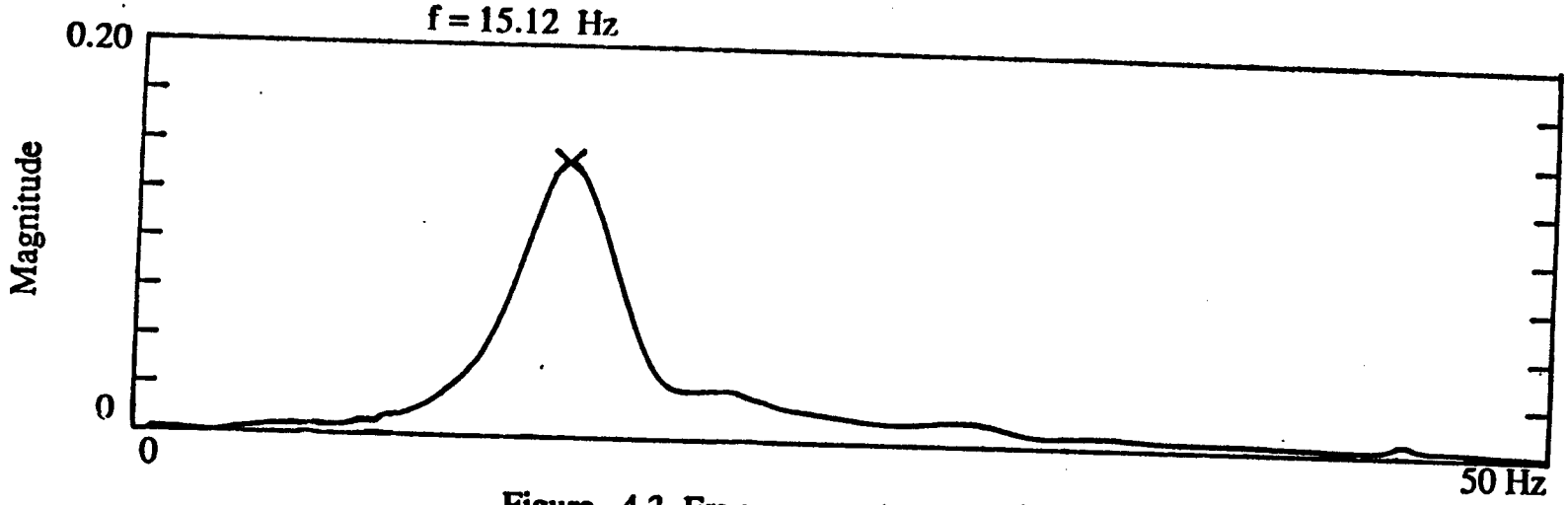

Figure 4.3 Frequency output, steel truss 2

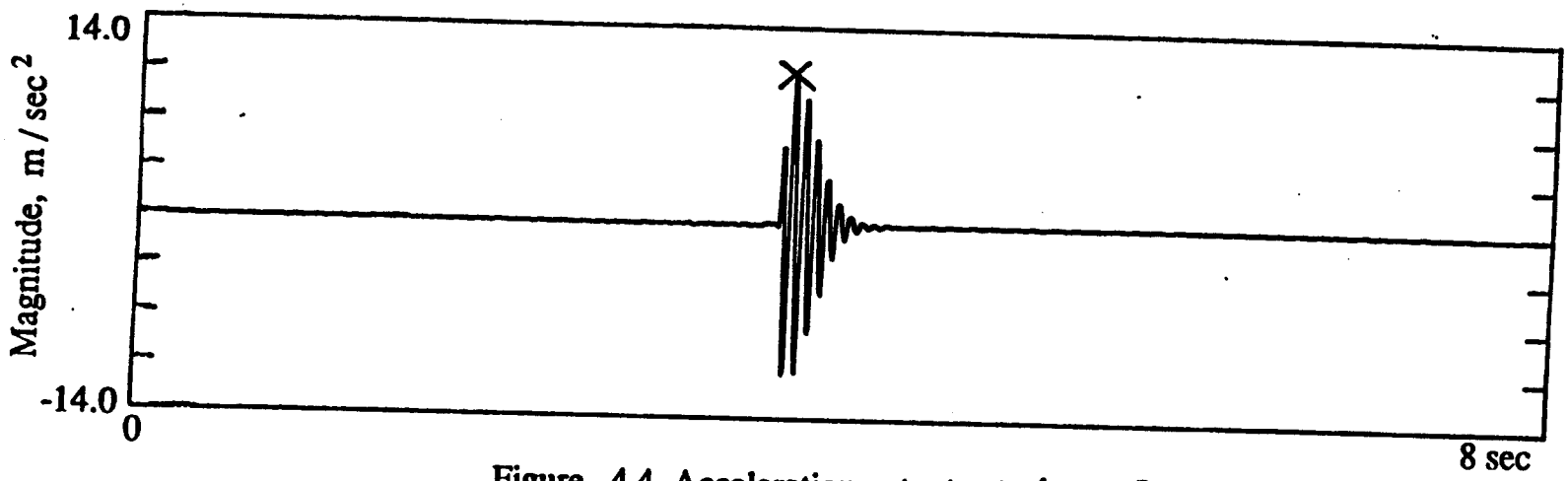

Figure 4.4 Acceleration output, steel truss 2

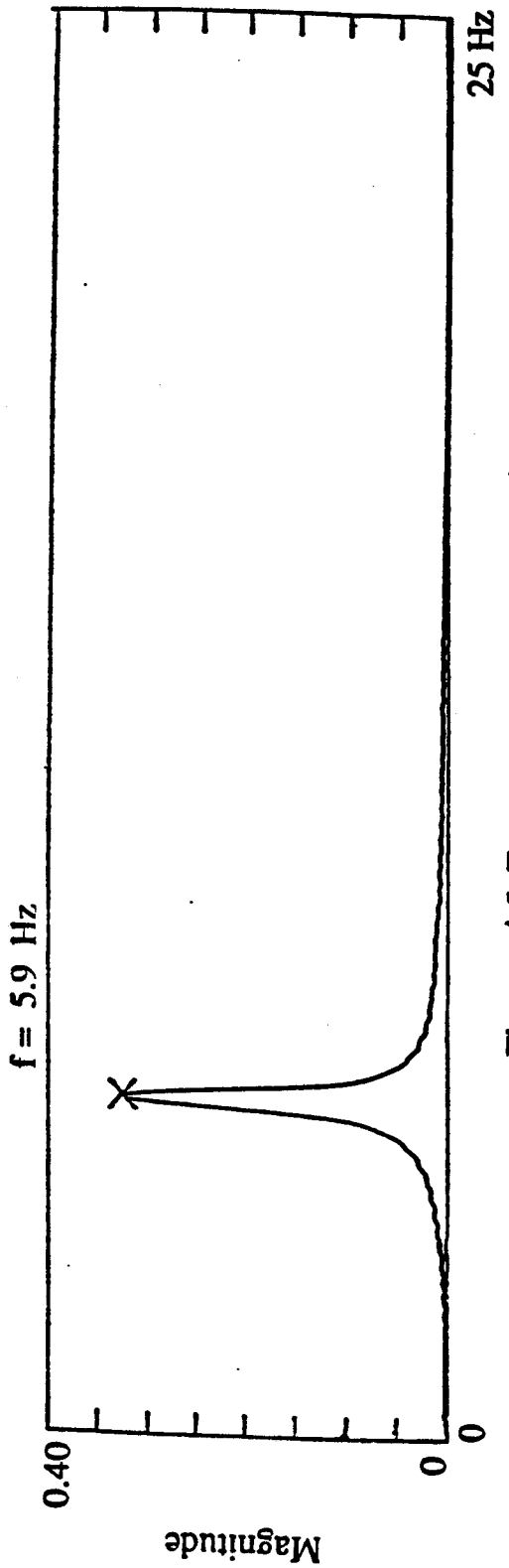

Figure 4.5 Frequency output, composite truss 1

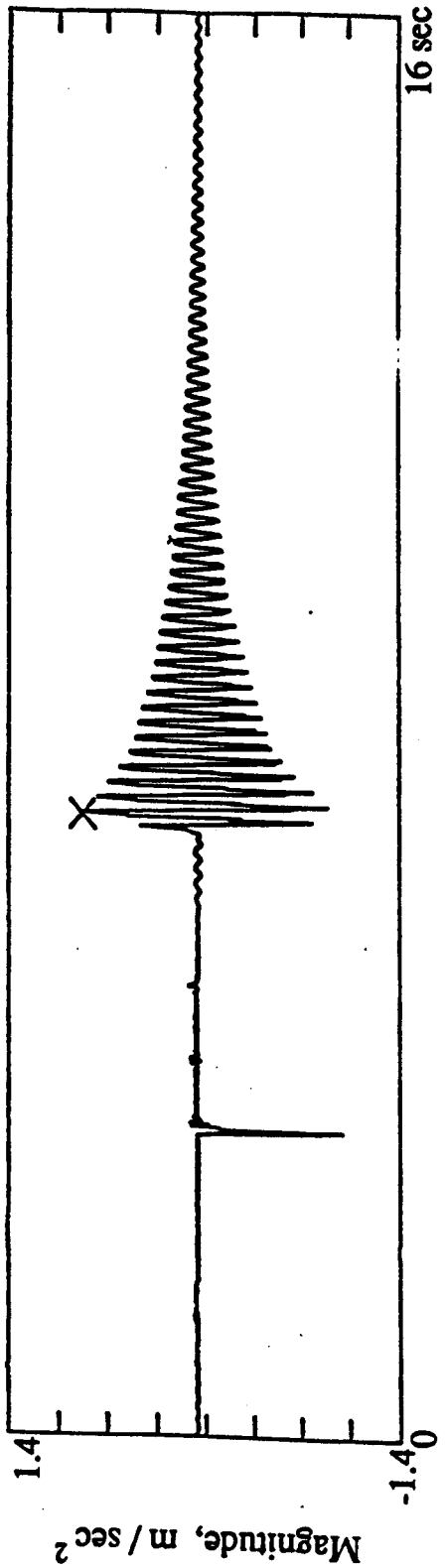

Figure 4.6 Acceleration output, composite truss 1

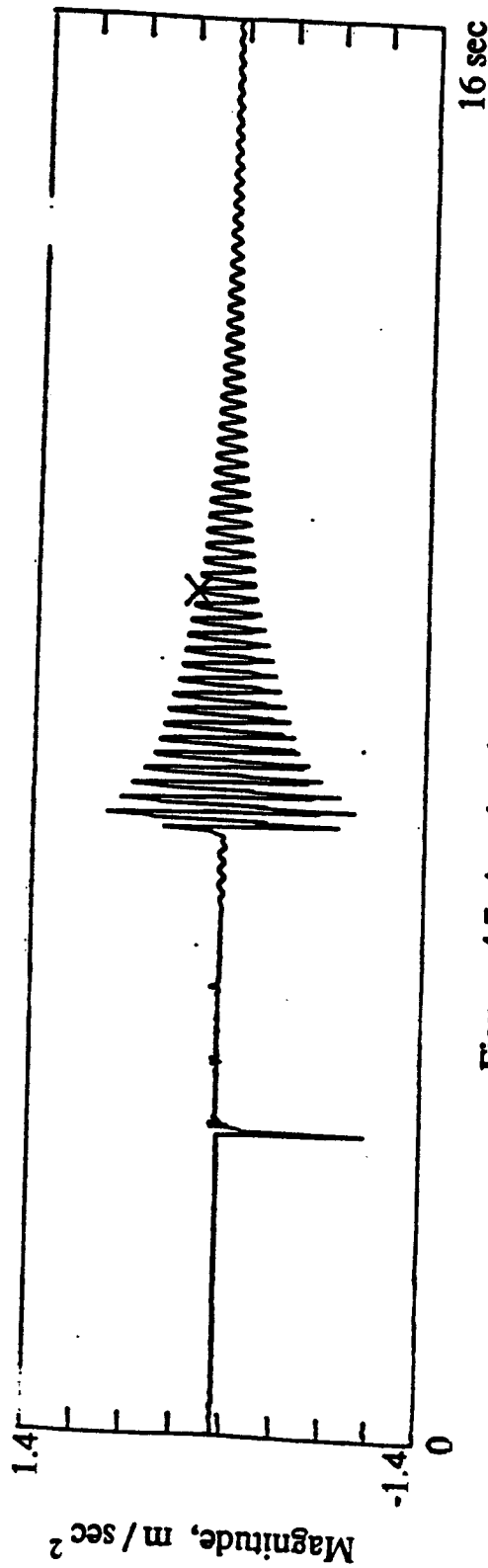

Figure 4.7 Acceleration output, composite truss 1

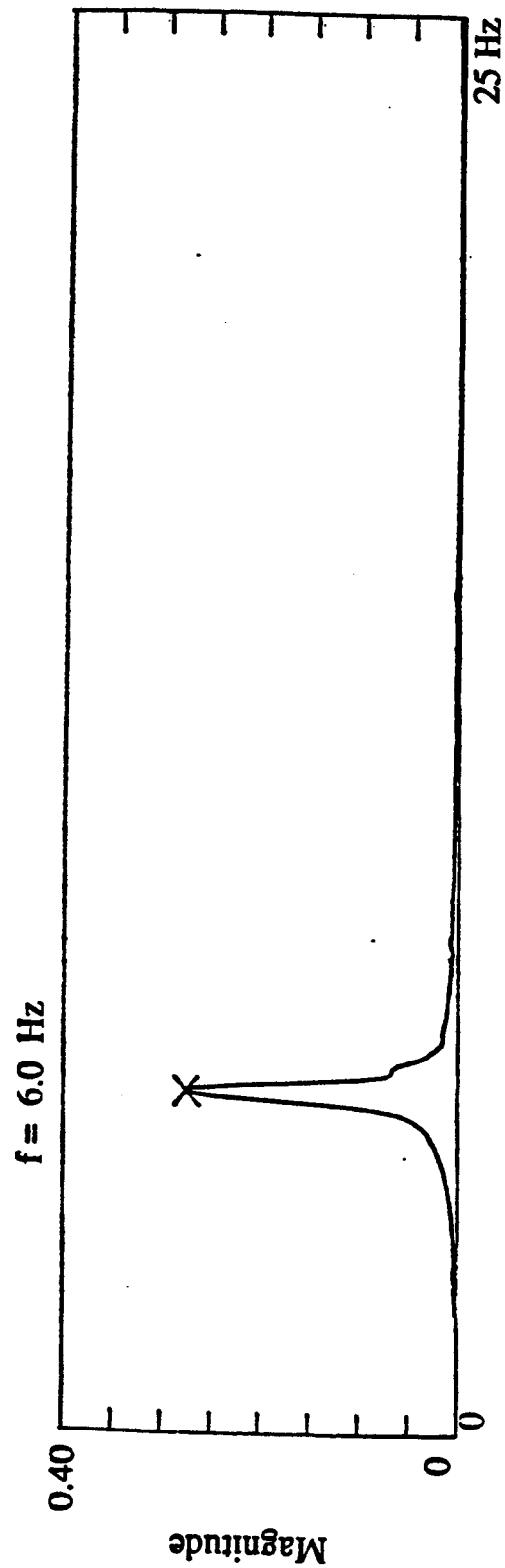

Figure 4.8 Frequency output, composite truss 2

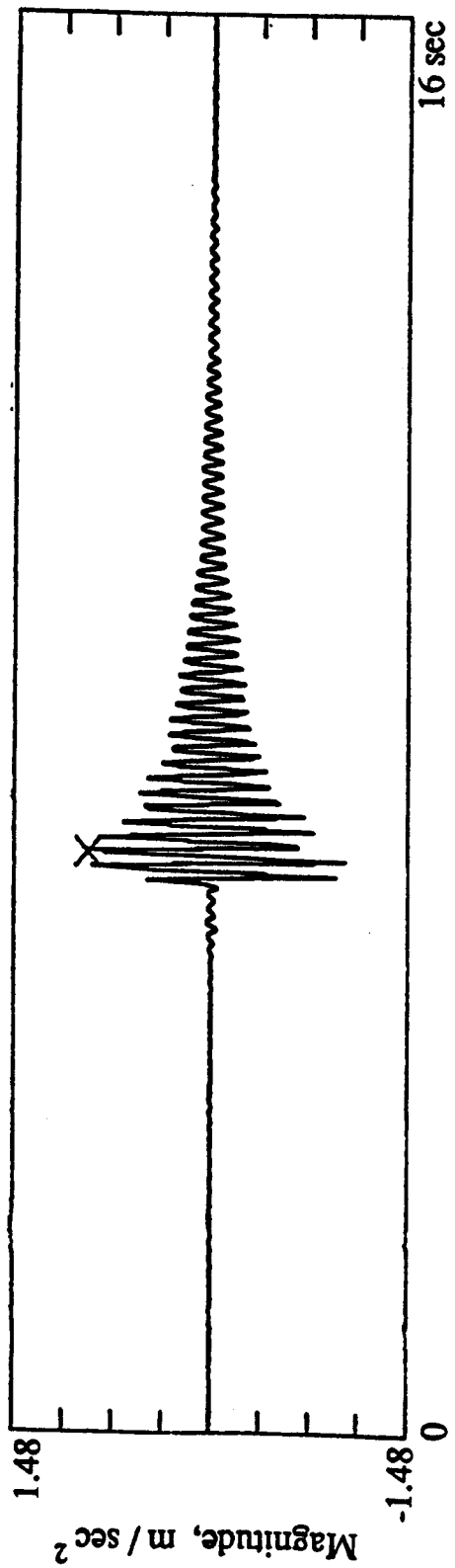

Figure 4.9 Acceleration output, composite truss 2

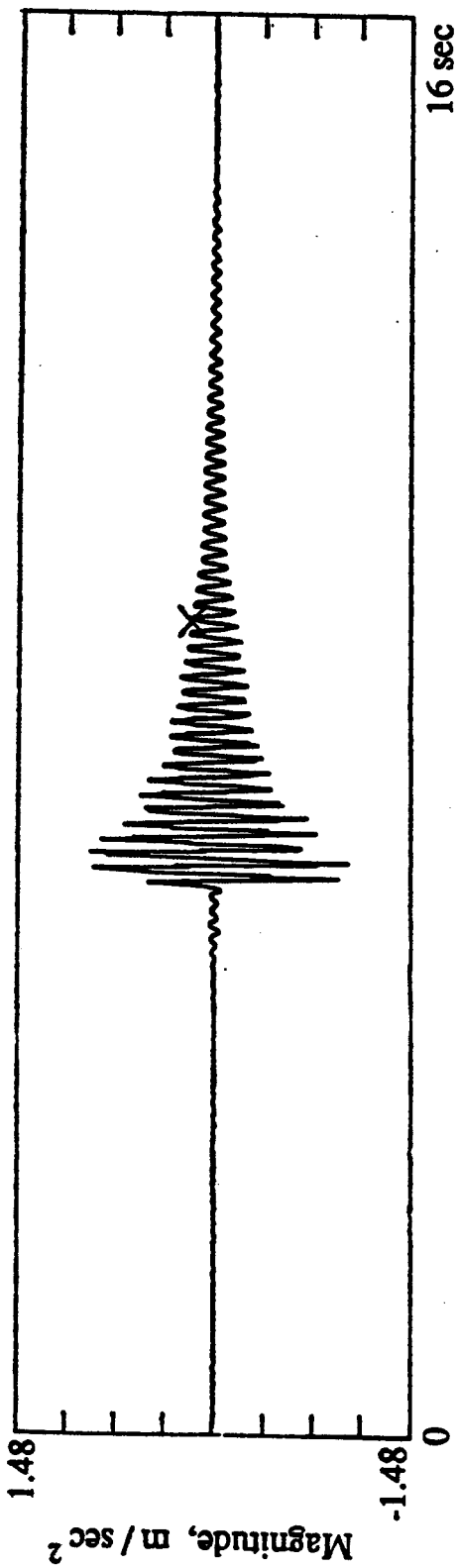

Figure 4.10 Acceleration output, composite truss 2

CHAPTER 5
SUMMARY AND CONCLUSIONS

1. The behaviour of non-interconnected double angle web members has been analyzed by examining strain data obtained at three locations along the length of the members. The web members, connected to the chords by weld on one leg, are eccentrically loaded. The strain analyses are also compared to a plane-frame-truss analysis where applicable.

2. Three plane-frame-truss analyses were carried out. A comparison of a pin-jointed truss analysis with that considering the member ends to be fixed shows, as would be expected, that the truss carries load primarily as axial forces in the members and that frame action contributes little to the overall strength.

3. Comparison of the pin-jointed analysis with the detailed analysis, taking into account the actual physical conditions as discussed subsequently, showed that the ratio of the axial force of the two analyses was 0.976 with the coefficient of variation of 0.019. This justifies the approach of positioning the web members such that their lines of actions intersect at mid-depth of the cover slab even though large joint eccentricities exist on the steel top chord.

4. As discussed in chapter 3 many different models were examined for the detailed plane frame analysis. That model considered to be most valid on the basis of the comparison with the results of the strain analyses, considered all members including shear connectors to be prismatic extending from node to node, considered all joint eccentricities, considered connection eccentricities by introducing

connection eccentricity moments at appropriate nodes, and considered the concrete cover slab to extend over its full width and thickness.

5. Multiple regression analyses were performed on the strain data obtained for eight web members at five load steps on two trusses. In the first of these, independent analyses of the strain data at the three levels served to check the accuracy of the strain data. The ratio of the maximum calculated axial load in a member to the minimum had a mean value of 1.037 and a coefficient of variation of 0.029.

6. The second set of multiple regression analysis was performed on all the strain data for particular load steps on given members. From these data the axial load and moments about the principal axes at the three locations were determined. These data were subsequently analyzed to establish the end moments and hence eccentricities about the principal axes. In turn these moments and eccentricities were resolved to establish the out-of-plane and in-plane eccentricities.

7. The out-of-plane end eccentricities were found to range from about one-fifth to two-fifths of the centroidal distance from the centroid of the angle to where the angles are connected to the chords. The out-of-plane eccentricity is reduced because of moments developed in the connections. The reduction is a function of the out-of-plane stiffness of the chord member and was found to be less (larger eccentricity) for the bottom chord having a more flexible side wall. Overall a mean end eccentricity of about one-third the centroidal distance is considered appropriate for the design of web members.

8 Ratios of the in-plane end eccentricities determined from the multiple regression analysis (the test or experimental values) divided by those determined from the detailed plane frame analysis, (the predicted value) were found for the bottom and top ends for five load steps for eight web members of trusses 1 and 2.

Chauvenet's criterion results in the rejection of some results as outliers as does the unusual behaviour of the bottom end of two web members. With these exclusions the mean value of the test-predicted bottom end eccentricity ratio is 0.846 with a coefficient of variation of 0.204 and of the top end eccentricity ratio 1.164 with a coefficient of variation of 0.152. The scatter in these results is considered to arise from the accumulative effect of the assumptions made in plane-frame-truss analysis and all the experimental errors.

9. The test values of the first fundamental frequency determined from the heel-drop tests for both the steel and composite trusses are in excellent agreement with the predicted values of about 15.0 and 5.8 Hz. respectively with test-predicted ratios of about 1.00 to 1.04.

10. The test values of the initial peak accelerations determined from the heel-drop tests for both the steel and composite trusses are in reasonable agreement with the predicted values. Those for the steel trusses are in the order of 97% of the predicted values while those for the composite trusses are about 170% of the predicted values. The ratios for the composite trusses are within the range reported by others.

11. The high damping ratios for the two steel trusses probably reflect the relative large mass of the test individual related to the masses of the trusses themselves and is considered unrealistic. The damping

ratio for composite trusses 1 and 2 of about 0.016 although relatively low are comparable to those reported by others. Unless increased in a real structure by furnishings and actual structural continuity such a damping ratio with the first fundamental frequency of 6 Hz. and an initial peak acceleration of about 10% g would exceed the annoyance threshold criterion of CSA Standard S16.1-M89.

REFERENCES

Adluri, S.M.R. and Madugula, M.K.S. 1992. Eccentrically loaded steel single angle struts. Engineering Journal, American Institute of Steel Construction, Vol.2, pp.59-66

Adluri, S.M.R. and Madugula, M.K.S. 1993. Behaviour of single-angle compression members. Discussion of Elgaaly et al., Journal of Structural Division, American Society of Civil Engineers. Vol.119, No.1, pp.359-360.

Allen, D.E. and Rainer, J.H. 1976. Vibration criteria for long span floors. Canadian Journal of Civil Engineering, Vol.3, No.2, pp.165-173.

Al-sayed, S.H. and Bjorhovde, R. 1989. Experimental study of single angle columns. Journal of Constructional Steel Research. Vol.12, No.2 pp. 83-102

American Institute of Steel Construction (AISC). 1986. Load and resistance factor design specification for structural steel buildings. Chicago, Illinois.

American Society of Civil Engineers (ASCE), 1988. Manuals and reports on engineering practice No.52; Guide for design of steel transmission towers. 2nd. edition. New York, N.Y.

Bathon, L., Mueller III, W.H. and Kempner jr., L. 1993. Ultimate load capacity of single steel angles. Journal of the Structural Division, American Society of Civil Engineers, Vol.119, No.1, pp. 279-300.

Bjorhovde, R. 1981. Full scale test of a composite truss. Structural Engineering Report. No.97, Department of Civil Engineering, University of Alberta.

Brattland, A. and Kennedy, D.J.L. 1986. Shrinkage and flexural tests of two full-scale composite trusses. Structural Engineering Report. No.143, Department of Civil Engineering, University of Alberta

Brattland, A. and Kennedy, D.J.L. 1992. Flexural tests of two full-scale composite trusses. Canadian Journal of Civil Engineering, Vol.19, No.2, pp. 279-295.

Canadian Standards Association(CSA). 1981a. General requirements for rolled or welded structural quality steel. National Standard of Canada CAN3-G40.20-M81, Canadian Standards Association, Rexdale, Ontario.

Canadian Standards Association(CSA). 1981b. Structural quality steels. National Standard of Canada CAN3-G40.21M81, Canadian Standards Association, Rexdale, Ontario.

Canadian Standards Association(CSA). 1989. Limit states design of steel structures, National Standard of Canada CAN/CSA- S16.1-M89, Canadian Standards Association, Ontario

Clough, R.W. and Penzien, J. 1975. Dynamics of structures. McGraw-Hill, Inc. N.Y.

Cran, J.A. 1972. Design and testing of composite open web steel joists. Technical Bulletin 11, Stelco.

Elgaaly, M. Dagher, H. and Davids, W. 1991. Behaviour of single angle compression members. Journal of Structural Engineering, American Society of Civil Engineers, Vol.117, No.12, pp.3720-3741

Kennedy, J.B. and Neville, A.M. 1986. Basic statistical methods for engineers and scientists, 3rd edition, Harper and Row, Publishers, New York

Lenzen, K.H. 1966. Vibration of steel joists, Engineering Journal, American Institute of Steel Construction, Vol.3, N0.3, p133.

Lenzen, K.H. and Keller, J.E. 1960. Vibrations of steel joist-concrete slab floor systems, Part I, The University of Kansas Center for Research in Engineering Science, Lawrence, Kansas.

Lenzen, K.H. and Murray, T.M. 1969. Vibration of steel beam-concrete slab floor systems, Studies in Engineering Mechanics, Report No.29, The University of Kansas Center for Research in Engineering Science, Lawrence, Kansas.

Lesik, D.F. and Kennedy, D.J.L. 1990. Ultimate strength of fillet welded connections loaded in plane. Canadian Journal of Civil Engineering 17(1), pp. 55-67.

Mendenhall, W. and Sincich, T. 1988. Statistics for the engineering and computer sciences, Dellen Publishing Company, California.

Nuttal, N.J. and Adams, P.F. 1970. Flexural and lateral-torsional buckling strength of double angle struts. Structural Engineering Report No.30, Department of Civil Engineering, University of Alberta.

Pernica, G. and Allen, D.E. 1982. Floor vibration measurements in a shopping center. Canadian Journal of Civil Engineering, Vol.9, pp.149-155.

Reiher, H. and Meister, F.J. 1931. The effect of vibration on people(in German), Forchung auf dem Gebeite des Ingenieurwesens, V.2,II, p381. (Translation: Report No.F-TS-616-Re H.Q. Air Material Command, Wright Field, Ohio, 1949).

Roark, R.J. 1943. Formulas for stress and strain, McGraw-Hill Inc. New York

Wiss, J.F. and Parmelee, R.A. 1974. Human perception of transient vibrations, Journal of the Structural Division, Proceedings of the American Society of Civil Engineers, Vol.100, No. ST4, pp. 773-787.

Recent Structural Engineering Reports

Department of Civil Engineering

University of Alberta

168. *Erection Analysis of Cable-Stayed Bridges* by Z. Behin and D.W. Murray, September 1990.

169. *Behavior of Shear Connected Cavity Walls* by P.K. Papinkolas, M. Hatzinikolas and J. Warwaruk, September 1990.

170. *Inelastic Transverse Shear Capacity of Large Fabricated Steel Tubes*, by K.H. Obaia, A.E. Elwi, and G.L. Kulak.

171. *Fatigue of Drill Pipe* by G.Y. Grondin and G.L. Kulak, April 1991.

172. *The Effective Modulus of Elasticity of Concrete in Tension* by Atif F. Shaker and D.J. Laurie Kennedy, April 1991.

173. *Slenderness Effects in Eccentrically Loaded Masonry Walls* by Mohammad A. Muqtadir, J. Warwaruk and M.A. Hatzinikolas, June 1991.

174. *Bond Model For Strength of Slab-Column Joints* by Scott D.B. Alexander and Sidney H. Simmonds, June 1991.

175. *Modelling and Design of Unbraced Reinforced Concrete Frames* by Yehia K. Elezaby and Sidney H. Simmonds, February 1992.

176. *Strength and Stability of Reinforced Concrete Plates Under Combined Inplane and Lateral Loads* by Mashhour G. Ghoneim and James G. MacGregor, February 1992.

177. *A Field Study of Fastener Tension in High-Strength Bolts* by G.L. Kulak and K. H Obaia, April 1992.

178. *Flexural Behaviour of Concrete-Filled Hollow Structural Sections* by Yue Qing Lu and D.J. Laurie Kennedy, April 1992.

179. *Finite Element Analysis of Distributed Discrete Concrete Cracking* by Budan Yao and D.W. Murray, May 1992.

180. *Finite Element Analysis of Composite Ice Resisting Walls* by R.A. Link and A.E. Elwi, June 1992.

181. *Numerical Analysis of Buried Pipelines* by Zhilong Zhou and David W. Murray, January 1993.

182. *Shear Connected Cavity Walls Under Vertical Loads* by A. Goyal, M.A. Hatzinikolas and J. Warwaruk, January 1993.

183. *Frame Methods for Analysis of Two-Way Slabs* by M. Mulenga and S.H. Simmonds, January 1993.

184. *Evaluation of Design Procedures for Torsion in Reinforced and Prestressed Concrete* by Mashour G. Ghoneim and J.G. MacGregor, February 1993.

185. *Distortional Buckling of Steel Beams* by Hesham S. Essa and D.J. Laurie Kennedy, April 1993.

186. *Effect of Size on Flexural Behaviour of High Strength Concrete Beams* by N. Alca and J.G. MacGregor, May 1993.

187. *Shear Lag in Bolted Single and Double Angle Tension Members* by Yue Wu and Geoffrey L. Kulak, June 1993.

188. *A Shear-Friction Truss Model for Reinforced Concrete Beams Subjected to Shear* by S.A. Chen and J.G. MacGregor, June 1993.

189. *An Investigation of Hoist-Induced Dynamic Loads* by Douglas A. Barrett and Terry M. Hrudey, July 1993.

190. *Analysis and Design of Fabricated Steel Structures for Fatigue: A Primer for Civil Engineers* by Geoffrey L. Kulak and Ian F.C. Smith, July 1993.

191. *Cyclic Behavior of Steel Gusset Plate Connections* by Jeffrey S. Rabinovitch and J.J. Roger Cheng, August 1993.

192. *Bending Strength of Longitudinally Stiffened Steel Cylinders* by Qishi Chen, Alla E. Elwi and Geoffrey L. Kulak, August 1993.

193. *Web Behaviour in Wood Composite Box Beams* by E. Thomas Lewicke, J.J. Roger Cheng and Lars Bach, August 1993.

194. *Experimental Investigation of the Compressive Behavior of Gusset Plate Connections* by Michael C.H. Yam and J.J. Roger Cheng, September 1993.

195. *Some Behavioural Aspects of Composite Trusses* by Berhanu Woldegiorgis and D.J. Laurie Kennedy, January 1994.